STUDY OF STRUCTURAL KINETICS IN THE EFFECT OF PARTLY SUBSTITUTION OF Fe BY Co IN FINEMET

M. Sc. Thesis

BY

KAUSHIK SARKAR

DEPARTMENT OF PHYSICS
KHULNA UNIVERSITY OF ENGINEERING & TECHNOLOGY
KHULNA - 9203, BANGLADESH
APRIL - 2018

STUDY OF STRUCTURAL KINETICS IN THE EFFECT OF PARTLY SUBSTITUTION OF Fe BY Co IN FINEMET

BY

KAUSHIK SARKAR
ROLL NO: 1655558
SESSION: JULY - 2016

A THESIS SUBMITED TO THE DEPARTMENT OF PHYSICS,
KHULNA UNIVERSITY OF ENGINEERING & TECHNOLOGY,
KHULNA - 9203 IN PARTIAL FULFILMENT OF THE
REQUIRMENT FOR THE DEGREE OF MASTER OF SCIENCE

DEPARTMENT OF PHYSICS
KHULNA UNIVERSITY OF ENGINEERING & TECHNOLOGY
KHULNA - 9203, BANGLADESH
APRIL - 2018

TO

MY PARENTS

DECLARATION

This is to certify that the thesis work entitled as "**Study of Structural Kinetics in the Effect of Partly Substitution of Fe by Co in FINEMET**" has been carried out in partial fulfillment of the requirement for M. Sc. degree in the department of Physics, Khulna University of Engineering & Technology, Khulna - 9203, Bangladesh. The above research work or any part of this work has not been submitted anywhere for the award of any degree or diploma. No other person's work has been used without due acknowledgement.

Supervisor	Candidate
----------	----------
(Prof. Dr. S. S. Sikder)	(Kaushik Sarkar)

Acknowledgements

I express, with due respect my deepest sense of sincere gratitude indebtedness to my supervisor Prof. Dr. Shibendra Shekher Sikder, Department of Physics, Khulna University of Engineering & Technology (KUET), Khulna for his indispensable guidance, erudite discussion, constructive suggestions, fruitful discussion and constant inspiration throughout the research work. He is always ready to provide a lucid explanation of the different concepts involved and critical reading of the script and subsequent corrections are much appreciated. Any mistake that remain is of course mine. Without his constant supervision this thesis work could not performed.

It is a matter of great pleasure for me to record the deepest sense of gratitude to Prof. Dr. Md. Mahbub Alam, Prof. Dr. Abdullah Elias Akther and Prof. Dr. Jolly Sultana, Department of Physics, KUET, have been given me a strong support in various ways during the entire period of my study in the department of Physics KUET. I am thankful to Mr. Alamgir Hossain, Assistant professor, Department of Physics, KUET of his tired less co-operation in my thesis work.

I am grateful to Dr. S. Manjura Hoque, Head & Chief Scientific Officer, Materials Science Division (MSD), Atomic Energy Centre, Dhaka (AECD) for providing kind opportunity to use the laboratory for experimental work. My thanks are also for Dr. Nazrul Islam Khan, PSO, Mr. H. N. Das and Mr. M. A. Mamun, Scientific Officer, MSD, AEC, Dhaka for providing me with technical assistance form time during my research work and providing kind opportunity to work in their laboratory for experimental purpose regarding my thesis.

I am grateful to Mr. Md. Kamrul Hasan Reza, Associate Professor Department of Physics, KUET, Mr. Sujith Kumar Shil, Mr. Suman Halder, Assistant Professor, Mr. Suman Deb Nath, Mr. Probal Roy, Mr. Saifullah, Lecture, Department of Physics, KUET for their tireless co-operation in my thesis work. I would also like to thank my well wishers and class fellows Al Masud and Prodip Kumar Mondal.

Many thanks are due to the Director, Atomic Energy Center, Dhaka for his kind permission to use the laboratory of Material Science Division, AEC, Dhaka.

I am thankful to Ms. Alhamra Parveen, Ms. Anjuman Ara Begum, Ms. Nazmunnahar Begum and Mr. Anawar Hossain of Material Science Division, AECD, for their co-operation during the experiments of my research work at the laboratory of AECD.

A very special thanks to Mrs. Nandita Saha, spouse of Prof. Dr. S. S. Sikder for her heartfelt encouragement, cares and helps throughout the entire period of M. Sc. program.

I also wish to thank the authority of Khulna University of Engineering & Technology (KUET), Khulna for providing me with the necessary permission and financial assistance for conducting this thesis work.

Kaushik Sarkar

ABSTRACT

This thesis is based on the experimental investigation of nanocrystalline formation partly substitution Fe by Co in FINEMET with composition $(Fe_{0.9}Co_{0.1})_{73.5}Cu_1Nb_3Si_{13.5}B_9$ alloy in the amorphous and annealed states. The sample has been prepared from high purity in gradients by rapid solidification technique using a method spinning technique and their amorphous nature has been confirmed by X-ray diffraction (XRD). The crystallization kinetics and the nanocrystal formation have been studied by differential thermal analysis (DTA) and XRD. Magnetization measurements have been carried out using vibrating sample magnetometer (VSM). The alloy has been annealed in a controlled way in the temperature range of 400 - 650^{o}C for constant annealing time one hour. The kinetics of primary crystallization α-FeCo(Si) phase and secondary crystallization Fe_2B phase in composition is studied as affected DTA and confirmed by XRD. The sample annealed at 450^{o}C at constant annealing time is almost unchanged is still lower than DTA scan that of primary crystallization phase but the same condition sample annealed at 600^{o}C completely diffused primary crystallization α-FeCo(Si) phase has already vanish. Thermal analysis experiment and from the obtained data activation energy of α-FeCo(Si) is 4.1eV and Fe_2B is 6.31eV. In the optimized annealing condition the grain size has been obtained in the range of 12 - 15 nm. The peak shifts indicate the change of the values of Si-content of nanograins and therefore, the change of the values of lattice parameter of nanograins. Saturation magnetization is maximum value is observed annealed at 600^{0}C. The M_S initially decreases with increasing annealing temperature and again increase M_S further decrease with increase annealing temperature may be connected with the enrichment of the residual amorphous phase with Nb that weakens the coupling between ferromagnetic nanograins. Lower applied field suffices to produce saturation the nanocrystalline material is said to be magnetically soft.

Contents

CHAPTER III

EXPERIMENTAL DETAILS

CHAPTER IV

RESULTS AND DISCUSSION

List of Figures

List of Tables

List of Symbols

a_0	=	Lattice parameter
B	=	Magnetic induction
D_g	=	Grain size
DTA	=	Differential Thermal Analysis
DSC	=	Differential Scanning Calorimetry
d	=	Average diameter
FWHM	=	Full Width at Half Maximum
H	=	Magnetic field
H_c	=	Coercivity
H_a	=	Applied magnetic field
[hkl]	=	Miller Indices
k	=	Magnetic hardness parameter
K_B	=	Boatman's constant
K_{eff}	=	Effective magnetic anisotropy constant
L	=	Self inductance of the sample core
L_o	=	Inductance of the winding coil without sample
L_{ex}	=	Ferromagnetic exchange length
M	=	Magnetization
M_s	=	Saturation magnetization
M_r	=	Remanence magnetization
nm	=	nano meter
NM	=	Nobel metal
S	=	Total spin angular momentum
T_{ij}	=	Exchange interaction between atoms at the position r_i and r_j .
T_a	=	Annealing temperature
T_c	=	Curie temperature
T_g	=	Glass transition temperature
T_x	=	Crystallization temperature
T_m	=	Melting point temperature
T_{x_1}	=	Primary crystallization temperature
T_{x_2}	=	Secondary crystallization temperature
T_{p_1}	=	Primary crystallization peak temperature

T_{p_2}	=	Secondary crystallization peak temperature
TG	=	Thermo gravimetric
TL	=	Transition metal
VSM	=	Vibrating Sample Magnetometer
XRD	=	X-ray diffraction
μ	=	Permeability
λ	=	Wave length
θ	=	Scattering angle
t_o	=	Time constant
β	=	Heating rate
δ_w	=	Domain wall Width
σ	=	Effective stress
ρ(r)	=	Atomic density
< K >	=	Average anisotropy
T_c^{am}	=	Curie temperature of residual amorphous matrix
ΔH	=	Enthalpy of crystallization
ΔE	=	Activation Energy

CHAPTER I

INTRODUCTION

CHAPTER II

THEORETICAL BACKGROUND

CHAPTER III

EXPERIMENTAL DETAILS

CHAPTER IV

RESULTS AND DISCUSSION

CHAPTER V

CONCLUSIONS

REFERENCES

INTRODUCTION

1.1 Introduction

Nanocrystalline materials designate a novel type of interface-controlled solids that are characterized by a structural modulation on the length scale of several nanometers. Considering the highly attractive application potentials e.g., ductility of nanocrystalline ceramics at low temperatures, high strength of nanostructure ceramic-metal composites, soft magnetic behavior of nanocrystalline alloys, or a tailoring of new types of alloys, the synthesis and structural studies of nanocrystalline materials have developed rapidly into a challenging field of materials science. The modified properties of nanocrystalline amorphous ribbon are considered as a consequence of the microscopic length scale of the crystal dimensions and in particular of the large number of interfaces. This thesis focuses on exploiting some of the scientific and technological aspect of nanostructure magnetic materials. Nanomaterials are generally materials that can have one dimension, two dimension or three dimension and can be specified within a size of 100 nanometer (1nm $=10^{-9}$m).

Nanomaterials can be classified into nanocrystalline materials and nanoparticles. The first are polycrystalline bulk materials devitrified from the synthesized amorphous precursor through appropriate thermal treatment with grain size into nanometer range (<100 nm) while the last refers to ultrafine dispersive particles with diameters <100 nm. Nanoparticles are interesting from the fundamental point of view due to their extremely small size. The increasing surface to volume ratio with decreasing size results in an increased significance of the grain boundaries (i.e. surface energies) especially in the "real" nanometer range (≤10nm). Nanocrystalline materials are distinguished from conventional polycrystalline materials by the size of crystallites that compose them. Defined broadly the term nanostructure is used to describe materials characterized by structural features in the range of 1-10nm corresponding typically to = 50-5×10^7atoms. The unique properties of FINEMET alloys include low losses, high permeability and near zero magnetostriction achieved by permalloys and Co-based amorphous alloys, but much higher saturation magnetization up to 1.3T, than these materials usually have ever offered.

In 1988 Yoshizawa, Oguma and Yamauchi at Hitachi Metals Ltd. developed the first nanocrystalline ultra soft magnetic alloy called FINEMET having composition $Fe_{73.5}Nb_3Cu_1Si_{13.5}B_9$ from the Fe-Si-B amorphous alloys to which the

addition of Cu and Nb were added [1.1] .Commercially known as FINEMET established a new approach to develop soft magnetic variable with high magnetic flux density, that is magneto crystalline anisotropy can be reduced by referring the grain size is less than a few tense of nanometer [1.2-1.3]. Nanocrystalline soft magnetic materials constitute a new class of condensed matter having interesting properties, which are mostly microstructure dependent. The FINEMET consists of a two phase microstructure in its optimally annealed condition. This micro structure is made up of a ferromagnetic bcc α-Fe (Si) phase and/ or Do_3 type of ordered Fe (Si) phase with grain size of 10-15 nm embedded in this residual ferromagnetic amorphous matrix. As the composition of a primary crystal differs from that of an amorphous matrix, the process of the crystal growth becomes diffusion controlled. In order to control the growth process of nanostructure alloys, it is important to investigate the kinetics of crystallization.

The crystallization of these metallic glasses enables the study of both nucleation and growth processes. Thus the main objective of this thesis is to describe the kinetics of solid phase transformation taking place on the nanoscale, i.e. the study of nanocrystallization which promotes the evolution of superior soft magnetic properties in the studied composition. These represent a new family of excellent soft magnetic core materials and have stimulated an amorphous research activity due to their potential application [1.4 – 1.7]. The unique properties of FINEMET alloys include low losses high permeability and near-zero magnetostriction achieved by permalloys and Co-based amorphous alloys, but much higher saturation magnetization up to 1.3 Tesla, than these materials usually have ever offered with a view to improve the soft magnetic behavior of FINEMET type alloys, partial substitution of Fe with various elements has been widely investigated [1.8 – 1.9]. Controlled Co addition [1.10 – 1.11] enhance the curie temperature of the resulting nanocrystalline material which good soft magnetic properties are also observed at elevated temperature, thus making these materials appropriate for working at high temperature [1.12]. Adding Co is also expected to be beneficial to induce in plane magnetic anisotropy to ribbons by magnetic field annealing, because the substitution of Fe with Co is known to be effective for increasing the magnetic anisotropy constant, K_u of Fe-Si-B amorphous alloys.

The magnetocrystalline anisotropy vanishes when the grain size is smaller than the ferromagnetic exchange length and magnetostriction goes towards zero due

to cancellation of positive magnetostriction of α-Fe(Si) crystallites and negative magnetostriction of the amorphous matrix. It is well known that the microstructure, noticeably the grain size, essentially determines the hysteresis loop of a ferromagnetic material, from the nanometer regime to microscopic grain size. The permeability shows a analogue behavior being essentially inversely proportional to the coercive force, lowest coercivities, however are again found for smallest structural correlation length like in amorphous alloys and in nanocrystalline alloys for grain sizes D_g < 20nm. To investigated that the partial substitution of Fe by Co leads to increasing of magnetic moment and Curie point of the amorphous state.

The effect of partly substitute of Fe by Co replaced FINEMET types alloys to improve the thermal stability against crystallization kinetics and higher Curie temperature of the amorphous phase. The aim of the present work is to improve the magnetic properties of these Co replaced FINEMET type alloys from melt spun amorphous ribbons; microstructure is an important parameter that can be controlled by heat treatment condition. In this work to understand the mechanism of the formation of nanocrystal phase transformation crystallization kinetics, size of the nanocrystal their volume fraction along with the effect on magnetic properties through controlled thermal treatment. Results have been aid in interpreting the effect of heat treatment on magnetic properties and application of this type of alloys.

1.2 The Aim and Objectives of the Present Work

The main objective of the present work is to the importance of partly substitution Fe by Co in FINEMET, there is scope for studying the crystallization kinetics and magnetic properties for the composition $(Fe_{0.9}\ Co_{0.1})_{73.5}Cu_1Nb_3Si_{13.5}B_9$ amorphous ribbon.

The objectives of the research work are us follows.

- To the kinetic of crystallization of amorphous to FINEMET type alloys were investigated by the use of DTA and XRD.
- To synthesis of the FINEMET alloy in the form of the ribbon with varying amount of Co and Fe in the amorphous state rapid solidification technique.
- To study growth of nanocrystals on amorphous matrix by thermal treatment.
- To characterization of nanostructure phases such as the size of nanograins, compositions of the nanograins and the volume of the nanograin.

- The formation nanocrystals with grain size distribution as affected by heat treatment with varying temperature and holding time.
- Correlation of evaluation of nanograins with the magnetic properties.
- Optimization of annealing temperature corresponding to the good magnetic properties.

1.3 Experimental Reason for this Research Work

In the present work, soft magnetic amorphous FINEMET ribbon type alloy with the nominal composition $(Fe_{0.9}Co_{0.1})_{73.5}Cu_1Nb_3Si_{13.5}B_9$ has been prepared from high purity in gradients by rapid solidification technique using a method spinning technique. As the composition of a primary crystal differs from that of an amorphous matrix, the process of crystal growth becomes diffusion controlled. In order to control the growth process of nanostrucred alloys, it is important to investigate the kinetics of crystallization. The crystallization of these metallic glasses enables the study of both nucleation and growth process. Thus the main objective of this thesis is to describe the kinetics of solid phase transformation taking place on the nanoscale, i.e., study of nanocrystallization which promotes the evolution of soft magnetic properties in studied sample. The experimental methods that would be used in this research work are as follows.

- Amorphousity of the sample will be checked by X-ray diffraction.
- Amorphous samples would be realized upon isothermal annealing based on the knowledge of crystallization temperature obtained from DTA.
- From DTA analysis evaluation of the crystallization activation energy of various phases will be done.
- The optimum heat treatment would be carried out in a microprocessor controlled high temperature furnace.
- Crystallization phase and grain size of the nanograins will be determined by XRD on sample annealed at different temperature.
- The combination of these two techniques is necessary for the compute description of the processes occurring during the nanocrystallization from amorphous precursors as well as microstructural evolution in FINEMET type alloy in its crystalline states.
- Temperature and field dependence magnetization will be performed using VSM.

1.4 Application of Nanocrystalline Ribbons

The more electric aircraft integrated power unit (MEA-IPU) is a specific example of a component in which bulk magnets, both had and soft are important. Such materials are critical to power generation, in power inversion (transformer), in magnetic bearing and magneto actuators. In the MEA-IPU, soft Fe-Co alloy laminate stakes are incorporated in the rotor and hard magnets in the IPU bearings. Operation of the IPU at the high temperatures associated with air cooling requires materials with excellent high temperature magnetic and mechanical properties. Realization of these exciting potentials will require:

(i) Development of high permeability, large saturation and remnant induction, low loss and hysteresis and eddy current for soft magnets of operating at high temperature.

(ii) Development of high energy product permanent magnets capable at operating at high temperatures.

(iii) Improved mechanical properties and corrosion resistance at higher operating temperatures.

(iv) Development of new magnetic device geometrics which exploit the materials.

Nanocrystalline materials have no microstructural discontinuities such as dislocations, grain boundaries or precipitates. This significantly reduces the possible spinning sites for domain walls, reducing the coactivity.

Nanocrystallization of amorphous precursors will also require compaction to produce shapes and to improve mechanical properties, as ribbons are quite brittle after nanocrystallization. The soft magnetic properties required for rotor applications in the more electric aircraft are in some senseless restrictive than those for the applications of FINEMET. Permeabilities of 10^2 – 10^3 are sufficient for this application. The frequency requirements, based on 10,000 rpm rotor speeds and 6 flux changes per cycle, require these permeabilities to only 1 KHz. The attractive technical characteristic of nanocrystalline alloys has no microstructural discontinuities such as dislocations, grain boundaries as or precipitates. This significantly reduces the possible pinning sites for domain walls, reducing the coercivity. The absence of microstructural discontinuities resulted in improved corrosion resistance. The highly elastic behavior of these alloys makes them less prone to degradation during handling.

1.5 Review of Researches on FINEMET

The pioneer alloy composition $Fe_{73.5}Cu_1Nb_3Si_{13.5}B_9$ known as FINEMET, has been thoroughly studied due to its novel magnetic properties. The study of Yoshizawa *et. al.*[1.13] on the role of nucleating Cu on the crystallization behavior of the composition FINEMET revealed that the average grain size is relatively large at crystallization temperature due to lower crystallization rate with no addition of Cu and annealing of this Cu free alloy leads to simultaneous or sequential formation of several crystalline phase.

Noh *et. al.***[**1.14] studied the effect of Cu on the crystallization behavior in $Fe_{74.5-x}Cu_1Nb_3Si_{13.5}B_9$ for x = 0 and x = 1.The crystallization behavior of this x = 0 is quite different and leads to a severe degradation of the soft magnetic properties compare to the original amorphous state. They also found that the average grain size just after the onset of crystallization is relatively large up to about 60nm with broad scattered and show a distinct variation with the annealing temperature. This indicates the significantly lower nucleation rate than in the Cu-doped alloy whose finer grain size is almost constant in wide range of annealing temperature [1.15]. Amorphous materials based on Fe-Si-B show good magnetic properties when they are heat rerated below their crystallization temperature. While the Fe-Cu-Nb-Si-B alloys exhibit extraordinary high permeability, two orders of magnitude higher than their conventional Fe-Si-B alloys due to heat treatment just above the crystallization temperature for a specific time. The great scope of technical application of this material $Fe_{73.5}Cu_1Nb_3Si_{13.5}B_9$ arises from this freedom of tailoring the magnetic properties [1.16 -1.17].

Müller *et. al* [1.18] showed that like Nb, the atomic volume of the refractory element grows V or VI elements (Cr,V, Mo, W or Ta) are larger than that of Fe that reduces diffusion co-efficient and thus stabilizes the amorphous matrix and slows down the for grain size refinement increases in the order of their atomic volume i.e. Cr < V< Mo ≈ W < Nb ≈ Ta. Thus, finest grain structures and superior magnetic properties require a certain amount of elements Nb and Ta.

Ayer's *et al.* [1.19] reported that the presence of Nb promotes the formation of Cu-rich clusters on a much finer scale than in an Nb free alloy composition. Small grain size is required for good soft magnetic properties, but at the same time needs to maintain the absence of boron compounds. Herzer [1.20] reported that the separation

between the primary crystallization of bcc Fe and the precipitation of Fe-B compounds decreases with increasing boron content. So, it is necessary to keep the boron concentration at a law or moderate level in order to obtain an optimum nanoscales structure. Kubaschewski [1.21] showed that in thermodynamically equilibrium, boron is practically insoluble in bcc Fe (<< 0.01 at. %); the solubilities of Cu and Nb are low: < 0.2 at. % Cu, < 0.1 at. % Nb.

This indicates the signifying lower nucleation rate than in the Cu-doped alloy whose finer grain size is almost constant in a wider range of annealing temperature [1.22] containing efforts. To improve the soft magnetic properties of FINEMET alloy have been made of modifying the alloy compositions. Ohnuma *et. al* [1.23] reported that the substitution of Fe by Co decreases the saturation magnetization in FINEMET type amorphous alloys. The magneto crystalline anisotropy of the small randomly oriented grains is averaged out of exchange integration. The research on Co substituted Fe-Nb-Ta-Mo-B amorphous alloys [1.24] showed that Co substitution increased saturation magnetization and Curie temperature (T_c) of the amorphous phase and decreased coercivity. As reported by Hakim *et. al.* [1.25], magnetic initial permeability of nanocrystalline amorphous ribbon strongly depends on annealing temperature and exhibits superparamagnetic behavior at $T > T_c$.

Franco *et al.* [1.26] also studied the super paramagnetic relaxation in FINEMET type of alloy Fe-Cu-Nb-Si-B without adding any extra refractory element and they have demonstrated that, this behavior is a general characteristics of this nanocrystalline alloys provided the volume fraction of crystallites are very low. If the size of the nanocrystals is small enough and the inter-granular amorphous matrix is sufficiently thick to minimize the magnetic interactions between them, of the nanocrystalline particles is expected.

Slawska-Waniewska *et. al.* [1.27] have observed temperature dependent magnetic response in partially and fully nanocrystallized FINEMET materials. They concluded that the sufficiently small nanocrystals with enough intergranular material between them to diminish or destroy coupling between grains that superparamagnetic response would be observed. This would not be the case for properly annealed samples with sufficient volume fraction of the nanocrystalline ferromagnetic. Characteristic of superparamagnetic response, first proposed by Bean [1.28] include: (i) a Lagevin function scaling of magnetization, (ii) disappearance of the coercivity

above a blocking temperature and (iii) time dependent magnetization, due to thermally activated switching of the magnetization.

The desire for large magnetic induction typically limits choices to alloys of Fe and Co (the elemental transition metal magnets with the largest atomic dipole moments). Curie temperature are also for elemental Fe (770^0C) and Co (1100^0C), suggesting the use of Fe or Co (or Fe-Co) alloys especially in high temperature applications. The development of advanced and newer magnetic materials with enhanced properties is closely related to the fundamental understanding and exploitation of influence of microstructures on the extrinsic magnetic properties. It is expected that the crystallization kinetics and the chemical partitioning occurring during crystallization will be described essentially. In particular, the role of the amorphous phase in exchange coupling magnetic nanoparticles at elevated annealing temperature and their magnetic properties. The effect of addition of the Co in FINEMET and thermal stability of the alloy draws much interest for the present research from the view point of application.

1.6 Organization of the Thesis

The thesis has been divided into five chapters.

Chapter I: Introduction followed by the aim and objectives of the present work, reason for choosing on FINEMET and organization of the thesis.

Chapter II: Theoretical background of the stability of amorphous alloys, theories of nanocrystalline substance and magnetization are discussed.

Chapter III: The preparation procedures of the nanocrystalline samples, experimental details including Differential Thermal Analysis (DTA), X-ray Diffraction (XRD) analysis, and Vibrating Sample Magnetometer (VSM) are described.

Chapter-IV: Details results regarding DTA, activation energy, corresponding crystallization temperature, XRD method after heat treatment of the sample at different temperatures, Lattice parameter, Silicon content, Grain size determination, field dependence of specific magnetization and annealing effects on saturation specific magnetization are discussed.

Chapter V: Conclusion and further suggestion of this work.

Finally a complete list of reference has been given towards the end of the chapters.

THEORETICAL BACKGROUND

2.1 History of Amorphous and Nanocrystalline Materials

Now a day tremendous advancement of science and technology for the last two decades the idea that should be able to economically arrange atoms in most of the ways permitted by physical law has gained fairly general acceptance. The recent advances in materials synthesis, characterization techniques and methods of advance measurement facilities on the nanometer scale have greatly assisted the expansion of nanotechnology. Amorphous soft magnetic alloys are now well accepted and mature materials. At first the great interest in amorphous metals stems from reports by Duwez et al. [2.1] on the preparation and properties of metallic alloys. The study of metallic glasses dates back to the pioneering work of Pol Duwez at Caltech in the 1950s. Duwez employed atomization prior to splat quenching [2.2 - 2.4]. Ferromagnetic amorphous alloy were first reported by Mader and Nowik [2.5]. Soon after, Tsuei and Duwez [2.6] reported splat quenched amorphous ferromagnetic with interesting soft magnetic properties.

Generally the optimum mechanical and magnetic properties of nanocrystalline soft magnetic materials are obtained for partially crystallized materials. This means that those materials are formed in two phases [2.7]. In general nanocrystalline alloys can be described as $TL_{1-x}(TE, M, NM)_x$ where

- TL denotes a late ferromagnetic transition metal element (TL= Co, Ni or Fe)
- TE denotes an early transition metal element (TE = Zr, Nb, Hf, Ta etc.)
- M is metalloid (M = B, P, Si, etc.) and
- NM is a noble metal (NM = Cu, Ag, Au etc.)

This composition usually has $x < 0.02$ i.e. with as much late ferromagnetic transition metal (TL of Fe, Co or Ni) as possible. The remaining early transition metals (TE = Zr, Nb, Hf, Ta, etc.) and metalloids (B, P, Si, etc.) are added to promote glass formation in the precursor. The noble metal elements (NM = Cu, Ag, Au, etc.) serve as nucleating agents for the ferromagnetic nanocrystalline phase. The compositions are limited by which glass formation can occur prior to the nanocrystallization route. These alloys may be single phase (Type-I) but are generally two phase materials with a nanocrystalline ferromagnetic phase and a residual

amorphous phase at the grain boundaries (Type-II).The type-II nanocrystalline alloys might have general properties:

- Relatively high resistivity (50 - 80μΩ-cm)
- Low magnetocrystalline anisotropy and
- Increase mechanical strength

With properties such as these, nanocrystalline alloys have great potential as soft magnetic properties. In the ongoing research we are any interested about the type-II. One of the important features of this magnetic system is that one can play with different compositions, annealing temperatures and time to control the grain size and their distribution upon, which the magnetic properties of these new materials strongly depend. In choosing the composition, one has to consider the magnetic component like Fe, Co of Ni, the crystallization initiating component e.g. Cu and the component Nb for stabilizing the nanocrystal by inhibiting the grain growth and glass forming materials like Si, B, etc.

Nanocrystalline soft magnetic alloys have received considerable attention due to their excellent soft magnetic properties [2.8]. Small addition of Cu and Nb into Fe-Si-B amorphous materials charges considerable their crystallization process, which is executed under appropriately controlled conditions and the specific purpose of these addition are

- The element is used for helping the formation of nuclei and ultra-fine grain and
- The element is used to impede the growth of the crystallites.

In this material, the nanocrystalline state is composed of a fine structure of α-Fe(Si) and is usually around 10nm. For such as average grain size the exchange interaction dominates the magnetic behavior of randomly oriented crystallites guided by random anisotropy [2.9].

2.1.1 Overview of Nanocrystalline Materials

Nanocrystalline materials represent one of the most active research areas in recent times for the atomic tailoring of materials with specific properties and property combinations. However, it is still in its infancy since its emergence as potential material has just began at this stage of development. There have been glimpses of exciting new properties like super plasticity, giant magneto resistance (GMR), transparency in opaque ceramics, enhanced homogeneity, unusual soft ferromagnetic

and giant magnetocaloric effects, processed by these material where reduced to nanometer dimension. In addition to the understanding of the usual properties possessed by nanophase materials, there are three other associated areas, which need serious attention:

i. Identification and development of suitable preparation methods, especially those which are capable of providing large industrial quantities of nanometer scale materials.
ii. Development of processing methods for manufacturing these materials into useful size and shapes without losing their desirable nanometer size feature and
iii. Identification of proper characterization methods, where the nanometer size range of these materials falls just below or at the resolution limit of the conventional tools.

2.2 Alloy Design Issues

Alloy designs issues are in many ways influenced by the processing routes used achieve desired microstructures. Alloy design issues include issues of chemistry and processing designed to:

(i) Optimize one of a number of important intrinsic and or extrinsic magnetic properties and
(ii) Optimize structural or microstructural features which promote important magnetic properties.

The first of these issues concerns the choice of chemistry so as to impact the intrinsic magnetization of the material. The second issue pertinent to alloy additions designed at aiding formation of an amorphous phase.

Since microstructure of alloy in influence extrinsic magnetic properties, the important microstructure features should be recognized including grain size, shape and orientation, defect concentration, compositional in homogeneities, magnetic domain and domain wall. The development of soft magnetic materials for application requires attention to a variety of intrinsic magnetic properties as well as development extrinsic magnetic properties though an appropriate optimization of the microstructure.

Alloy design issues are influenced by processing routes used to achieve desired microstructures. In figure 2.1 illustrates a flowchart for the considerations in designing and developing nanocrystalline soft magnetic material from an amorphous

precursor route as an example of the design process. Here we consider first, the effects of alloy composition on intrinsic magnetic properties. This is followed by consideration of alloying additions necessary to produce an appropriate amorphous precursor. Typical experimental steps used to identify the structure and properties of the resulting materials are also illustrated.

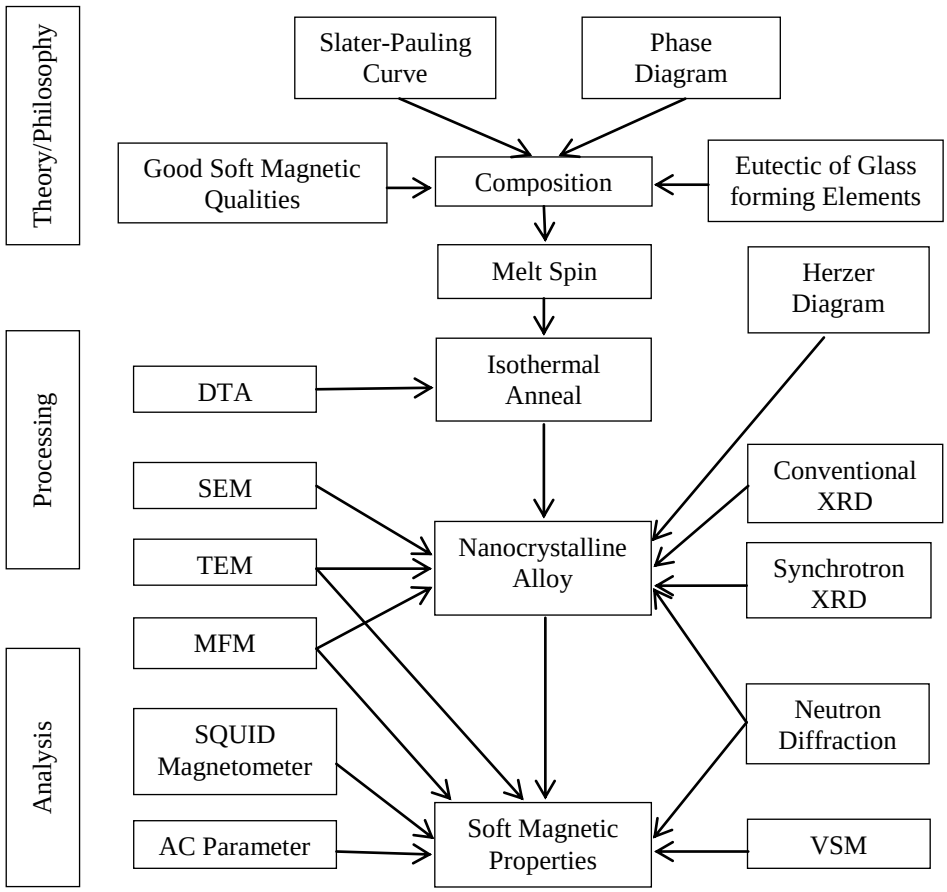

Fig. 2.1 Flowchart for the consideration in designing and developing nanocrystalline soft magnetic material from an amorphous precursor route

2.2.1 Stages of Evolution of Microstructure

It has been established that controlled crystallization of the amorphous alloys in the form of their ribbons prepared by rapid solidification technique using melt-spinning machine appeared to be the most suitable method available until now to synthesize nanocrystalline alloys with attractive soft magnetic properties. The basic principle for the crystallization method from amorphous solids is to control the crystallization kinetics by optimizing the heat treatment condition such as annealing

temperature and time, heating rate, etc. The nanocrystalline microstructure and the accompanying soft magnetic properties are rather insensitive to the precise annealing condition within a wide range of annealing temperature $T_a \approx 525$ - 580^0C. They develop in a relatively short period of time (about 10-15 minutes) and do not much latter even after prolonged heat treatment of several hours [2.10]. A typical heat treatment like T_a at 540^0C in most cases yields a nanocrystalline microstructure to the

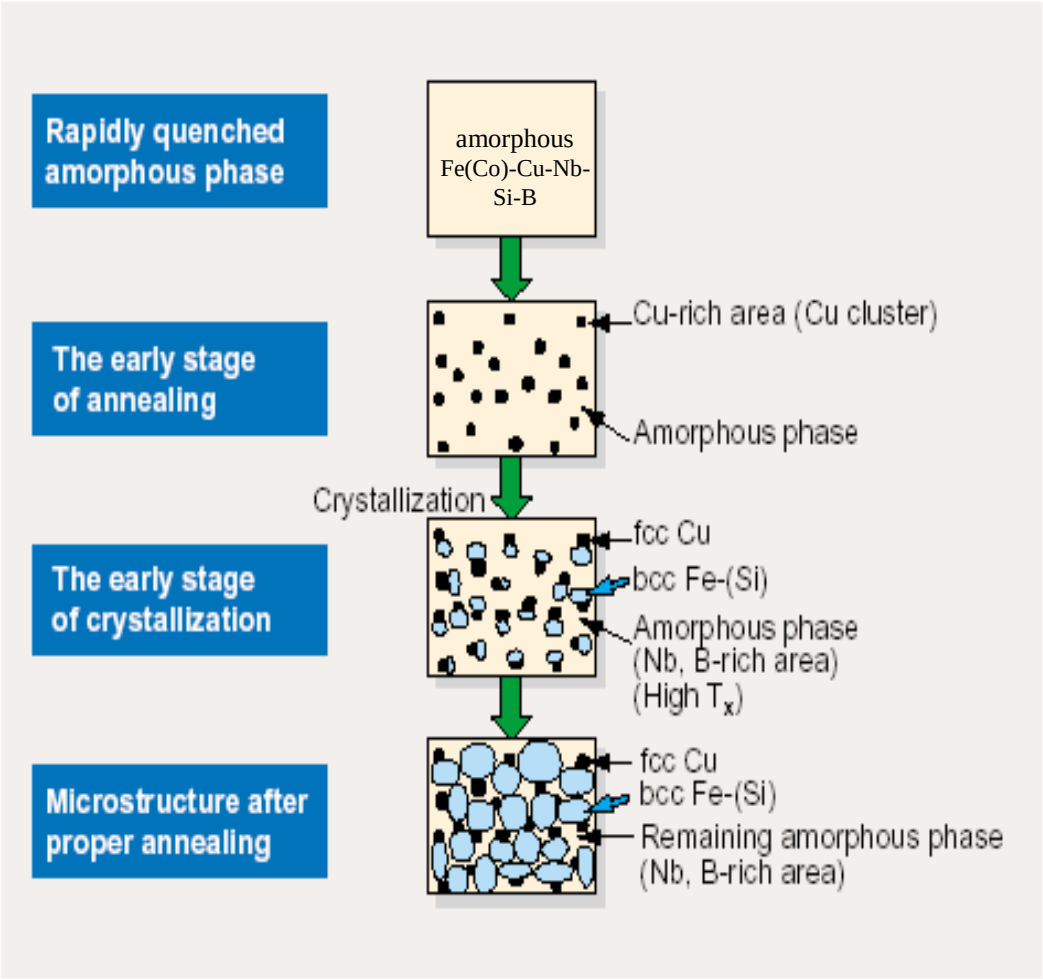

Figure 2.2: Schematic illustration of the formation of nanocrystalline structure in Fe(Co)-Cu-Nb-Si-B alloys.

Only annealing at more elevated temperature above about 600^0C leads to the precipitations of small fractions of boride compounds like Fe_2B or Fe_3B with typical dimensions of 50 nm to 100nm, while the ultrafine grain structure of bcc Fe-Si still persists. Further increase of the annealing temperature above 700^0C finally yields grain coarsening. Both the formation of Fe borides and grain coarsening deteriorates the soft magnetic properties significantly. The evolution of microstructure during

annealing is depicted schematically in figure 2.2 and summarized as follows according to Hono *et al*. [2.11-2.12].

The formation of the particular nanocrystalline structure is essentially related to the combined addition of Cu and Nb (or other group IV or VI elements) and their low solubility in Fe-Si (< 0.2 at % Cu, < 0.1 at % Nb). Cu enhances the nucleation of bcc grains while Nb impedes grain coarsening and at the same time, inhibits the formation of boride phase. The microstructure evolution is schematically illustrated in figure 2.2 can be summarized as follows.

Annealing at temperatures in general between about 500^{o}C to 600^{o}C leads to primary crystallization of the bcc Fe. At the initial stage of annealing, before the onset of crystallization, the phase separation tendency between Cu and Fe leads to the formation of Cu-rich clusters, with 5 nm size and probably still amorphous [2.13-2.14]. The presence of Nb seems to promote the formation of these Cu-rich clusters on a much finer scale than in an Nb free alloy composition [2.15]. This happens when the annealing treatment is carried out at around 550^{o}C when Cu clusters are formed with a few nanometer diameters. Because the investigators [2.16] observed that Cu clusters and bcc phase simultaneously at the early stage of the nanocrystallization.

This cluster formation causes a concentration fluctuation of Fe, since Cu substitutes for Fe. Thus, the regions in between Cu-rich clusters provide a significantly increased density of nucleation sites for the crystallization of Fe. The consequence is an extremely fine nucleation of Fe-Si crystallites at high rate which subsequently grow in a diffusion controlled process [2.17] as the annealing proceeds further annealing at higher temperature at the initial stage of crystallization α-Fe(Si) phase forms. At this stage Nb and B are excluded from α-Fe(Si) and are enriched in the remaining amorphous phase, because they are insoluble in the α-Fe(Si) phase.

Thus the regions in between the Cu rich clusters provide a significantly increased density of nucleation sites for the crystallization of bcc Fe. The consequence is an extremely fine nucleation of bcc Fe-Si crystallites at a high rate, which subsequently grow in a diffusion-controlled process as the annealing proceeds further as annealing goes on the grain size of the α-Fe(Si) increases. At the same time the Si content of this phase keeps increasing since Si tends to be partitioned to the bcc α-Fe(Si) phase. Since the Nb and B enrichment in the amorphous phase stabilizes the remaining state, the grain growth of the bcc phase eventually stops. The presence of

Nb at the same time inhibits the formation of Fe-B compounds. The Cu concentration of the clusters also increases as the crystallization proceeds.

At the optimum stage, three distinct phases are present based on the chemical composition. As the bcc Fe-Si phase forms, Nb and B are excluded from the crystallite because of their low solubility in bcc Fe and are enriched in the residual amorphous matrix. At a time all the Si tends effectively to be partitioned into the bcc Fe-Si phase [2.16, 2.18]. The particular enrichment with B and Nb increasingly stabilizes the residual amorphous matrix, thus, hinders coarsening of the bcc grains. The presence of Nb at the time inhibits the formation of Fe Boride compounds. The transformation finally ceases in a metastable two-phase microstructure of bcc Fe-Si embedded in an amorphous Fe-Nb-B matrix.

2.2.2 Advantages of Soft Nanocrystalline Alloys

The unique properties of FINEMET alloys include low losses, high permeability and near zero magnetostriction achieved by permalloys and Co-based amorphous alloys, but much higher saturation magnetization up to 1.3 Tesla, than these materials usually have ever offered. Nanocrystalline amorphous ribbons are produced by the melt-spinning technique to produce an amorphous metal and then heat treating this alloy at temperature higher than its crystallization temperature. The choice of soft magnetic materials for applications has been guided by recent developments in the field of soft magnetic materials. Amorphous and nanocrystalline magnetic materials, in terms of combined induction and permeability are now competitive with Fe-Si bulk alloys and the Fe-Co alloys. In figure 2.3 [2.19], figures of merit for Fe-based amorphous alloys, Co-based amorphous alloys and nanocrystalline alloys are summarized. Co-based amorphous alloys, Fe-based amorphous alloys and nanocrystalline alloys have evolved over the past decades with soft magnetic properties which now exceed those of the bulk alloys based on Fe, Co and Fe-Co.

This FINEMET material is still in its immaturity since its emergence although much research work has been carried out for the potential utility of this unique material.

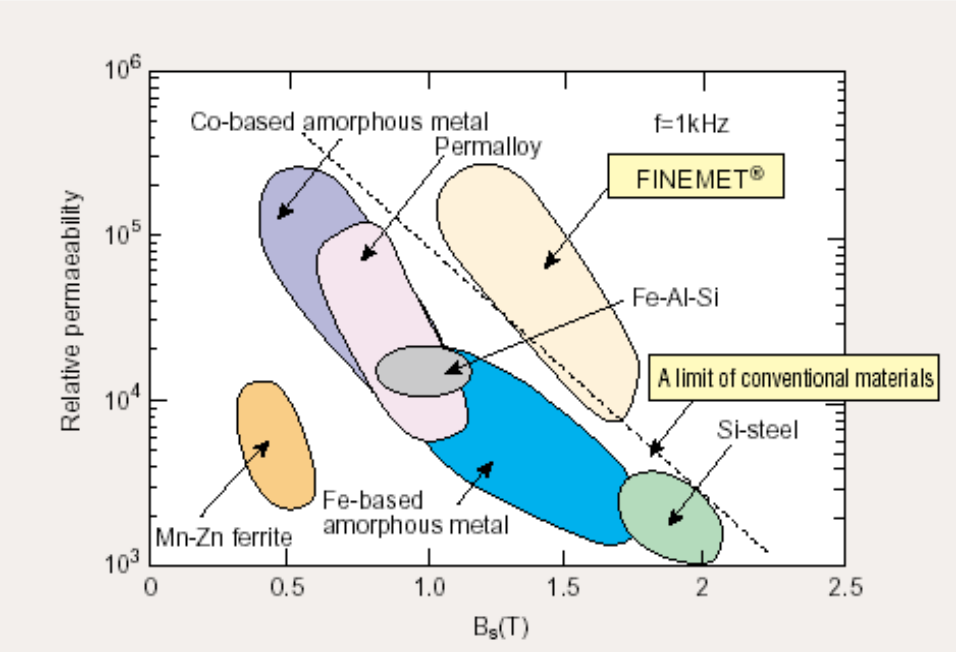

Figure 2.3: FINEMET is superior compared to conventional materials

At the stage of development, this material has the following advantages:

- High saturation magnetic flux density more than 1 Tesla or 10 kOe.
- High permeability over $\mu_i \approx 10{,}000$ at 100 kHz.
- Excellent temperature characteristics.
- Less affected by mechanical stress.
- Audio noise emission is very low, lower magnetostriction significantly reduces audible noise emission when the voltage and current is applied to the core at audible frequency range.
- Flexible to control the magnetic properties, "B-H curve shape" during the annealing, and three types of B-H curve squareness, high, middle and ion resonance ratio, corresponding to various application.

2.2.3 Viscosity Condition for the Formation of Metallic Glass

In the terms of viscosity and diffusion co-efficient are as follows:

(i) Metallic atomic bonding of the metals; the viscosity is lower than the diffusion co-efficient and mobility is high.

(ii) Viscosity becomes high and the diffusion co-efficient decreases in the amorphous state. An atomic bond tends to be covalent as in the case of Silicate (SiO_2).

2.3 Conditions for the Formation of Nanocrystalline Alloys

The essential conditions for preparing of nanocrystalline materials are.

(i) The magnetic properties are highly dependent on the grain size; if the grain size is larger; the magnetic anisotropy would be very high, which is turn will have diverse effect on the soft magnetic properties specially the permeability.

(ii) For the crystallization process there should be nucleation centers initiated to be distributed throughout the bulk of amorphous matrix.

(iii) For stabilizing the crystallites there must be a nucleation.

(iv) Nanocrystalline materials obtain from crystallization must be controlled that crystallites do not grow too big. The grain growth should be controlled so that the grain diameter is within 15-20nm.

(v) The size of the grain can be limited to nanometer scale by doping group-II metals are

→ Cu (Au ……)

→ Nb, W, Mo, Cr, Ta etc.

(vi) The stability must be lower and the crystallization must be higher.

There is additional understanding of the unusual properties possessed by nanophase materials; there are three other associated areas, which need serious attention:

- Identification and development of suitable preparation methods, especially which are capable of providing large industrial quantities of nanometer scale.
- For manufacturing of these materials processing methods should be develop useful size and shape without losing their nanometer size feature.
- Identification of proper crystallization methods, where the nanometer size range of these materials falls just below or at the resolution limit of the conventional tools.

2.4 Stability of the Amorphous and Nanocrystalline Materials

Amorphous materials are always metastable state which leads to transform into more stable crystalline phase. There are three kinds of stability of significance for magnetic ribbons;

(i) Their resistance to the initiation of crystallization.

(ii) Structural relaxation effect, and

(iii) The relaxation or reorientation of directional order.

The glass forming materials the melting point of the alloys and thereby the separation between the glass forming temperature and the crystallization temperature is reduced. Controlled crystallization seems from the amorphous state to be the only method presently available to synthesize nanocrystalline alloys with attractive soft magnetic properties. The formation and the resultant stability of amorphous alloys are important topic both for theoretical understanding and technically. The theoretical analyses of the factors controlling the case of formation and the stability of the resultant amorphous alloys have been extensively reviewed [2.20 - 2.21]. From the thermodynamic view point [2.22 - 2.23], the ability of an alloy to be quenched into the glassy state is generally measured by the magnitude of the quantity.

$$\Delta T_g = T_m - T_g \qquad (2.1)$$

Where T_m and T_g are the melting and glass temperature respectively. The stability of the glass after formation in a similar manner is generally measured by the magnitude of the quantity.

$$\Delta T_x = T_x - T_g \qquad (2.2)$$

Where T_x is the temperature for the onset of crystallization. As the temperature decrease from T_m, the rate of crystallization will increase rapidly but then fall rapidly as the temperature decrease below T_g. The amorphous alloy composition most favorable for glass formation is near eutectic i.e. the composition in which the transformation from the liquid state to solid state takes place instantaneously without passing through liquid plus solid mixed phase. The deeper the eutectic the better is the glass formation ability [2.24]. There have been three approaches for relating the stability of the glass, i.e. its microstructure:

(i) Barnaul's model of randomly packed hard sphere's [2.25]. The atoms of the metal are assumed to from a random network of close packed hard spheres and the smaller metalloid atoms fill the holes inherent in such structure.

(ii) The effect of atomic sizes and inter atomic interactions [2.26], i.e. chemical bonding suggested that it is chemical bonds which are dominating factors in glass formation and stability.

(iii) The third approach [2.27] is based on the role of the electron gas and showed that under certain circumstances a nearly free electron gas will produce a barrier against crystallization.

The transition to the glassy state and the crystalline state is accompanied by an exothermic heat effect giving rise to a sharp peak in temperature dependence of the heat flow. Therefore, DTA is a widely used technique to study thermally induced transformations in amorphous alloys and to determine T_g and T_x. The magnitude of T_g and T_x are very different for amorphous materials and depend strongly on composition. The activation energy ranges typically between 2 and 6 eV [2.28].

2.4.1 Characteristics of the Glass Transition Temperature

When the time scale of molecular rearrangements occurs glass transition temperature (T_g) are too long for equilibrium to be maintained:

(i) T_g means the time scale of the experiment maters.

(ii) A high frequency/short time scale experiment allows less long for equilibrium to be established – even for an identical cooling rate.

(iii) NMR (high frequency technique 10^{15} Hz.) always measures a higher T_g than DTA (1 Hz.).

(iv) In the glass itself, entropy is similar to the crystal and original in vibrational modes, which are still present.

(v) Long range transitional motions are frozen out. The temperature T_g configuration relaxation (including translational motion) but vibrational relaxations are still in equilibrium.

(vi) T_g decreases as melt cooled more and more slowly.

(vii) When the timescale of the experiment and the configuration relaxation time coincide, begin to see departure from equilibrium.

(viii) The time scale for configuration relaxation will be related to rotational or translational diffusion coefficient.

(ix) Optional definition of T_g is when the viscosity of the super-cooled liquid exceeds 10^{13} NSm^{-2}. Where as in the liquid there is an Arrhenius type with a Boltzmann factor containing activation energy.

2.4.2 Differential Thermal Analysis and its Application

Differential thermal Analysis (DTA) is an important technique for the study of structural change both in solid and liquid materials under heat treatment. During this process, the temperature difference between a substance and reference material is measured as a function of temperature whilst the subject and the reference material are subjected to some controlled temperature program. The transition of an amorphous or glassy state to crystalline state is accompanied by an exothermic heat effect that gives rise to a sharp peak in temperature dependence of the heat flow. To study this thermally induced transformation in amorphous alloys, DTA is a widely used technique. DTA detects the release or absorption as they are heated or cooled. Such information is essential for understanding thermal properties of materials. Analysis of decomposition of glass materials, crystalline phase charges, chemical reactions and glass transition temperature are some of the properties with DTA.

Amorphous alloys are in a metastable state and tend to transition into stable crystalline phases. At temperature below the crystallization temperature, structural relaxation effect takes place which are caused by atomic rearrangements. DTA is an important technique for the study of structural change both in solid and liquid materials under heat treatment. The principle of DTA is widely used to understand the crystallization nature of the amorphous. Differential thermal analysis is a direct and effective technique for analyzing the kinetics of amorphous materials and stability with respect to crystallization process.

The crystallization is associated with the nucleation and growth process. Since the formation of an amorphous alloy depends on the absence of LRO, change of composition is expected to affect T_g and T_x. This is because long range ordering of atoms depends on the free energy difference between the crystalline state and the amorphous state. The magnitude of T_g and T_x are very different for amorphous materials and depend strongly on composition. Using DTA technique it is possible to determine T_g and T_x. Nanocrystalline amorphous ribbons prepared by rapid quenching method have been subjected to DTA using a Shimadzu Thermal Analyzer. Different peaks, crystallization temperatures, crystallization activation energies are obtained from this analysis.

2.4.3 Evaluation of Activation Energy Based on DTA Technique

Based on the work of Murray and White [2.29 – 2.31], the kinetics of materials can be understood by interpretation of DTA patterns of the materials. The dependence of T_x on the heating rate $\beta = \frac{dT}{dt}$ can be used to determine the activation energy of crystallization [2.32]. Considering the fraction x of amorphous material transformed into the crystalline state in time t and at temperature T obtains for the first-order rate process [2.33- 2.34]

$$\left(\frac{\delta x}{\delta t}\right)_T = K(1-x) \tag{2.3}$$

For thermally activated process, the rate constant K obeys an Arrhenius type of equations

$$K = K_o e^{-\left(\frac{\Delta E}{RT}\right)} \tag{2.4}$$

where K_o is a constant and ΔE is the activation energy. Combining equation (2.3) and (2.4) and using $dx = \left(\frac{\delta x}{\delta t}\right)_T dt + \left(\frac{\delta x}{\delta t}\right)_t dT$ with $\left(\frac{\delta x}{\delta t}\right) dt \cong 0$, are obtains

$$\frac{dx}{dt} = K_o(1-x)e^{-\left(\frac{\Delta E}{RT}\right)} \tag{2.5}$$

$$\frac{d^2x}{dt^2} = \frac{d}{dt}\left[K_o(1-x)e^{-\left(\frac{\Delta E}{RT}\right)}\right]$$

$$= -K_o \frac{dx}{dt} e^{-\left(\frac{\Delta E}{RT}\right)} + K_o(1-x)\frac{d}{dT}\left\{e^{-\left(\frac{\Delta E}{RT}\right)}\right\}\frac{dT}{dt}$$

$$= -K_o \frac{dx}{dt} e^{-\left(\frac{\Delta E}{RT}\right)} + \frac{dx}{dt}\left(\frac{\Delta E}{RT^2}\right)\beta$$

At the peak of the exothermic heat, the change of the reaction rate $\frac{d^2x}{dt^2} = 0$, yielding with $T = T_x$ but $\frac{dx}{dt} \neq 0$

$$K_o e^{-\left(\frac{\Delta E}{RT_x}\right)} = \left(\frac{\Delta E}{RT_x{}^2}\right)\beta \tag{2.6}$$

From equation (3.6) it is easily seen that

$$\frac{d\left(ln\frac{\beta}{T_x^2}\right)}{d\left(\frac{1}{T_x}\right)} = -\frac{\Delta E}{R} \tag{2.7}$$

Here $\beta = \frac{dT}{dt}$ the heating rate. $\Delta T_x$for the stability of amorphous alloys as given by equation (2.5) and is obtained from DTA. Similar correlation between thermal stability as measured by ΔT_x and ΔE appears too small.

From the measured data of the heating rate (β) and the respective crystallization temperature (ΔT_x), the activation energy can be deduced from the slope of a plot $ln\frac{\beta}{T_x^2}$ versus $\frac{1}{T_x}$from equation (2.7) can be derived from transformation theory, where ΔE is the activation energy for versus flow and other terms have been omitted because they an insignificant temperature dependence in this region of temperature. The values of ΔE also appear to correlate well with the number of atomic species in the alloy; the more complex the alloy the grater is ΔE.

2.5 Determination of Nanometric Grain Size by X-Ray Diffraction

Nanocrystalline alloys are basically crystalline and because of their crystalline and they exhibit Bragg scattering peaks in X-ray diffraction experiments. However, due to their small size, significant fine particle broadening is observed in the Bragg peaks. The X-ray scattering from a crystalline solid is given by Bragg's law:

$$2d \sin\theta = n\lambda \qquad (2.8)$$

This equates the path difference scattered from parallel crystalline planes spaced d = d_{hkl} apart to an integral number (n) of X-Ray wavelength λ. Here θ is the X-Ray angle of incidence (and of diffraction) measured with respect to the crystalline planes. Bragg scattering occurs at discrete values of 2θ satisfying the Bragg condition for an infinite crystal, i.e. Bragg peaks are δ-functions. The peaks are broadened over a range of angles for finite sized crystals as shown in figure 2.4.

The better understand of the phenomenon of fine particle broadening following argument of Cullity [2.35] is outlined below. We consider a finite crystal of thickness, D_g = md, where is an integer and d is the distance between crystalline planes, i.e., there are m planes in D_g. considering figure 3.4, if the broadened Bragg peak begins at an angle $2\theta_2$ and ends at $2\theta_1$, the breadth of the peak or full width at half maximum is given as:

$$\beta = \frac{1}{2}(2\theta_1\text{-}2\theta_2) = \theta_1\text{-}\theta_2 \qquad (2.9)$$

Now consider the path differences for each of the two angles $\theta_1$andθ_2, for X-rays travelling the full thickness of the crystal. The width β is usually measured in

radians; intensity is equal to half the maximum intensity. As a rough measure of β , we can take half the difference between the two extreme angles at which the intensity is zero, which amounts to assuming that the diffraction line triangular in shape.

We now write the path difference equations for those two angles related to the entire thickness of the crystal rather to the distance between adjacent planes.

$$2D_g \sin\theta_1 = (m+1)\lambda \tag{2.10}$$

$$2D_g \sin\theta_2 = (m-1)\lambda \tag{2.11}$$

By the subtraction;

$$D_g\,(\sin\theta_1 - \sin\theta_2) = \lambda \tag{2.12}$$

$$2D_g \cos\left(\frac{\theta_1+\theta_2}{2}\right)\sin\left(\frac{\theta_1-\theta_2}{2}\right) = \lambda \tag{2.13}$$

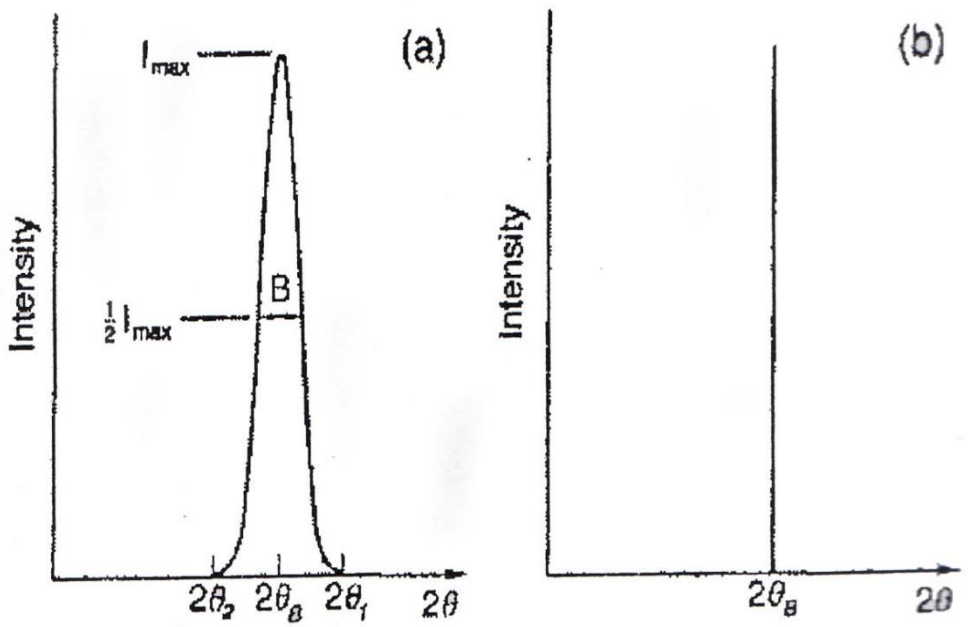

Figure 2.4: Effect of fine particle broadening in XRD (a) fine particle and (b) perfect crystal

But $\theta_1$and θ_2 are both very nearly equal to θ, so that $\theta_1 + \theta_2 \approx 2\theta$ and $\sin\left(\frac{\theta_1-\theta_2}{2}\right) \approx \left(\frac{\theta_1-\theta_2}{2}\right)$ thus the eq^n can be written as:

$$2D_g \cos\theta.\,(\tfrac{\theta_1-\theta_2}{2}) = \lambda \tag{2.14}$$

From the equation (2.9) and equation (2.14) we get:

$$\beta . D_g \cos\theta = \lambda \tag{2.15}$$

$$D_g = \frac{\lambda}{\beta cos\theta} \tag{2.16}$$

A more exact empirical treatment yields:

$$D_g = \frac{0.9\lambda}{\beta cos\theta} \tag{2.17}$$

This is known as the Scherrer's formula. It is used to estimate the particle size of very small crystals from the measured width of their diffraction curves.

2.6 Magnetic Dipole Moments and Magnetization

The vast majority of soft magnetic materials have one or more of the ferromagnetic transition metal elements Fe, Co or Ni, or the rare earth metal as a majority component. The vast majority of soft magnetic materials have one or more of the ferromagnetic transition metal element. The magnetic dipole moments of the elemental and alloy magnets are almost completely understood through the Band Theory of Solids [2.36]. The band theory of solids considers the broadening of localized atomic states with discrete Eigen values into a continuum of states for more itinerant electrons over arrange of energies. The theory allows for calculation of energy dispersion (i.e. energy as a function of wave vector) and orbital angular momentum specific and spin-resolved densities of states. The calculation of spin-resolved energy band and densities of states allows for the dispersion of atom resolved magnetic dipole moments, therefore spontaneous magnetization of element and alloy magnetic solids. Among the success of the band theory descriptions of magnetic properties are:

(i) The prediction of non-integral of half integral atomic dipole moments and resulting ground state magnetization in the metals and alloys.
(ii) The prediction that band widths and exchange splitting (energy differences between spin up and spin down bands) are intimately dependent on magnetic coordination number and atomic volume.

The electronic potential is more accurately, but still not at the level of consideration of all individual electron-electron interactions. In densities of states are

more structures within free electron model and in more accurate description of the magnetic states in solids. The results of band theory, in describing alloying affects on magnetic dipole moment in solid.

The variation of the mean atomic magnetic dipole moment as a function of composition in the transition metal alloy system. Spin resolved densities of states $g_+(E)$ and $g_-(E)$ for Co and Fe atoms, in an equi-atomic Fe Co alloy, as a function of energy (where the Fermi energy, E_F is taken as the Zero of energy). The number of spin up, n_+ and spin down, n_- electrons in each band can be calculated again by integrating these densities of state:

$$n_+ = \int_0^{E_F^+} g_+(E)dE \tag{2.22}$$

and $$n_- = \int_0^{E_F^-} g_-(E)dE \tag{2.23}$$

Here the Fermi energies, E_F, are the same and the zero's of energy are different for the two spin bands and the atom resolved (i.e. Fe and Co) magnetic dipole moments can be calculated as:

$$\mu_m = (n_+ - n_-)\mu_B \tag{2.24}$$

Knowledge of atomic values or alloy density, then allows for the direct calculation of the alloy magnetization

2.6.1 Magnetization of the Nanocrystalline Ribbon

The saturation magnetization of a material at a temperature of 0 K is one of its basic properties. Measurements are usually expressed as average moment per magnetic atom in units of the Bohr magnetron, μ_b as specific saturation magnetization for the amorphous alloy, σ_s in units for Am^2/kg. The moments of most amorphous alloys are lower than those of the structural disorder on the moments is very small.

This points out the importance of chemical instead of structural disorder. The reduction is least in B-based and highest in p-based glass. The observed moments on TM-M glasses can approximately fitted to a formula [2.37].

$$\mu = \left(\frac{\mu_{TM} C_{TM} - C_B - 2C_{sc} - 3C_\rho}{C_{Tm}} \right) \tag{2.25}$$

Where μ_{TM} is the magnetic moment of TM-M atoms, taken as 2.6, 1.6 and 0.6 respectively in Bohr magneto for Fe, Co and Ni. C's are respective concentrations. This clearly demonstrates the change transfer from metalloid to d-band of transition metal and seems to suggest that 1, 2 or 3 electrons are transferred from each of B, Si (C, Ge) or P atom. The relative number of electrons donated can be listed as – $P_{13}C_7$ > -$S_{15}B_{10}$ > -$P_{16}B_6AI_3$ > -$P_{14}B_{13}$ > -B_{20} Based on the relative magnitudes of M_s.

EXPERIMENTAL DETAILS

3.1 Methods used for preparation of Nanocrystalline Alloy

The different experimental techniques developed to produce amorphous metallic glass can be classified into two groups:

(i) The atomic deposition methods.

(ii) The fast cooling of the melt.

As we know, controlled crystallization from the amorphous state is the only method which presently available to synthesize nanocrystalline alloys with superior soft magnetic properties. In this thesis work amorphous ribbons have been prepared by fast cooling of the melt.

3.1.1 The Fast Cooling of the Melt

Atomic arrangement, bonding and atomic size effects are related in the structural factors. The structural factors as discussed Turnbull [3.1] are the nucleation, crystal growth rate and diffusion rate compared to the cooling rate. The interest in this method stems from the wide variety of alloys that can be made as well as from the potential low cost of preparation. In the pioneering work Duwez, *et al* [3.2], number of devices has been reported for obtaining the necessary high quenching rates and producing continuous filaments. The methods using the principle of fast cooling of melt techniques are:

(i) The gun techniques

(ii) Single roller rapid quenching techniques

(iii) Double roller rapid quenching techniques

(iv) Centrifuge and rotary splat quencher techniques

(v) Torsion catapult techniques

(vi) Plasma-jet spray techniques

(vii) Filamentary casting techniques

(viii) Melt extraction techniques

(ix) Free-jet spinning techniques

(x) The melt spinning techniques

Although the different methods used in preparing amorphous metallic ribbons are mentioned here, only the single roller rapid quenching technique, which is widely used to prepare the amorphous ribbons.

3.2.1 Master Alloy Preparation

Amorphous ribbons with the nominal composition $(Fe_{0.9}Co_{0.1})_{73.5}Cu_1Nb_3Si_{13.5}B_9$ were prepared in an arc furnace on a water-cooled copper hearth under an atmosphere of pure Ar. Their purity and origin of the constituent elements were Fe (99.9%), Co (99.9%), Nb (99.9%), Cu (99.9%), Si (99.9%) and B (99.9%) as obtained from Johnson Mathey (Alfa Aesar Inc.). The required amounts of the constituent elements were taken from pure metal bars or flakes, weighed carefully with a sensitive electronic balance and placed on the copper hearth inside the arc furnace. Before melting, the furnace chamber was evacuated (10^{-4}torr), and flashed with Ar gas. The process was repeated several times to get rid of residual air and finally the furnace chamber were kept in an Ar atmosphere.

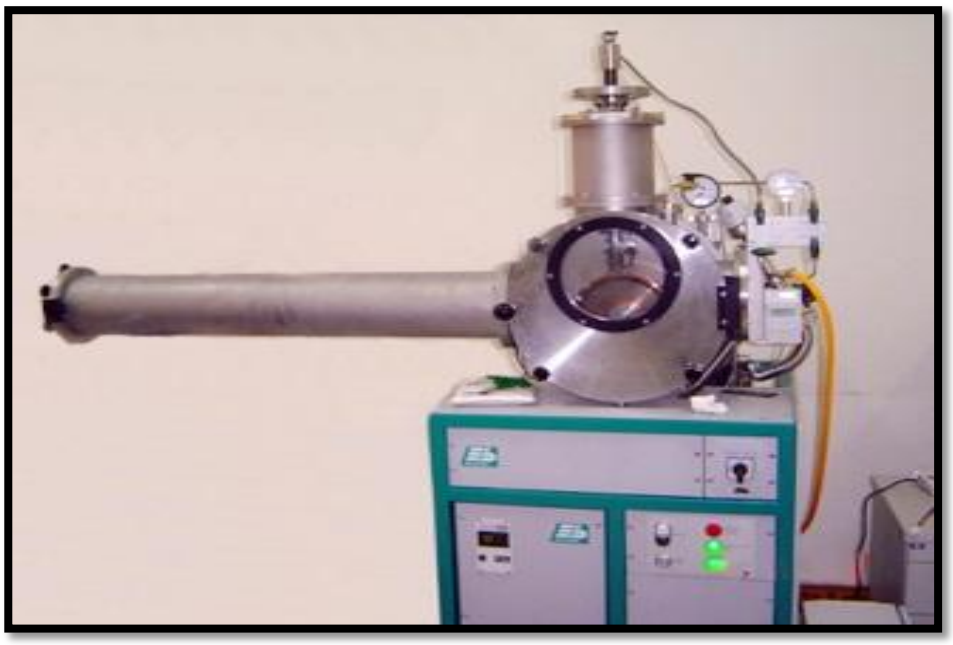

Figure 3.1 : Vacuum Arc Melting Machine

A substantial amount of pure Titanium getter, placed inside of the chamber on the side of the copper hearth was melted first in order to observe any oxygen present in the furnace chamber. The constituent elements were then melted in the shape of buttons. The arc melting facilities used to prepare the sample are installed at the Centre for Materials Science, National University of Hanoi, Vietnam. The arc furnace used in the preparation of master alloy is shown in Figure 3.1

3.2.2 Preparation of Ribbon by Melt Spinning Technique

Melt spinning is a widely used production method for rapidly solidifying materials as well as preparing amorphous metallic ribbon [3.3-3.4]. In order to prepare amorphous of $(Fe_{0.9}Co_{0.1})_{73.}Cu_1Nb3Si13_{.5}B_9$ alloys, the melt spinning facilities was used at the Centre for Materials Science, National University of Hanoi, Vietnam. After proper cleaning of the roller surface and adjusting its speed to the desired value, as measured by stroboscope the induction furnace is powered using high frequency generator. The arc melted master alloy was crashed into small pieces and put inside the quartz tube crucible for re-melting by induction furnace using a medium frequency generator with maximum power of 25kW at a nominal frequency of 10kHz. When the melting temperature is reached as observed through a protective spectacle, the injection pressure is applied by opening the pressure valve. To avoid the turbulence of the wind, arising from the high speed of the roller in disturbing the melt puddle, cotton pad and metallic shield are usually used just beneath the roller. To avoid oxidation of the ribbon during its formation an inert atmosphere can be created around the roller by a slow stream of Ar-gas.

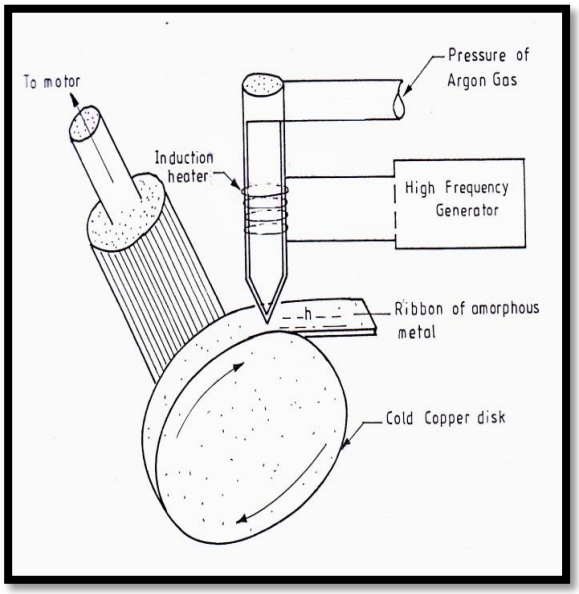

Figure 3.2: Schematic diagram Figure 3.3: Melt-Spinning Machine

Figure 3.2 shows schematic diagram and Figure 3.3 shows the pictorial view of the Melt-Spinning Machine. The Quartz crucible has in its bottom part, a rectangular nozzle tip of 8 mm length and 0.7 mm width. The position of the nozzle

tip can be adjusted with respect to cooper wheel surface, so that the molten alloy was perpendicularly ejected onto the wheel surface from a distance of about 0.3 mm. The small piece of the master alloy samples were inductively remelted inside the quartz tube crucible followed by ejecting the molten metal with an over pressure of 250 mbar of 99.9% pure Ar supplied from an external reservoir through a nozzle onto a rotating copper wheel with surface velocity of 30m/sec. The temperature was monitored by an external pyrometer from the upper surface of the molten alloy through a quartz window. The metal alloys were ejected at a temperature of about 150 to 250 K above the melting point of the alloy. The resulting ribbon samples had thickness of about 20-25μm and width ~6 mm. Processing parameters such as the thermal conductivity of the rotating quench wheel, wheel speed, ejection pressure, thermal history of the melt before ejection, distance between nozzle of quartz tube and rotating wheel, as well as processing atmosphere have influenced on the microstructure and properties of melt-spun ribbons.

The lower pressure of 250 mbar as mentioned above stabilizes the turbulence between melt pull and rotating copper wheel enhancing the heat transfer resulting in a more uniform quenching. As a result, a more uniform ribbon microstructure can be obtained at relatively low wheel speed. With increasing wheel speeds for a given ejection rate, the increasing extraction rate results in thinner ribbons. The speed of the roller, the volumetric flow rate, the orifice diameter, the substrate orifice distance, the injection angle etc. are adjusted by trial and error to get the best result in respect of the quality and geometry of the ribbons.

3.2.3 Important Factors to Control the Thickness of Ribbons

(i) Rotating speed

- Angular velocity ω = 2000rev/min
- Surface velocity V = 20 m/s to 30 m/s

(ii) Gap between nozzle and rotating copper drum (h) = 200 to 30 μm.

(iii) Oscillations of the rotating copper drum both static and dynamic has maximum displacement 1.5 to 5 μm

(iv) Pressure = 0.2 to 3.0 bar at argon atmosphere

(v) Temperature of molten metal's $T_m \approx 1500^0$C; the temperature did not exceed 1800^0 C otherwise quartz tube would be melted.

(vi) A steady flow of the molten metal's on the surface of the rotating drum needs to be ensured.

3.2.4 Confirmation of Amorphousity of Ribbons

The amorphousity of the ribbons has been cheeked by X-ray diffraction using Cu-K_α radiation using Philips (PW 3040) X 'Pert PRO XRD System located at Materials Science Division, Atomic Energy Centre, Dhaka (AEC).

From the X-ray diffraction pattern of the samples in Figure 3.4, there have no peaks observed within the scanning range. The ribbons showed broad diffraction maximum and no low angle scattering. These ribbons were also ductile and those cases for which low angle scattering appear and the broad diffraction peak are subdued there is some presence of micro crystalline phase. Although there are few small humps shown in the diffraction pattern around $2\theta = 45^o$; but it cannot be regarded due to the crystalline effects. So from all the pattern of X-ray diffraction is confirmed that the samples are in pure amorphous state.

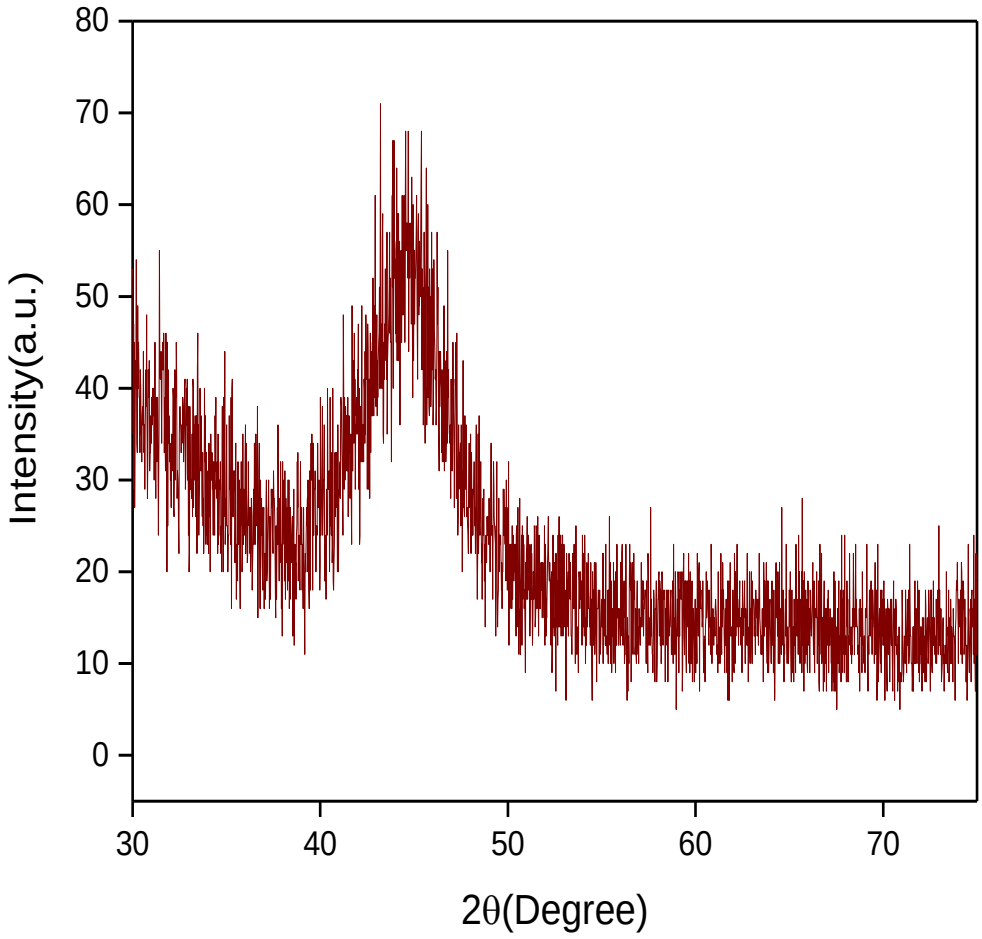

Figure 3.4: X-ray diffraction of as-cast nanocrystalline amorphous ribbons with Composition $(Fe_{0.9}Co_{0.1})_{73.5}Cu_1Nb_3Si_{13.5}B_9$.

3.3 Thermal Analysis Techniques

The differential Thermal Analysis (DTA) is an important technique for studying the structural change occurring both in solid and liquid materials under heat treatment. These changes may be due to dehydration, transition from one crystalline variety to another, destruction of crystalline lattice, oxidation, decomposition etc. The principle of DTA consists of measuring the heat changes associated with the physical or chemical changes that occur when a standard substance is gradually heated. This technique can also be used to identify magnetic ordering of nanocrystalline amorphous ribbons.

This technique has been used in determining the first crystallization temperature (T_{x_1}) and second crystallization temperature (T_{x_2}) of our nanocrystalline soft magnetic material. The first crystalline temperature is defined as the temperature at which the alloy passes from the solid to liquid state. For our study, it is sufficient to describe T_{x_1} as the temperature at which atomic mobility is great enough to allow diffusive rearrangement to occur in a matter of minutes. The crystallization temperature T_{x_2} is defined as the temperature at which crystallization occurs with long range ordering. DTA technique has been used in determining T_{x_1} and T_{x_2} of our nanocrystalline ribbon of composition $(Fe_{0.9}Co_{0.1})_{73.5}Cu_1Nb_3Si_{13.5}B_9$ based on Kissinger plots, crystallization activation energy of T_{x_1} and T_{x_2} phases have been evaluated.

3.3.1 The Principle of Differential Thermal Analysis

The DTA technique was first suggest by Le Chatelier [3.5] in 1887 and was applied to the study of clays and ceramics. DTA involves heating or cooling a test sample and inert reference under identical conditions, while recording any temperature difference between the sample and reference. Then this differential temperature is plotted against time, or against temperature. When a sample and reference substance are heated or cooled at a constant rate under identical environment, their temperature differences are measured as a function of time or temperature as shown by the curve in Figure 3.5 (a).

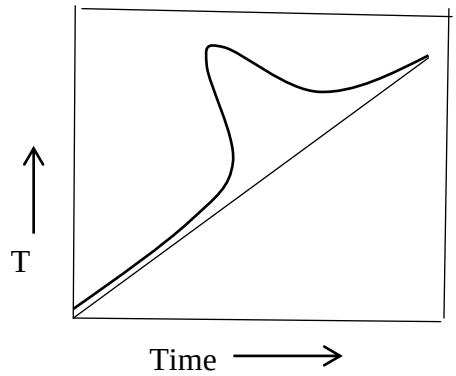

Figure 3.5(a): Heating curve of sample and reference substance

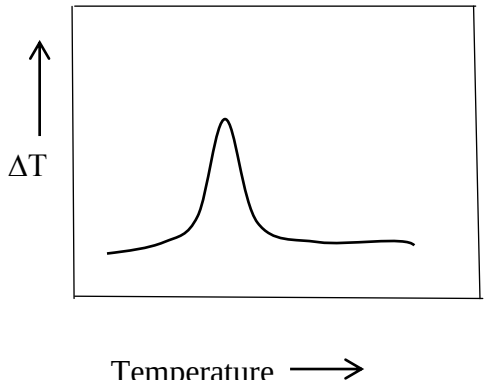

Figure 3.5(b): DTA Curve

The temperature of the reference substance, which is thermally inactive, rises uniformly when heated, while the temperature of the sample under study changes anomalously when there is physical or a chemical change of the active specimen at a particular temperature. When there is an exothermic reaction there is a peak in the temperature versus time curve, heat supplied from outside is consumed by the reaction. And when the reaction is over, the sample temperature gradually catch up the temperature of the inactive specimen. The temperature difference ΔT is defined, amplified and recorded by a peak as shown in Figure 3.5 (b).

For any endothermic reaction or change the active specimen absorbs heat which is reflected in the corresponding the trough in temperature versus time curve. Changes in the sample, which leads to the absorption or evolution of heat, can be detected relative to the inert reference. Differential temperatures can also arise between two inert samples when their response to the applied heat treatment is not identical. DTA can therefore be used to study thermal properties and phase changes which do not lead to a change in enthalpy.

Changes in the sample, either exothermic or endothermic, can be detected relative to the inert reference. Thus, a DTA curve provides data on the

transformations that have occurred, such as glass transitions, crystallization, melting and sublimation. The baseline of the DTA curve showed then exhibit discontinuities at the transition temperatures and the slope of the curve at any point will depend on the microstructural constitution at that temperature. The area under a DTA peak can be related to the enthalpy change and is not affected by the heat capacity of the sample. DTA may be defined formally as a technique for recording the difference in temperature between a substance and a reference material against either time or temperature as the two specimens are subjected to identical temperature regimes in an environment either heated or cooled at a controlled rate.

3.3.2 Apparatus

The key features of a DTA kit are as shown in Figure 3.6 sample holder comprising thermocouples, sample containers and a ceramic or metallic block, a furnace, temperature programmer, recording system. The essential requirements of the furnace are that it should provide a stable and sufficiently large hot-zone and must be able to respond rapidly to commands from the temperature programmer. A temperature programmer is essential in order to obtain constant heating rates. The recording system must have a low inertia to faithfully reproduce variations in the experimental set-up.

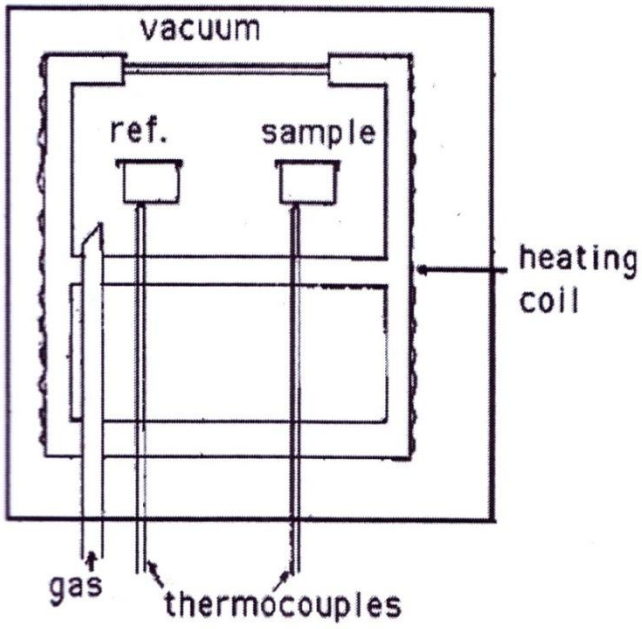

Figure 3.6: Schematic illustration of a DTA cell

The key feature is the existence of two thermocouples connected to a voltmeter. One thermocouple is placed in an inert material such as Al_2O_3 while the

other is placed in a sample of the material under study. As the temperature is increased, there will be a brief deflection of the voltmeter if the sample is undergoing a phase transition. This occurs because the input of heat will raise the temperature of the inert substance, but be incorporated as latent heat in the material changing phase.

The temperature in the sample holder is measured by a thermocouple, the signal of which is compensated for the ambient temperature and fed to the temperature controller. This signal is compared with the program signal and the voltage impressed to the furnace is adjusted. Thus signal is compared with the program signal and the voltage impressed to the furnace is adjusted. Thus the sample and the reference substance is heated and cooled at a desired rate. The temperature in the sample holder is digitally displayed on the DTA measurements model STA7200 and is also recorded on the recorder.

3.3.3 Experimental Factors

It is necessary in care to selecting the experimental parameters. For example, the effects of specimen environment, composition, size and surface to volume ratio all affect powder decomposition reactions, whereas these particular variables may not affect solid state phase changes. In some circumstances, the rate of heat evolution may be high enough to saturate the response capability of the measuring system; it is better than to dilute the test sample with inert material. For the measurement of phase transformation temperatures, it is advisable to ensure that the peak temperature does not vary with sample size. The shape of a DTA peak does depend on sample weight and the heating rate used. The influence of heating rate on the peak shape and disposition can be used to advantage in the study of decomposition reactions, but for kinetic analysis it is important to minimize thermal gradients by reducing specimen size or heating rate.

3.3.4 Interpretation and Presentation of DTA

With porous, compacted or heaped samples, the gas filling the pores can alter the thermal conductivity of the atmosphere surrounding the DTA container and lead to large errors in the peak area. The situation is made worse when gases are evolved from the sample, making the thermal conductivity of the DTA-cell environment different from that used in calibration experiments. The DTA apparatus is calibrated for enthalpy by measuring peak areas on standard samples over specified temperature

ranges. The calibration should be based upon at least two different samples, conducting both heating and cooling experiments.

Figure 3.7: TA7000 Series Simultaneous Thermogravimetric Analyzer

In the present work, HITACHI Instruments TA7000 Series Simultaneous Thermogravimetric Analyzer TG/DTA/DSC which is situated at Khulna University of Engineering and Technology (KUET) has been used for thermal analysis shows in Figure 3.7. The Thermo gravimetric/Differential Thermal Analyzer (TG/DTA) combines the flexibility of DTA with the proven capabilities of the TG measurement technology, providing property information for a verity of samples. Thus simultaneous TG/DTA/DSC System can be used for such application as oxidation, heat resistance, and the amount of water, compositional analysis and measurement of ash contents in a sample. This system is also used to cover such need as reaction rate and accelerated degrading tests.

All experiments are run at atmospheric pressure in continuous flow of purified inert gas Nitrogen. Gases are normally purged into the furnace chamber at the lower end through a purification train in which oxygen and water are removed by heated copper wool and exhausted from the top into a condensate trap for collecting the condensable volatile products.

A. The Features are:

(i) The TG/DTA can operate in either DSC or DTA mode. In DSC mode it displays heat flow signal.

(ii) The horizontal differential balance provides high sensitivity and accuracy.

(iii) Gas control unit automatically control the environment of the furnace between measurements.

(iv) Auto sampler with 30 samples positions provides laboratory automation and increase productivity.

(v) Through the utilization of an automatic cooling unit, the instrument is now automatically cooled to a set temperature after measurements, which raises the effectiveness of measurements.

B. Specification:

Temperature Range	: Room temperature to 1500°C (normally around 1300°C)
Balance Method	: Horizontal differential type
Maximal sample weight	: 200mg;
Program rate	: 0.01 to 100°C/min
Automatic Cooling unit	: Force Air Cooling
Gas flow rate	: 0 to 1000ml/min
Cooling rate	: less than 15 min from 1000 to 50°C
Atmosphere	: Air, Inert gas, Vacuum(10^{-2} Torr)
Sample pan material	: Platinum, Alumina and Aluminum.
TG measurement Range/Sensitivity	: 200 mg /0.2µg
DTA measurement / Sensitivity	: +1000µV/ 0.06µV

3.4 Annealing

Annealing in metallurgy and materials science, is heat treatment wherein a material is altered, causing changes in its properties such as strength and hardness. It is a process that produces conditions by heating to above the critical temperature, maintaining a suitable temperature, and then cooling. Annealing is used to induce ductility, soften material, relieve internal stresses, refine the structure by making it homogeneous, and improve cold working properties.

In the cases of copper, steel, silver and brass, this process is performed by substantially heating the material (generally until glowing) for a while and allowing it to cool. Unlike ferrous metals, which must be cooled slowly to anneal, copper, silver and brass can be cooled slowly in air or quickly by quenching in water. In this fashion

the metal is softened and prepared for future work such as shaping, stamping, or forming.

Annealing occurs by the diffusion of atoms within a solid material, so that the material progresses towards its equilibrium state. Heat is needed to increasing the rate of diffusion by providing the energy needed to break bonds. The movement of atoms has the effect of redistributing and destroying the dislocations in metals and (to a lesser extent) in ceramics. This alternation in dislocations allows metals to deform more easily, so increases their ductility.

3.4.1 Stages

There are three stages in the annealing process, with the first being the recovery phase, which results in softening of the metal through removal of crystal defects (the primary type of which is the linear defect called a dislocation) and the internal stresses which they cause. Recovery phase covers all annealing phenomena that occur before the appearance of new strain-free grains. The second phase is recrystallization, where new strain-free grains nucleate and grow to replace those deformed by internal stresses. If annealing is allowed to continue once recrystallization has been completed, grain growth will occur, in which the microstructure starts to coarsen and may cause the metal to have less than satisfactory mechanical properties.

3.4.2 Setup and Equipment

Typically, large ovens are used for the annealing process. The inside of the oven is large enough to place the work piece in a position to receive maximum exposure to the circulating heated air. For high volume process annealing, gas fired conveyor furnaces are often used. For large work piece or high quantity parts, car-bottom furnaces will be used in order to move the parts in and out with ease. Once the annealing process has been successfully completed, the work pieces are sometimes left in the oven in order for the parts to have a controlled cooling process. While some work pieces are left in the oven to cool in a controlled fashion, other materials and alloys are removed from the oven. After being removed from the oven, the work pieces are often quickly cooled off in a process known as quench hardening. Some typical methods of quench hardening materials involve the use of media such as air,

water, oil or salt. Quench hardening is generally applicable for some ferrous alloys, but not copper alloys.

3.5 Thermal Treatment of the Nanocrystalline Amorphous Ribbon

With a view to study nanocrystallization behavior by XRD and magnetic properties upon evaluation of nanocrystalline phase on amorphous matrix, thermal treatment, i.e. annealing is required to perform. For XRD, as prepared amorphous ribbon were cut into small pieces of about 2cm lengths for annealing treatment. MTI Corporation built KSL-1700X-S high temperature muffle furnace used for this purpose shown in Figure 3.8. The samples were put into the tube and filled up with Nitrogen gas before the tube furnace heated to a predefined temperature and kept for the time (60 minute) required completing the annealing. In this way all the isothermal annealing as a function of time were performed.

Figure 3.8: MTI - KSL-1700X-S High Temperature Muffle Furnaces

3.6 Powder/ Polycrystalline Diffraction

About 90% of all solid materials can be described as crystalline. When X-ray interacts with a crystalline substance (phase) one get a diffraction pattern. The X-ray diffraction pattern of a pure substance is, therefore, like a fingerprint of the substance.

The powder diffraction method is thus ideally suited for characterization and identification of polycrystalline phases. Today about 50000 inorganic and 25000 organic single components, crystalline phase and diffraction patterns have been collected and stored on magnetic or optical media as standers. The main use of powder diffraction is to identify components in a sample by a search match procedure. Furthermore, the areas under the peak are related to the amount of each phase present in the sample.

3.6.1 Experimental Technique for X-ray Diffractometer

X-ray diffraction (XRD) is a versatile non-destructive analytical technique for identification and quantitative determination of various crystalline phases of powdered or solid samples of any compound. For each set of composition, ribbons are cut into several pieces; each of length 20 mm. Heat treatment was performed on the amorphous ribbons using a muffle furnace, where each piece of ribbon was wrapped by aluminum foil separately. After the heat treatment, samples were removed from the furnace tube carefully and kept separately for XRD experiment.

For XRD experiment each sample was set on a glass slides and fixed the sample by putting adhesive tape at the two ends of the sample. After the pattern is obtained the value of 2θ is calculated for each diffraction line; set of 2θ values is the raw data for the determination of the lattice parameters of the unit cell. Figure 3.9: Shows the block diagram of the PHILIPS PW 3040 X'Pert PRO X-ray diffractometer. The PHILIPS PW 3040 X'Pert PRO X-ray diffractometer was used for the lattice parameter determination in the Materials Science division, Atomic Energy Centre, Dhaka. Figure 3.10 shows the inside view of the PHILIPS PW 3040 X'Pert PRO XRD system. The PHILIPS PW 3040 X'Pert PRO diffraction system utilizes a modular system approach to provide performance for application ranging from routine characterization to in-depth research investigation.

The powder diffraction technique was used with a primary beam power of 40 kV and 30mA for Cu radiation. A nickel filter was used to reduce Cu-K_α radiation and finally Cu-K_α radiation was only used as the primary beam. A (θ- 2θ) scan was taken from 30^o to 90^o to get possible fundamental peaks of the sample with the sampling pitch of 0.02^o and time for each step data collection was 1.0 sec. Both the programmable divergence and receiving slits were used to control the irradiated beam area and output intensity from the sample respectively.

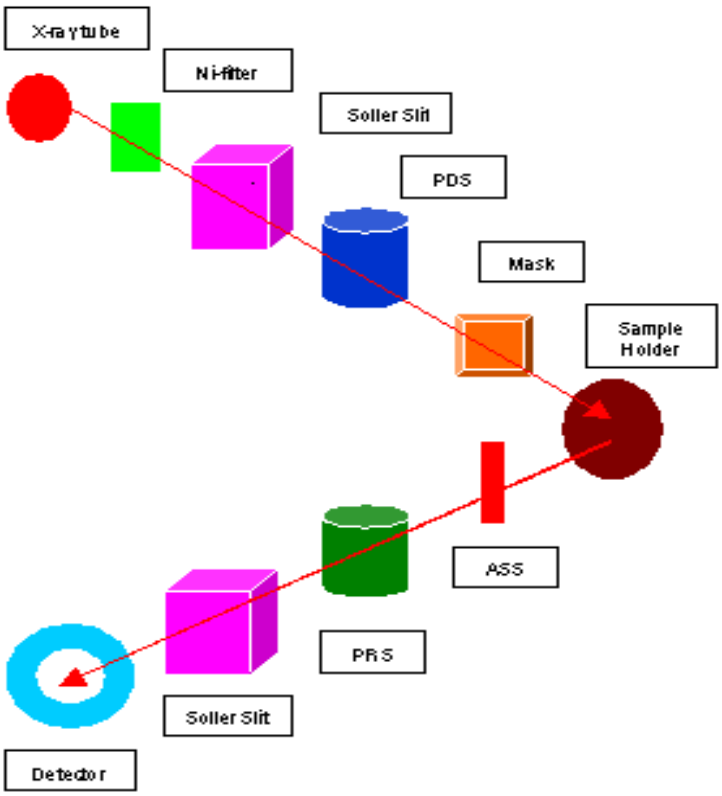

Figure 3.9: Block diagram of the PHILIPS PW 3040 X'Pert PRO XRD system.

An anti-scatter slit was used just after the sample holder to reduce air scattering. Two solar slits were used just after the tube and in front of the detector to get parallel beam only. All the data of the samples were stored in the computer memory and later analyzed that using computer software "X PERT HIGHSCORE".

The PHILIPS X' Pert PRO XRD system comprised of the following parts;

(i) Cu-Tube with maximum input power of 60 kV and 55 mA,

(ii) Ni- Filter to remove Cu-K_α component,

(iii) Solar slit to pass parallel beam only,

(iv) Programmable Divergent slits (PDS) to reduce divergence of beam and control irradiated beam area,

(v) Mask to get desired beam area,

(vi) Sample holder for powder sample,

(vii) Anti Scatter slit (ASS) to reduce air scattering back ground,

(viii) Programmable Receiving slit (PRS) to control the diffracted beam intensity and

(ix) Solar slit to stop scattered beam and pass parallel diffracted beam only

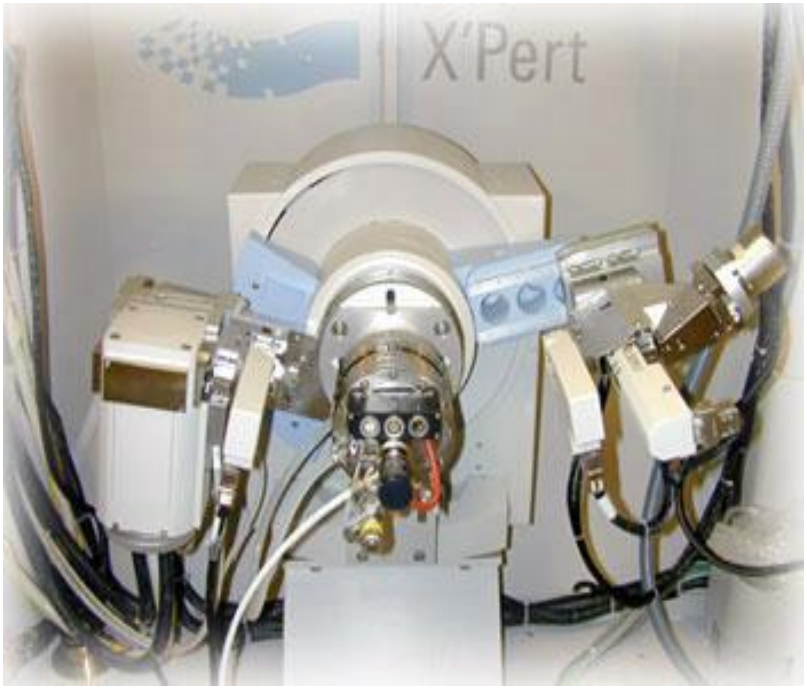

Figure 3.10: Internal arrangement of a PHILIPS X' Pert PRO X-ray diffractometer

3.6.2 Analysis of XRD data

The XRD data consisting of $\theta_{hkl}$and d_{hkl} values corresponding to the different planes from which the following structural information of the nanocrystalline ribbon sample was evaluated.

(i) Identification of phases

(ii) Lattice parameter determination

(iii) Average grain size determination

(iv) Si- content determination in nanograins

(i) Identification of phases

XRD has become a very popular and useful instrument for routine X-ray analysis of nanocrystalline amorphous ribbon samples. In fact the diffractometer technique is often preferred to Debye-Scherrer technique owing to its several inherent merits. The most striking difference between the two methods is in the use of different intensity detection and measuring devices. XRD pattern of as-cast indicates just amorphous pattern of the given composition. The XRD patterns are identified as bcc α-Fe (Si) solid solution, which are developed on the nanocrystalline amorphous ribbon after heat treatment. The peak pattern is observed for all the samples at

different heat treatment temperatures indicating the bcc α-Fe (Si) phase, which is developed on amorphous ribbons after heat treatment. Present experiment revels that 450°C is not sufficient temperature to start forming of crystalline nanograins of bcc Fe (Si) on the amorphous ribbon of the studied alloy composition.

(ii) Lattice Parameter Determination

Lattice parameter of crystalline bcc Fe-Si nanograin has been determined for all the two different amorphous compositions at different heat treatment temperatures. Normally, lattice parameter of an alloy composition is determined by the Debye-Scherrer method after extrapolation of the curve. In the present case, only one reflection (110) is prominent in all XRD patterns and we would like to understand how the value of lattice parameter changes with annealing temperature. We have, therefore, determined the lattice parameter using only that particular reflection using equation $2d\sin\theta = \lambda$ and $a_0 = d\sqrt{2}$, where $\lambda = 1.54178\,\text{Å}$ for $Cu - K_\alpha$ radiation and a_0 is the determined lattice parameter within an error estimated to be $\pm 0.0001\,\text{Å}$.

(iii) Grain Size Determination

The main aim (vital point) of the present study is to determine the nanocrystalline grain size for all the heat treated samples of the alloy composition by using Scherrer method. The XRD pattern of (110) reflection for different steps of heat treatment temperature of the alloy composition is used to calculate grain size. Grain size is determined using the following formula,

$$D_g = \frac{0.9\lambda}{\beta\cos\theta} \qquad (3.3)$$

Where $\lambda = 1.54178\,\text{Å}$ for $Cu - K_\alpha$ radiation and β = FWHM (full width at half maximum) of the peak in radian. Considering β in degree we get the following relation

$$D_g = \frac{79.5}{\beta\cos\theta} \qquad (3.4)$$

All the values of grain size for every steps of heat treatment temperature of the alloy composition were determined. The FWHM of the peak is large at the early heat treatment temperature and with the increase of heat treatment temperature the value of FWHM becomes smaller which means that the grain size is increasing gradually.

(iv) Si-content in Nanograins

Crystalline nanograins were formed on the amorphous matrix of the ribbon in the process of heat treatment having the composition of Fe-Si. It is, therefore important to determine the concentration of Fe and Si in the nanograin. As because the alloy consists of Fe and Si and are experimentally determined the lattice parameter of the alloy nanograin for the two compositions at different temperatures. It is easy to calculate the Si content in the nanograins from the data of Pearsons who was established the relationship between the lattice parameter as dependent on Si content in Fe-Si alloys covering a wide range of composition [3.6]. From the relationship, are constructed a simple equation to calculate Si content from lattice parameter. The equation is

$$X = \frac{(a_0 - 2.8812)}{0.0022} \qquad (3.5)$$

Where X is at. % Si in the nanograins, a_0 is the determined lattice parameter of nanograins. Si-contents for the nanograins develop during the isothermal annealing at various temperatures have been calculated.

3.7 Magnetization Measurement Techniques

In the present study magnetization has been performed using a Vibrating Sample Magnetometer (VSM). A VSM operates on Faraday's Law of Induction, which tells us that a changing magnetic field will produce an electric field. This electric field can be measured and can tell us information about the changing magnetic field. A VSM is used to measure the magnetic behavior of magnetic materials.

3.7.1 Vibration Sample Magnetometer

The principle of vibrations sample magnetometer (VSM) is the measurement of electromotive force induces by magnetic sample when it is vibrate at a constant frequency in the presence of a static and uniform magnetic field. A small part of the (10 - 50 mg) was weighted and made to avoid movements inside the sample holder shown in Figure 3.11. VSM is a versatile and sensitive method of measuring magnetic properties developed by Foner [3.7 - 3.8] and is based on the flux change in a coil when the sample is vibrated near it. The VSM is designed to continuously measure the magnetic properties of materials as a function of temperature and field. In this type of magnetometer, the sample is vibrated up and down in a region surrounded by

several pickup coils. The magnetic sample is thus acting as a time-changing magnetic flux, varying inside a particular region of fixed area. From Maxwell's law it is known that a time varying magnetic flux is accompanied by an electric field and the field induces a voltage in pickup coils. This alternating voltage signal is processed by a control unit system, in order to increase the signal to noise ratio. The result is a measure of the magnetization of the sample.

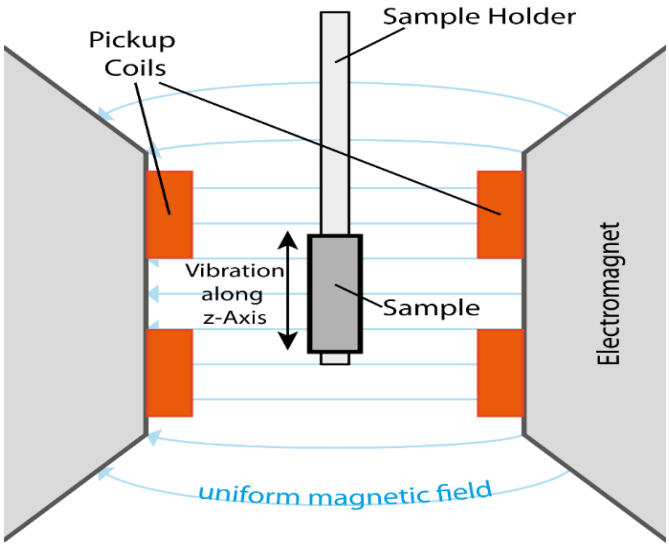

Figure 3.11: Vibrating Sample Magnetometer - sample holder and detection mechanism

The simplest of these is the rotating coil which rotates at a fixed angular velocity. Therefore the amplitude of the generated voltage by rotating coil is proportional to the magnetic induction and therefore the amplitude can be used to measure magnetic induction or magnetic field in free space. The signal can be read directly as an AC voltage or converted to a DC voltage which is proportional to the amplitude.

Figure 3.12 shows VSM of Model EV7 system. The magnetic properties measurement system model EV7 is a sophisticated analytical instrument configured specially for the study of the magnetic properties of the small samples over a broad range of temperature from 103K to 800K and magnetic field from -20kOe to +20kOe. The VSM is designed to continuously measure the magnetic properties of materials as a function of temperature and the field. In this type of magnetometer, the sample is vibrated up and down in a region surrounded by several pick up coils. The magnetic sample is thus acting as a time-changing magnetic flux, varying the electric flux is

accompanied by an electric field and the field induces a voltage in pick up coils. This alternating voltage signal is processed by a control unit system, in order to increase the signal to noise ratio. The result is a measure of the magnetization of the sample.

Figure 3.12: Vibrating Sample Magnetometer at Materials Science Division, AECD

By using a compact gradiometer pickup coil configuration, relatively large oscillation amplitude (1- 3mm peak) and a frequency of 40 Hz, the system is able to resolve magnetization changes of less than 10^{-6} emu at a data rate of 1 Hz. The VSM option for the PPMS consists primarily of a VSM line a motor transport (head) for vibrating the sample, a coil set puck for detection, electronics for driving the linear motor transport and detecting the response from the pickup coils. If a sample is placed in a uniform magnetic field, created between the poles of electromagnet, a dipole moment will be induced. If the sample vibrates with sinusoidal motion sinusoidal electrical signal can be induced in suitable placed pick-up coils. The signal has same frequency of vibration and its amplitude will be proportional to the magnetic moment.

The sample is attached to the end of a sample rod that is driven sinusoidal. The center of oscillation is positioned at the vertical center of a gradiometer pickup coil. The precise position and amplitude of oscillation is controlled from the VSM motor

module using an optical linear encoder signal read back from the VSM linear motor transport. The voltage induced in the pickup coil is amplified and lock-in detected in the VSM detection module.

The sample is fixed to sample holder located at the end of a sample red mounted in a electromechanical transducer. The transducer is driver by a power amplifier which itself is driver by an oscillator at a frequency of 90Hz. So, the sample vibrates along the 2-axis perpendicular to the magnetizing field. The latter induce a signal in the pick-up coil system that is fed to a differential. The output of the differential amplifier is subsequently fed into a tuned amplifier and an internal lock in amplifier that receives signal supplied by the oscillator. The output of the lock-in amplifier, or the output of the magnetometer itself, is a DC signal proportional to the magnetic moment of the sample being studied. Calibration of the VSM is done by measuring the signal of a pure Ni standard of Known saturation magnetic moment placed in the saddle point. The basic instrument included the electromechanical system and the electronic system including in personal computer. Laboratory electromagnet coils of various maximum field strengths may be used.

RESULTS AND DISCUSSION

4.1 Crystallization Behavior of $(Fe_{0.9}Co_{0.1})_{73.5}Cu_1Nb_3Si_{13.5}B_9$ Alloys

The understanding of the crystallization kinetics of magnetic amorphous alloys is of scientific interest as it represents a phase transformation occurring under extreme situations far from equilibrium. The calorimetric studies of amorphous alloys deliver substantial fundamental information concerning the kinetics of the crystallization and structural relaxation effect. The kinetics of the onset of crystallization has been studied calorimetrically by Clements and Cantor [4.1] and both calorimetrically and magnetically by Luborsky [4.2] in a variety of amorphous magnetic alloys. Crystallization kinetics of magnetic material is often determined from Differential Scanning Calorimetry (DSC), Differential Thermal Analysis (DTA) and Thermomagnetic Analysis (TMA) [4.3 - 4.5].

The change of composition affects the growth kinetics in complicated way, which can only be determined experimentally. The composition of the alloy affects both the primary and secondary crystallization phases, because the time needed for the constituent atom to have long range order depends on their bond energies [4.6-4.7]. Good soft magnetic properties of the materials require not only small grain size but at the same time the absence of boron compound. The separation between the primary crystallization of α-Fe(Si) phase and the secondary crystallization product of Fe_2B phase not only is determined by the Cu and Nb addition but also on boron content, with the increase of boron content the separation between the two products decreases [4.8]. We kept at a moderate level of boron content in the nominal composition in order to obtain an optimum nanoscaled structure.

In the present investigation DTA technique has been used to study the crystallization behavior of nanocrystalline amorphous alloys $(Fe_{0.9}Co_{0.1})_{73.5}Cu_1Nb_3Si_{13.5}B_9$. DTA is a direct and effective technique for analyze the kinetics of nanocrystalline materials in respect of phase transitions. DTA has been performed to identify the crystallization temperatures as well as a activation energy required for crystallization.

4.1.1 DTA Results of Nanocrystalline Amorphous Ribbon with composition $(Fe_{0.9}Co_{0.1})_{73.5}Cu_1Nb_3Si_{13.5}B_9$ Alloy

DTA traces of as-cast nanocrystalline amorphous ribbon $(Fe_{0.9}Co_{0.1})_{73.5}Cu_1Nb_3Si_{13.5}B_9$ alloy taken in nitrogen atmosphere with the heating rates of 10^0C to 60^0C/minute at the step of 10^0C with continuous heating from room temperature to 800^0C, are presented in figure 4.1 (a) to figure 4.1 (f), respectively. In each of the figure, two exothermic peaks are distinctly observed which corresponds to two different crystallization events at temperature primary crystallization (T_{x_1}) and secondary crystallization (T_{x_2}) respectively. The soft magnetic ribbon corresponds to close in which T_{x_1} of α-FeCo(Si) takes place. T_{x_2} of Fe_2B and/ or FeCoB caused magnetic hardening of the nanocrystalline alloy. Phase identification cannot be done from a DTA scan. XRD has been used for the identification of phases and would be discussed later on. Thus, the identification of these two temperature, is necessary to understand the appropriate temperature range for heat treatment in order to achieve the nanocrystalline phase and thereby, suitable range of temperature for application of alloy. Both are the samples display exothermic peak, i.e. release of heat during the crystallization of α-FeCo(Si) and Fe_2B and/ or FeCoB phase since the transition from amorphous solid to crystalline solid is an exothermic process. In the Table 4.1 shows the T_{x_1}, T_{x_2}, and crystallization peak temperature of T_{p_1} & T_{p_2} are given for different heating rate.

The temperature gap between T_{x_1} and T_{x_2} are 126.54^0C, 130.69^0C, 134.40^0C, 134.44^0C, 133.04^0C and 132.95^0C for heating rates 10^0C, 20^0C, 30^0C, 40^0C, 50^0C and 60^0C per minutes respectively. From different investigations [4.9] it was reported that this temperature gap evolutions for addition of Cu in FINEMET type alloys. Since only the product of primary crystallization i.e. the nanocrystalline α-FeCo(Si) phase is responsible for the desired ultra soft magnetic behavior.

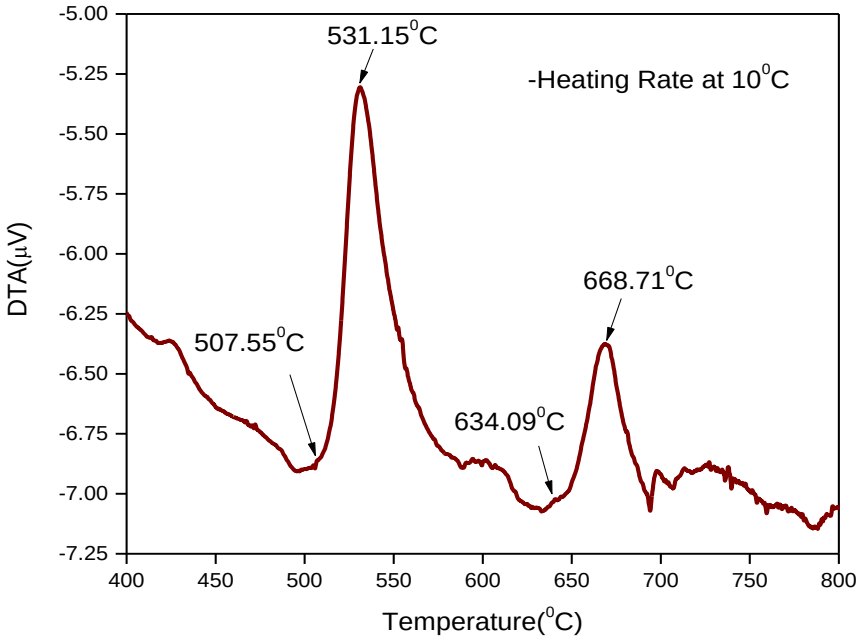

Figure 4.1(a): DTA trace of as-cast nanocrystalline amorphous ribbon $(Fe_{0.9}Co_{0.1})_{73.5}Cu_1Nb_3Si_{13.5}B_9$ at the heating rate of 10^0C/min

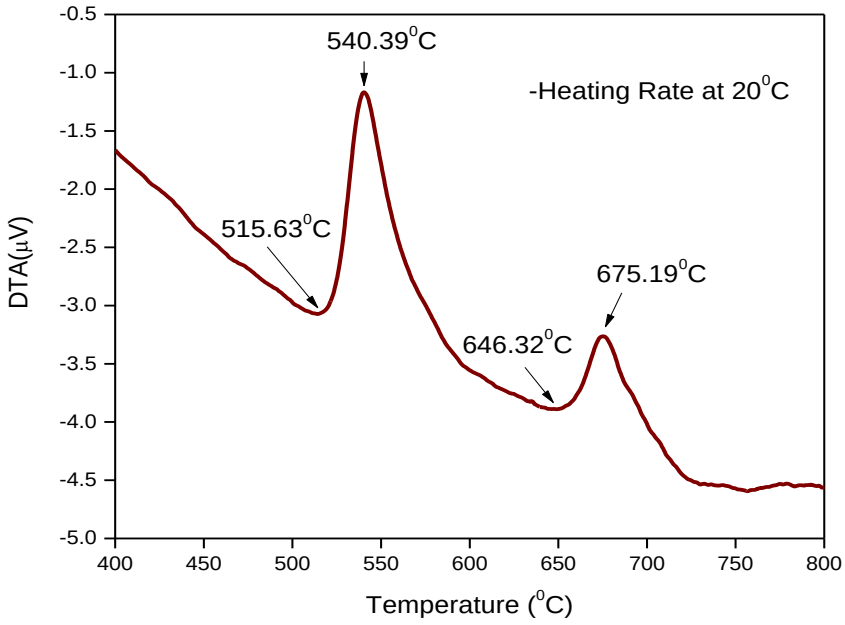

Figure 4.1(b): DTA trace of as-cast nanocrystalline amorphous ribbon $(Fe_{0.9}Co_{0.1})_{73.5}Cu_1Nb_3Si_{13.5}B_9$ at the heating rate of 20^0C/min

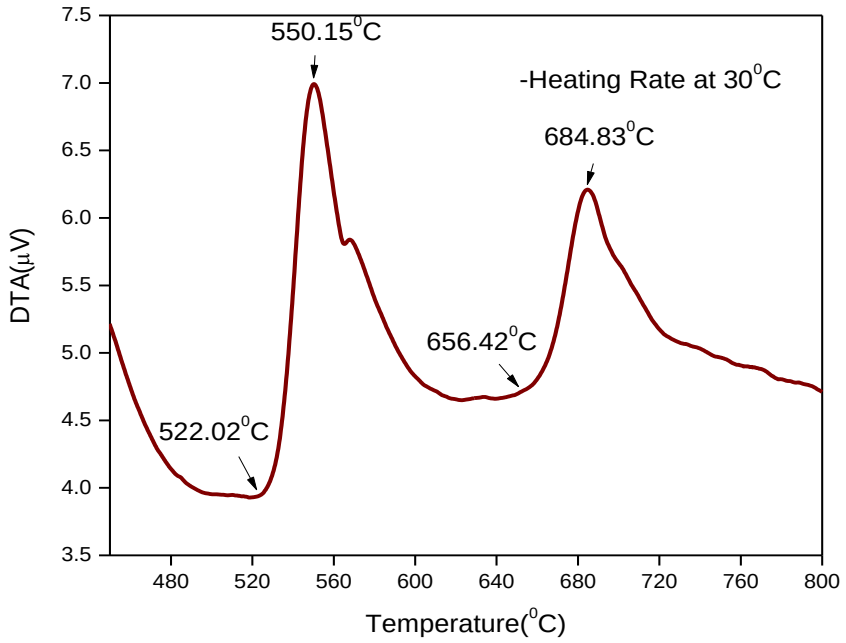

Figure 4.1(c): DTA trace of as-cast nanocrystalline amorphous ribbon $(Fe_{0.9}Co_{0.1})_{73.5}Cu_1Nb_3Si_{13.5}B_9$ at the heating rate of 30^0C/min

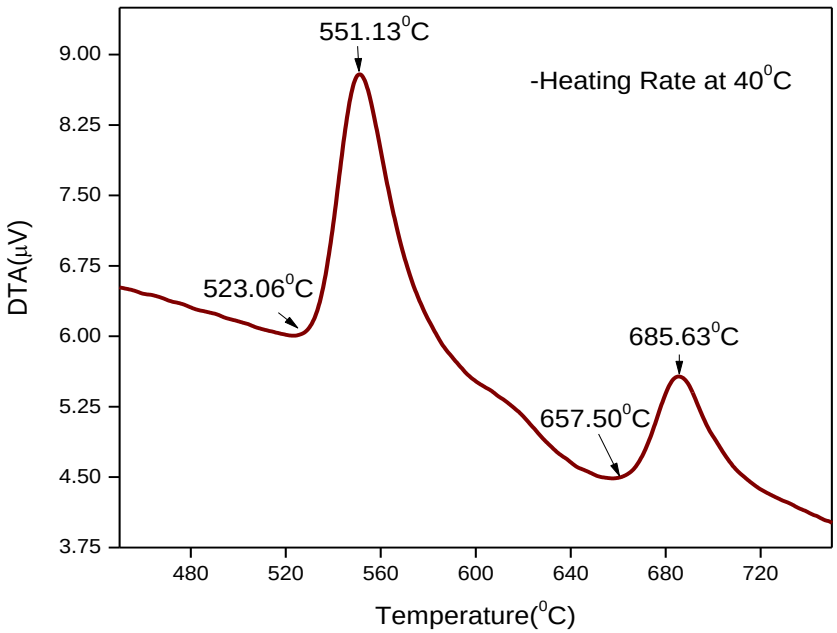

Figure 4.1(d): DTA trace of as-cast nanocrystalline amorphous ribbon $(Fe_{0.9}Co_{0.1})_{73.5}Cu_1Nb_3Si_{13.5}B_9$ at the heating rate of 40^0C/min

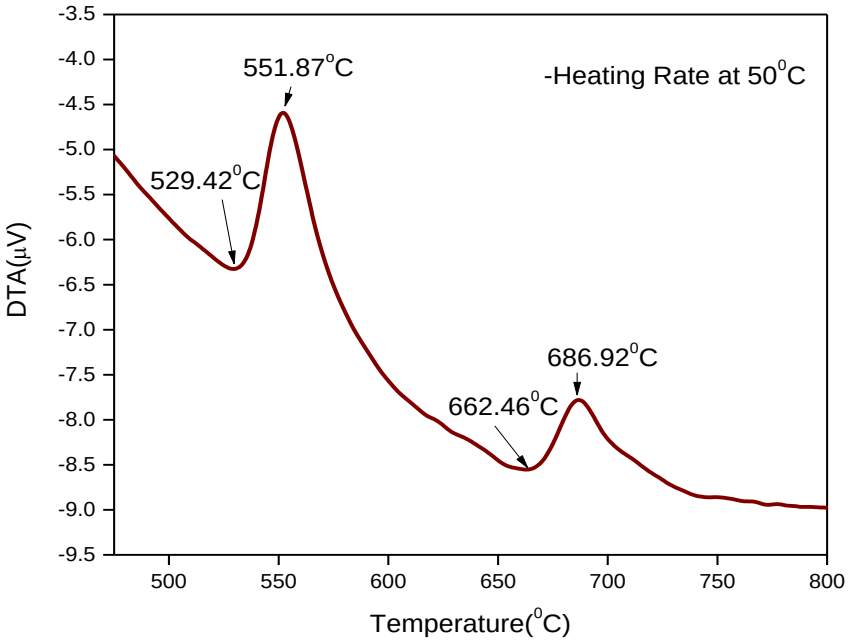

Figure 4.1(e): DTA trace of as-cast nanocrystalline amorphous ribbon $(Fe_{0.9}Co_{0.1})_{73.5}Cu_1Nb_3Si_{13.5}B_9$ at the heating rate of 50^0C/min

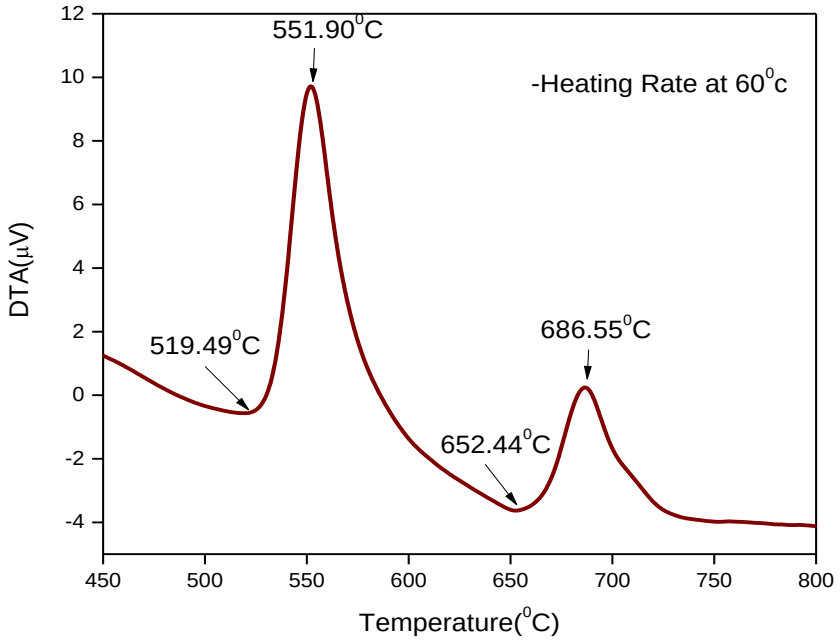

Figure 4.1(f): DTA trace of as-cast nanocrystalline amorphous ribbon $(Fe_{0.9}Co_{0.1})_{73.5}Cu_1Nb_3Si_{13.5}B_9$ at the heating rate of 60^0C/min

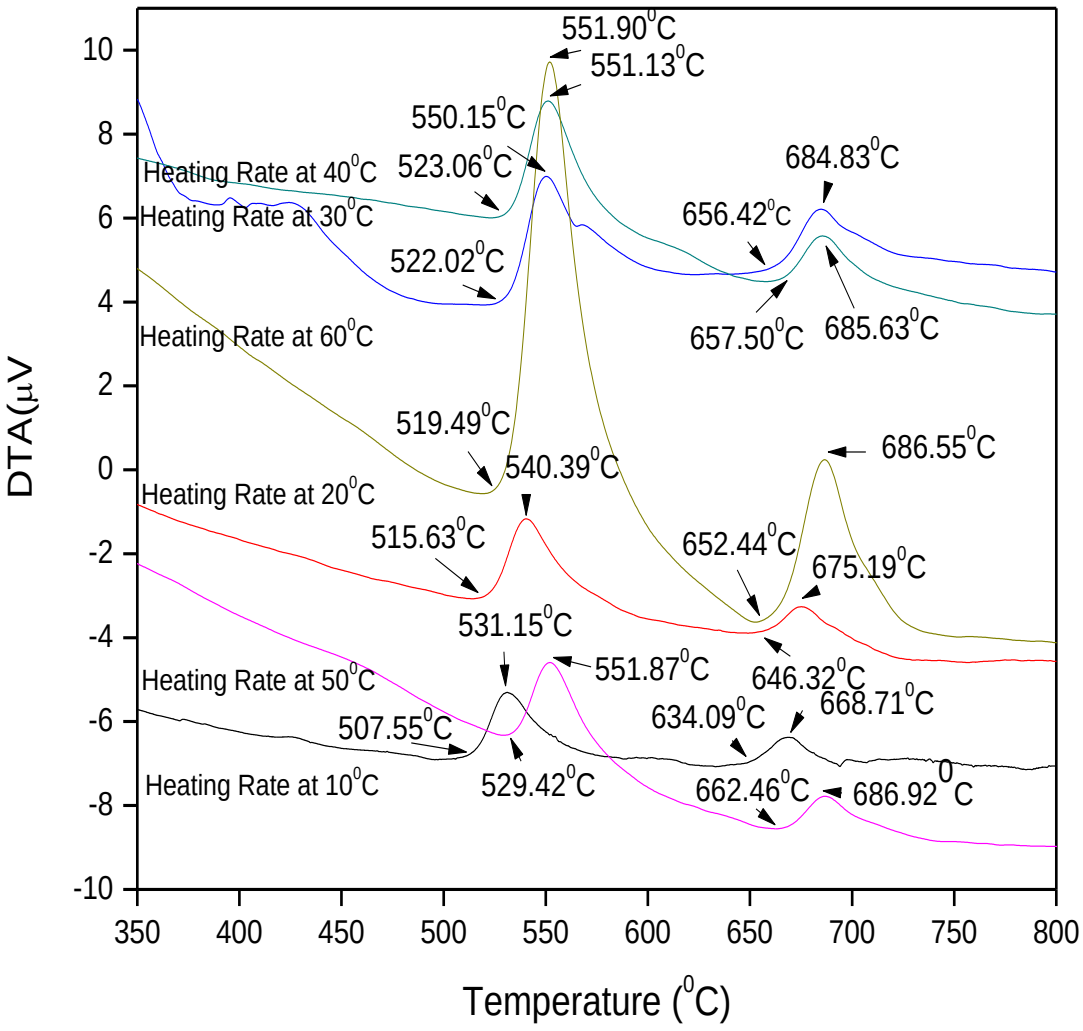

Figure 4.2: Effects of heating rate on DTA traces of nanocrystalline amorphous ribbon $(Fe_{0.9}Co_{0.1})_{73.5}Cu_1Nb_3Si_{13.5}B_9$ at the heating rate of 10°C to 60°C/min.

The secondary crystalline Fe_2B phase cause magnetic hardening, so keeping a suitable temperature gap between T_{x_1} and T_{x_2} is important. This is to note that for obtaining good soft magnetic properties T_{x_1} and T_{x_2} corresponding to primary and secondary crystallized phases should be well separated from each other at a annealing temperature $T_{x_1} < T < T_{x_2}$. So that only primary crystallization product α-FeCo(Si) is crystallized. The reason is that the secondary crystallization product Fe_2B and/ or FeCoB is extremely detrimental for the soft magnetic properties. Since Cu helps nucleation of α-FeCo(Si) phase and Nb delays the formation of boride phase [4.10],

the observed anomalies of crystallization temperatures in thus studied samples are clearly understood from their compositional variation of Cu and Nb.

Table 4.1 Effect of heating rate on 1st and 2nd crystallization states of the nanocrystalline amorphous ribbon with composition $(Fe_{0.9}Co_{0.1})_{73.5}Cu_1Nb_3Si_{13.5}B_9$

Heating rate β^0C/min	1st starting $T_{x_1}{}^0$C	1st peak $T_{p_1}{}^0$C	Temperature range of 1st state in ^{0}C	2nd starting $T_{x_2}{}^0$C	2nd peak $T_{p_2}{}^0$C	Temperature range of 2nd state in ^{0}C	T_{x_2}- T_{x_1} in ^{0}C	T_{p_2}- T_{p_1} in ^{0}C
10	507.55	531.15	23.60	634.09	668.71	34.62	126.54	137.56
20	515.63	540.39	24.76	646.32	675.19	28.87	130.69	134.9
30	522.02	550.15	28.13	656.42	684.83	28.41	134.4	134.68
40	523.06	551.13	28.07	657.50	685.63	28.13	134.44	134.5
50	529.42	551.87	22.45	662.46	686.92	24.46	133.04	135.05
60	519.49	551.90	32.41	652.44	686.55	34.11	132.95	134.65

The transition from amorphous to crystalline state is an exothermic process. It means both the peaks arise due to release of heat energy at particular temperature. At that temperature, atoms are arranged in a crystalline periodic order, i.e. in a long range atomic order by consuming heat energy supplied though the process. The first crystallization peak temperature (T_{p_1}) corresponding to structural relaxation i.e. release of stress initially formed by rapid solidification process. The secondary crystallization peak temperature (T_{p_2}) corresponding to recrystallization i.e. reordering of atoms to form another crystalline phase.

From each of the DTA traces, it is obvious that the area under the first crystallization peak is larger than the area covered by the second crystallization peak. In the Table 4.1 crystallization two phases T_{x_1} & T_{x_2} and crystallization peak temperature of two phases T_{p_1} & T_{p_2} are given for different heating rates. It has been observed that the crystallization temperature range of first phase occurred within 22.45^0C to 32.41^0C but this range for the second crystallization phase is 24.46^0C to 34.11^0C. So it is notable that the crystallization temperature range for first peak is

always smaller than the second peak. It is also observed that the peak temperature shift to higher values and crystallization temperature range increase with the heating rates.

Figure 4.2 represents a combination of all DTA traces of amorphous $(Fe_{0.9}Co_{0.1})_{73.5}Cu_1Nb_3Si_{13.5}B_9$ ribbons. It is observed that the crystallization of each phase has occurred over a wide range temperatures and that the peak temperatures shift to higher values with the increase of heating rate. That means, it is requires more heat energy for the formation of crystalline phases with increasing heating rates. Two crystallization phenomena have taken within a large temperature gap of around 134.5^0C to 137.56^0C, evaluated from the difference between two successive peak temperatures.

Table 4.2: Effect of heating rate on 1st and 2nd crystallization peak position and energy product of the nanocrystalline amorphous ribbon with composition $(Fe_{0.9}Co_{0.1})_{73.5}Cu_1Nb_3Si_{13.5}B_9$

Heating rate β^0C/min	1st peak in $T_{p_1}{}^0$C	Energy products 1st peak, ΔE μV-S/mg	2nd peak in $T_{p_2}{}^0$C	Energy products 2nd peak, ΔE μV-S/mg	T_{p_2}- T_{p_1} in^0 C
10	531.15	29.8	668.71	9.74	137.56
20	540.39	26.4	675.19	7.28	134.90
30	550.15	24.6	684.83	5.40	134.86
40	551.13	21.4	685.63	7.80	134.50
50	551.37	10.8	686.92	5.37	135.05
60	551.90	19.4	686.55	5.20	134.65

The crystallization phase activation energies products are determined and are shown in table 4.2. Energy products decrease with linearly increasing heating rate but except heating rate 60^oC/min for T_{p_1} and 40^oC/min for T_{p_2} in this amorphous ribbon. The kinetics anisotropy reorientation depends on the instantaneous structural astate and may be described in terms of activation energy products. It may qualitatively be

said the activation energy products for anisotropy reorientation decreases upon heating rate. Low values of activation energy products are similar in magnitude to that found structural phase in amorphous ferromagnetic ribbons.

4.1.2 The Activation Energies for Formation of Nanocrystalline Phase

The activation energy of crystallization of T_{p_1} and T_{p_2} phases has been calculated using Kissinger equation [4.11].

$$\beta = T_p^2 e^{-E/KT_p}$$

$$\ln(\frac{\beta}{T_p^2}) = -\frac{E}{KT_p}$$

$$E = -KT_p \ln(\frac{\beta}{T_p^2}) \qquad (4.1)$$

Where β is the heating rate, T_p is the crystallization temperature, E is the activation energy and K is the Boltzmann constant.

Table 4.3: Effect of heating rate on 1st and 2nd crystallization of the nanocrystalline amorphous ribbon with composition $(Fe_{0.9}Co_{0.1})_{73.5}Cu_1Nb_3Si_{13.5}B_9$ state's calculative data for activation energy

Heating rate β^0C/min	Heating rate β^0K/min	1st Peak $T_{p_1}{}^0$K	$1/T_{p_1}\times10^3$	$\ln(\beta/T_{p_1}{}^2)$	2nd Peak $T_{p_2}{}^0$K	$1/T_{p_2}\times10^3$	$\ln(\beta/T_{p_2}{}^2)$
10	13.41	804.31	1.243	-10.78	941.87	1.061	-11.10
20	26.89	813.55	1.229	-10.11	948.35	1.054	-10.42
30	40.24	823.31	1.214	-9.73	957.99	1.043	-10.03
40	53.66	824.29	1.213	-9.45	958.79	1.042	-9.75
50	67.07	825.03	1.212	-9.23	960.08	1.041	-9.53
60	80.46	825.06	1.212	-9.04	959.71	1.041	-9.35

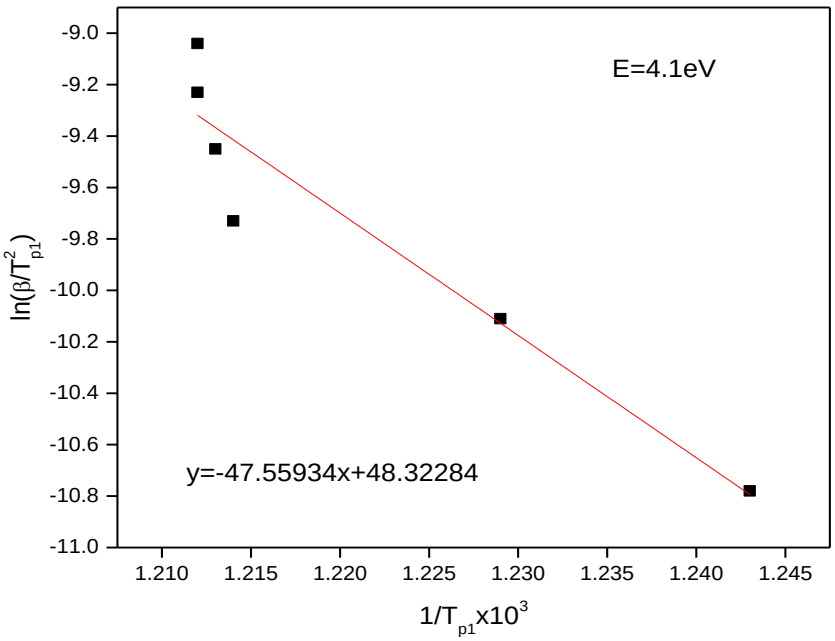

Figure 4.3(a): Kissinger's plot to determine the activation of α-FeCo(Si) phase for $(Fe_{0.9}Co_{0.1})_{73.5}Cu_1Nb_3Si_{13.5}B_9$

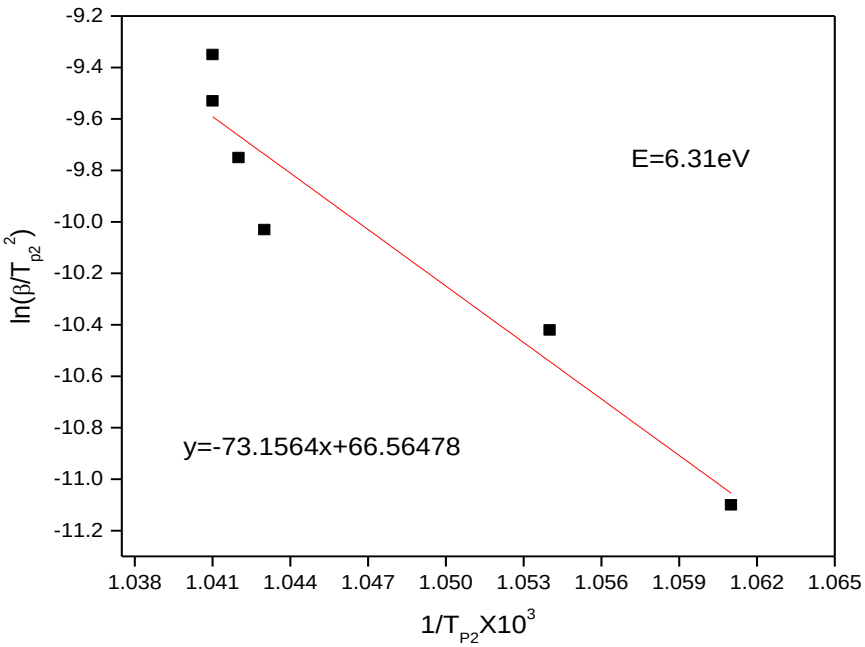

Figure 4.3(b): Kissinger's plot to determine the activation of Fe_2B phase for $(Fe_{0.9}Co_{0.1})_{73.5}Cu_1Nb_3Si_{13.5}B_9$

The activation energy of T_{p_1}[α-FeCo (Si)] and T_{p_2} (Fe_2B) phases has been calculated from table 4.3 and using Kissinger's plot shown in figure 4.3(a) and figure 4.3(b). It shows that first thermal crystallization activation energy of α-FeCo(Si) phase E_1 is 4.10eV and second Fe_2B phase E_2 is 6.31eV. As depicted above, the apparent energy in fact composed of two parts: nucleation and growth with respect to activation energy E_n and Eg respectively. At this stage, formation of Cu clusters leads to a small higher activation energy for preferential nucleation. However, with the increase of crystalline volume fraction, the Cu-rich regions gradually run out.

4.1.3 Annealing effects on the Kinetics of Structural Relaxation of $(Fe_{0.9}Co_{0.1})_{73.5}Cu_1Nb_3Si_{13.5}B_9$ Nanocrystalline Amorphous Ribbon Studied by DTA

The experimental data have been interpreted in terms of different annealing effects on amorphous ribbon of DTA traces at constant heating rate 20°C/min. The DTA traces of $(Fe_{0.9}Co_{0.1})_{73.5}Cu_1Nb_3Si_{13.5}B_9$ alloy in the as cast state and annealed at different temperatures for constant one hour annealing time are shown in figure 4.4(a) to 4.4(c) respectively. Effect of annealing at different temperatures of the amorphous ribbons on their crystallization behavior by DTA scan have been performed on both the samples with continuous heating at 20°C/min heating rate.

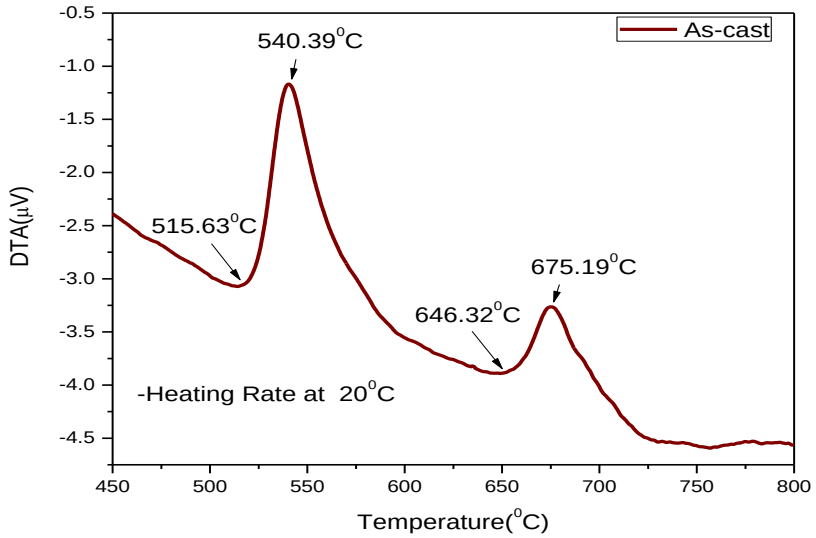

Figure 4.4(a): DTA trace of as-cast nanocrystalline amorphous ribbon $(Fe_{0.9}Co_{0.1})_{73.5}Cu_1Nb_3Si_{13.5}B_9$ at the heating rate of 20°C/min

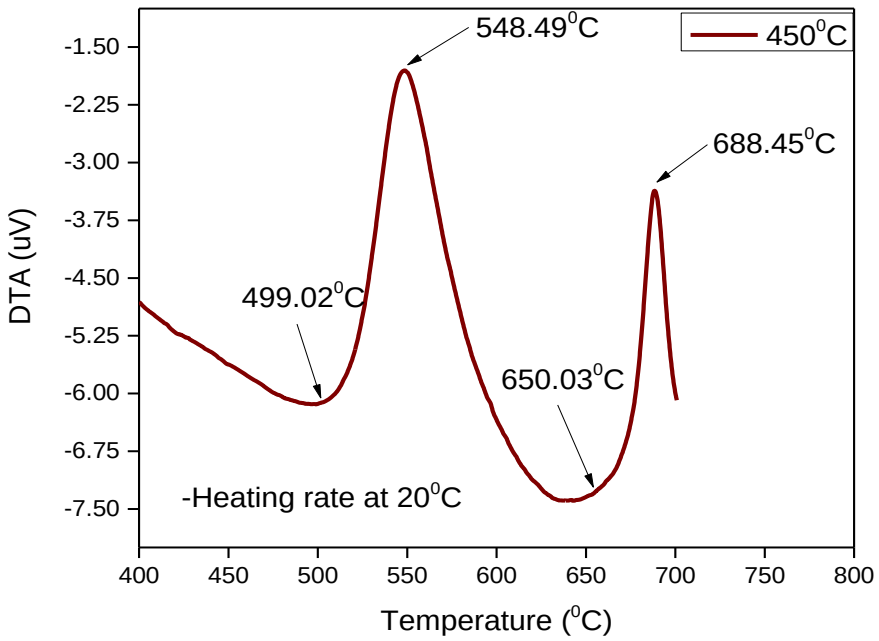

Figure 4.4(b) Effects on DTA trace of annealing temperature 450^{0}C on the nanocrystalline amorphous ribbon with composition $(Fe_{0.9}Co_{0.1})_{73.5}Cu_1Nb_3Si_{13.5}B_9$ at the heating rate of 20^{0}C/min at constant annealing time 1 hour

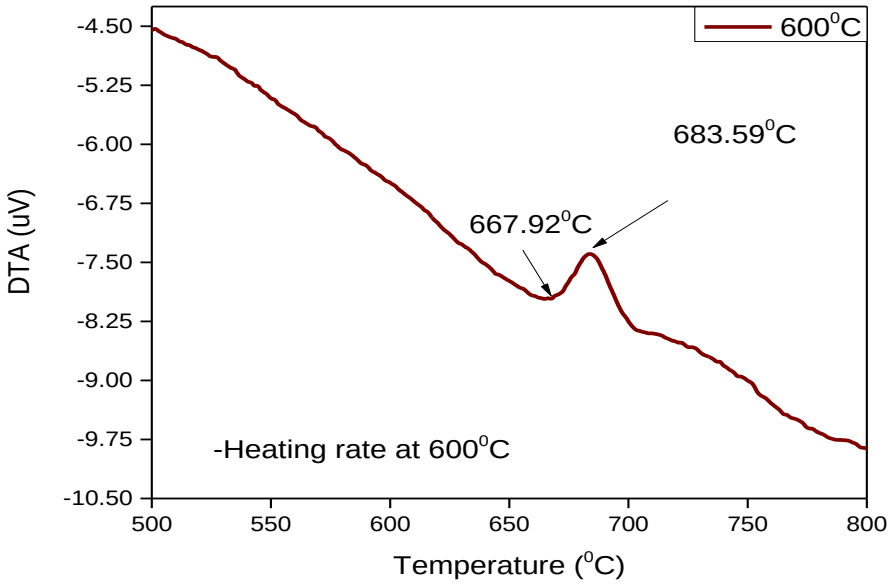

Figure 4.4(c): Effects on DTA trace of annealing temperature 600^{0}C on the nanocrystalline amorphous ribbon with composition $(Fe_{0.9}Co_{0.1})_{73.5}Cu_1Nb_3Si_{13.5}B_9$ at the heating rate of 20^{0}C/min at constant annealing time 1 hour

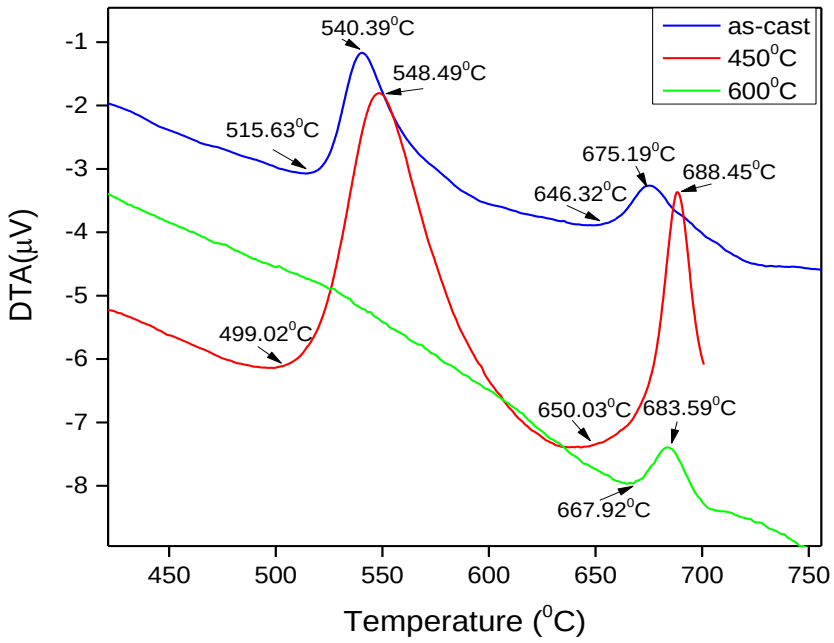

Figure 4.5: Effects on DTA trace of as-cast and different annealing temperature on the nanocrystalline amorphous ribbon with composition $(Fe_{0.9}Co_{0.1})_{73.5}Cu_1Nb_3Si_{13.5}B_9$ at the heating rate of 20^0C/min at constant annealing time 1 hour

It is observed from the DTA scan that the onset temperature for the sample $(Fe_{0.9}Co_{0.1})_{73.5}Cu_1Nb_3Si_{13.}5B_9$ annealed temperature at constant annealing time one hour at 450°C is almost unchanged with respect to its amorphous precursor which is quite logical since 450°C is still lower than its T_{x_1}= 540.39°C. But the same sample when annealed at and 600^0C at constant annealing temperature one hour which are higher than the onset of crystallization temperature of T_{x_1}= 540.39°C, the T_{p_1} has completely diminished and display diffused character meaning that substantial amount of primary crystallization, α-FeCo(Si) phase has already vanish for annealed at 600^0C at constant annealing time one hour.

The area under the first peak of DTA curve corresponds to the crystallization enthalpy, ΔH of α-FeCo(Si) from which the volume fraction of crystallization (X_f) can be estimated according to the formula,

$$X_f = \frac{\Delta H_a - \Delta H_t}{\Delta H_a} \qquad (4.2)$$

Where, ΔH_a and ΔH_t are the crystallization enthalpy of the as-cast alloy and that of the alloy annealed for a time t, respectively. This shows that with increasing annealing temperature X_f is expected to increase. The effect of annealing temperature 450^oC on the secondary crystallization is insignificant since the 450^oC is very low compared to T_{x_2}. The results of DTA scan on annealing of the sample with as-cast sample with the parameter such as T_{x_1}, T_{x_2}, T_{p_1}, T_{p_2} and ΔT are depicted in table 4.4. As cast and annealed samples at annealed 450^0C do not show any significant changes area under the T_{p_1} to the crystallization enthalpy, ΔH of α-FeCo(Si). This means that at 450^0C, no crystallization occurred which is quite obvious since $T_{x_1}= 540.39^0C$ for this sample. This demonstrates that even annealing at 450^0C, the material still remained amorphous. Therefore crystallization enthalpy ΔH area under the peak is almost equal that of, it's amorphous state. But when annealed at 600^0C, there is broad diffused first peak meaning that substantial amount of primary crystallization, α-FeCo(Si) has already vanished for constant annealing time one hour at $T_{x_1}= 540.39^0C$. For annealed at 600^0C first DTA peak is almost not visible; i.e α-FeCo(Si) phase has almost completed. A critical scrutiny of T_{p_1} does not show any significant changes are shown in figure 4.4(c).

Table 4.4: Annealing effects on 1^{st} and 2^{nd} crystallization states of the nanocrystalline amorphous ribbon with composition $(Fe_{0.9}Co_{0.1})_{73.5}Cu_1Nb_3Si_{13.5}B_9$ at constant heating rate 20°C/min.

Annealing Temperature	1^{st} starting $T_{x_1}{}^0C$	1^{st} peak $T_{p_1}{}^0C$	Temperature range of 1^{st} state in ^0C	2^{nd} starting $T_{x_2}{}^0C$	2^{nd} peak $T_{p_2}{}^0C$	Temperature range of 2^{nd} state in ^0C	$T_{x_2} - T_{x_1}$ in ^0C	$T_{p_2} - T_{p_1}$ in^0 C
As- cast	515.63	540.39	24.76	646.32	675.19	28.87	130.69	134.90
450^0C	499.02	548.49	49.47	650.03	688.45	38.42	151.01	139.96
600^0C	……	……	…….	667.92	683.59	15.67	……...	……

Figure 4.5 represents a combination of all DTA traces of amorphous $(Fe_{0.9}Co_{0.1})_{73.5}Cu_1Nb_3Si_{13.5}B_9$ ribbons. It is observed that the crystallization of each phase has occurred over a wide range temperatures and that the peak temperatures shift to higher values with the increase of annealing temperature. Two crystallization phenomena have taken within a large temperature gap of around 134.90^0C to 139.96^0C, evaluated from the difference between two successive peak temperatures.

It is observed from the table that the T_{x_1}, T_{x_2}, T_{p_1}, T_{p_2} as well as the difference between the two crystallization events are almost not affected by annealing, just below the crystallization temperatures. When the samples are annealed above the T_{p_1} as evidenced from their DTA curves are so diffused and smeared that they give signals of nearly completion of the primary crystallization of α-FeCo(Si) crystallites. Therefore no characteristic temperatures in this range could be determined. Activation energy products increase with increasing annealed 450^oC but higher annealed decrease at 600^oC at constant annealing time one hour are shown in Table 4.5.

Table 4.5: Annealing effects on 1st and 2nd crystallization peak position and energy product of the nanocrystalline amorphous ribbon with composition $(Fe_{0.9}Co_{0.1})_{73.5}Cu_1Nb_3Si_{13.5}B_9$ at constant heating rate 20°C/min.

Annealing Temperature In ^{0}C	1st peak T_{p_1} ^{0}C	Energy products 1st peak, ΔE μV-S/mg	2nd peak T_{p_2} ^{0}C	Energy products 2nd peak, ΔE μV-S/mg	T_{p_2}- T_{p_1} in^0 C
As-cast	540.39	26.4	675.19	7.28	134.90
450	548.49	43.9	688.45	8.19	139.96
600	…….	……..	683.59	4.29	…… ……..

The DTA traces of$(Fe_{0.9}Co_{0.1})_{73.5}Cu_1Nb_3Si_{13.5}B_9$ alloy at annealed temperature 450^0C constant annealing time one hour of different heating rate are shown in figure 4.6(a) to 4.6(c) respectively.

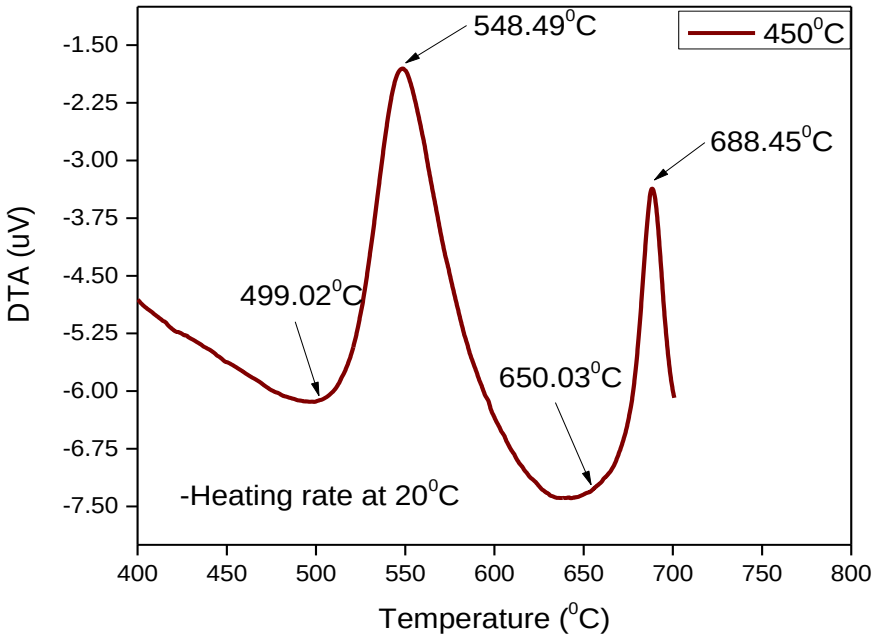

Figure 4.6(a): Effects on DTA trace of annealing temperature 450^0C at constant annealing time one hour on the nanocrystalline amorphous ribbon with composition $(Fe_{0.9}Co_{0.1})_{73.5}Cu_1Nb_3Si_{13.5}B_9$ at the heating rate of 20^0C/min

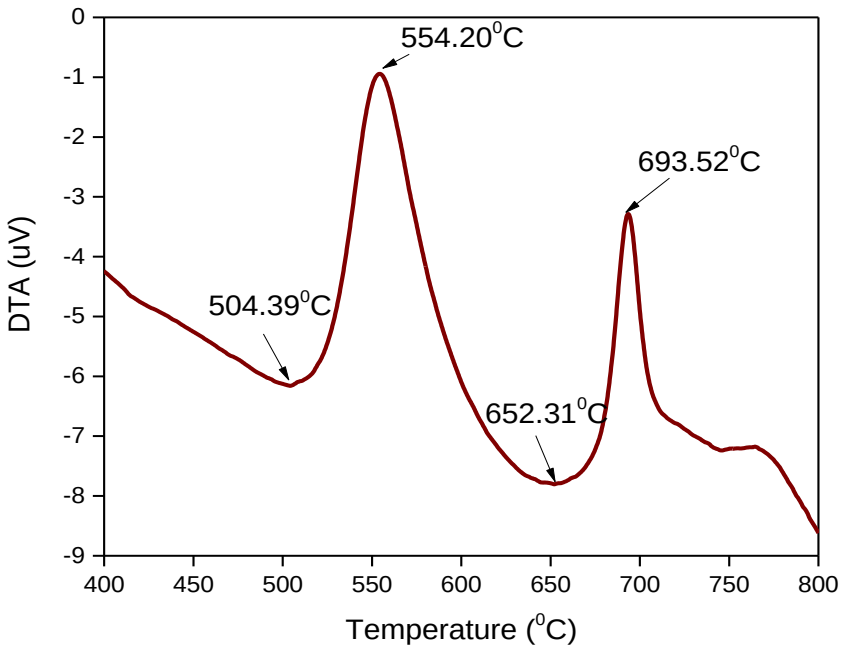

Figure 4.6(b): Effects on DTA trace of annealing temperature 450^0C at constant annealing time one hour on the nanocrystalline amorphous ribbon with composition $(Fe_{0.9}Co_{0.1})_{73.5}Cu_1Nb_3Si_{13.5}B_9$ at the heating rate of 30^0C/min

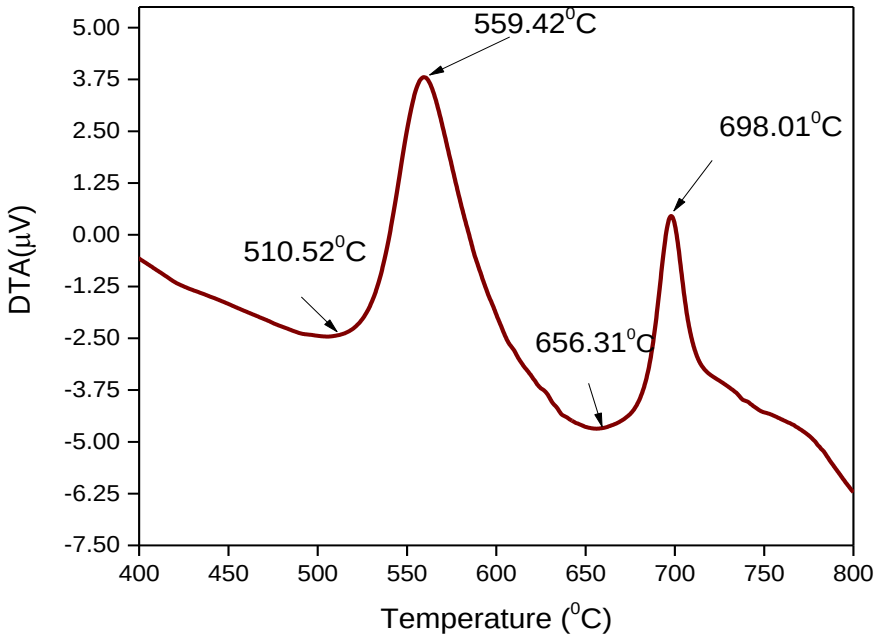

Figure 4.6(c): Effects on DTA trace of annealing temperature 450^0C at constant annealing time one hour on the nanocrystalline amorphous ribbon with composition $(Fe_{0.9}Co_{0.1})_{73.5}Cu_1Nb_3Si_{13.5}B_9$ at the heating rate of 40^0C/min

Table 4.6: Annealing effects on 1st and 2nd crystallization states of the nanocrystalline amorphous ribbon with composition $(Fe_{0.9}Co_{0.1})_{73.5}Cu_1Nb_3Si_{13.5}B_9$ at annealed 450^0C constant annealing time one hour.

Heating rate β^0C/min	1st starting $T_{x_1}{}^0$C	1st peak $T_{p_1}{}^0$C	Temp. range of 1st state in ^{0}C	2nd starting $T_{x_2}{}^0$C	2nd peak $T_{p_2}{}^0$C	Temp. range of 2nd state in ^{0}C	$T_{x_2} - T_{x_1}$ in ^{0}C	$T_{p_2} - T_{p_1}$ in^0 C
20	499.02	548.49	49.47	650.03	688.45	38.42	151.01	139.96
30	504.39	554.20	49.81	652.31	693.52	41.21	147.92	139.32
40	510.52	559.42	48.9	656.31	698.01	41.70	145.79	138.59

Table 4.7: Annealing effects of heating rate on 1st and 2nd crystallization peak position and energy product of the nanocrystalline amorphous ribbon with composition $(Fe_{0.9}Co_{0.1})_{73.5}Cu_1Nb_3Si_{13.5}B_9$ at constant annealed 450^0C at constant annealing time one hour.

Heating rate β^0C/min	1st peak $T_{p_1}{}^0$C	Energy products 1st peak, ΔE μV-S/mg	2nd peak, $T_{p_2}{}^0$C	Energy products 2nd peak, ΔE μV-S/mg	T_{p_2}- T_{p_1} in^0 C
20	548.49	43.9	688.45	8.19	139.96
30	554.20	40.7	693.52	11.0	139.32
40	559.42	46.8	698.01	11.3	138.59

The crystallization phase activation energies products are determined at annealed temperature 450^oC and are shown in table 4.7. Energy products linearly increase with increasing heating rate in the annealed amorphous ribbon. The kinetics of structural relaxation is virtually reorientation structural state.

Table 4.8: Annealing effect of heating rate on 1st and 2nd crystallization of the nanocrystalline amorphous ribbon with composition $(Fe_{0.9}Co_{0.1})_{73.5}Cu_1Nb_3Si_{13.5}B_9$ state's calculative data for activation energy annealed at 450^0C for constant annealing time one hour.

Heating rate β^0C/min	Heating rate β^0K/min	1st Peak $T_{p_1}{}^0$K	$1/T_{p_1}\times10^3$	$\ln(\beta/T_{p_1}{}^2)$	2nd Peak $T_{p_2}{}^0$K	$1/T_{p_2}\times10^3$	$\ln(\beta/T\,T_{p_2}{}^2)$
20	26.89	821.56	1.217	-10.13	961.61	1.04	-10.44
30	40.24	827.36	1.209	-9.742	966.68	1.034	-10.053
40	53.66	832.58	1.201	-9.466	971.17	1.03	-9.774

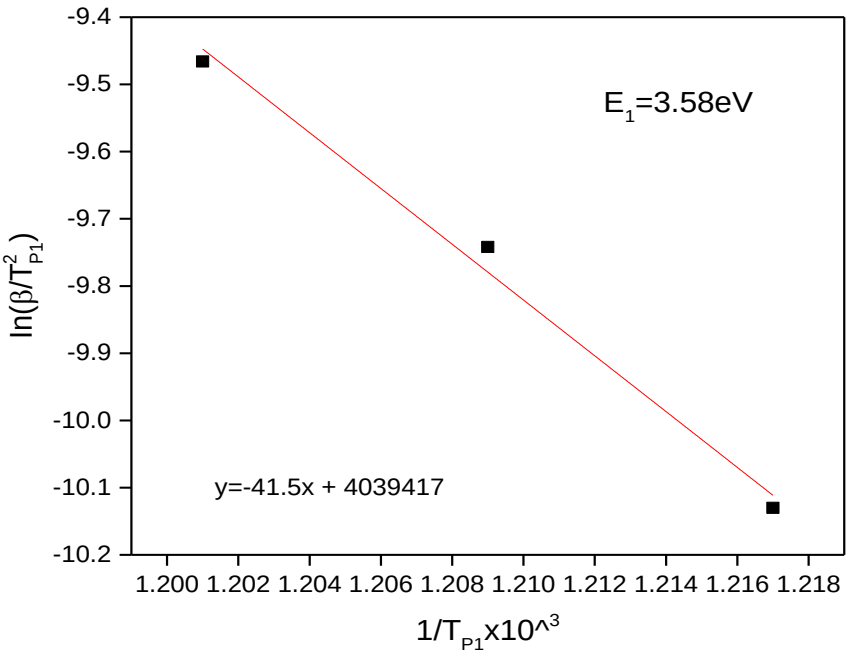

Figure 4.7(a): Kissinger's plot to determine the activation of α-FeCo(Si) phase for $(Fe_{0.9}Co_{0.1})_{73.5}Cu_1Nb_3Si_{13.5}B_9$ annealed at 450°C for constant annealing time one hour.

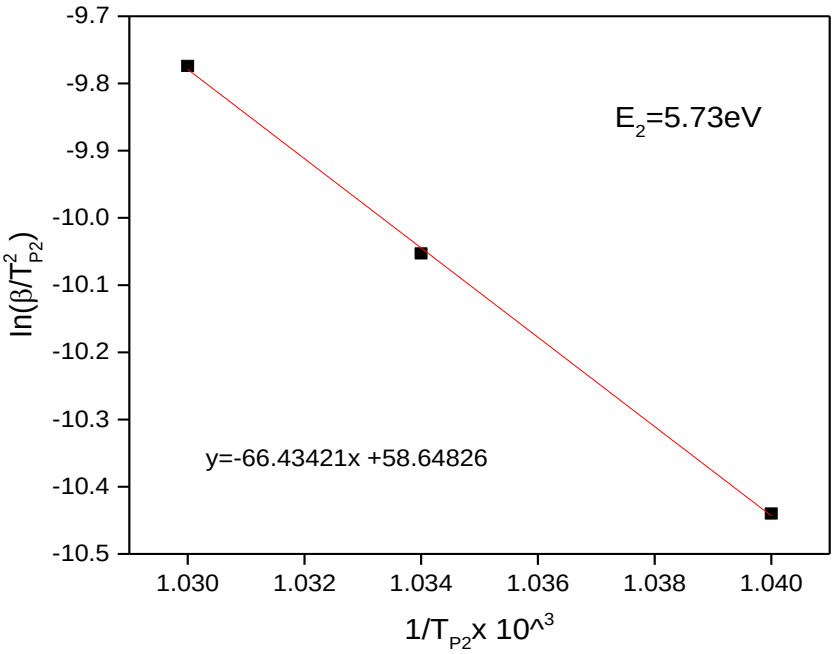

Figure 4.7(b): Kissinger's plot to determine the activation of Fe_2B phase for $(Fe_{0.9}Co_{0.1})_{73.5}Cu_1Nb_3Si_{13.5}B_9$ annealed at 450°C for constant annealing time one hour.

The activation energy of crystallization of $T_{x_1}$and T_{x_2} phases have been calculated using Kissinger equation (4.1).The activation energy of α-FeCo(Si) and Fe_2B phases has been calculated from table 4.8 and using Kissinger's plot shown in figure 4.7(a) and figure 4.7(b). It shows that first thermal crystallization activation energy of α-FeCo(Si) phase E_1 is 3.58eV and second Fe_2B phase E_2 is 5.73eV. It is seen that the therma 1st and 2nd crystallization activation energy at annealed 450°C decreases than as-cast sample. The general consensus seems to be that the local structural state of the amorphous ferromagnetic alloys with annealing.

4.1.4 Comparison between DTA Results of $(Fe_{0.9}Co_{0.1})_{73.5}Cu_1Nb_3Si_{13.5}B_9$ alloy and FINEMET

Table 4.9(a): Comparison of peak temperature of original FINEMET[4.12], $(Fe_{0.9}Co_{0.1})_{73.5}Cu_1Nb_3Si_{13.5}B_9$ as-cast and annealed at 450°C alloy

Heating rate in °C/min	$(Fe_{0.9}Co_{0.1})_{73.5}Cu_1Nb_3Si_{13.5}B_9$ as-cast ribbon			$(Fe_{0.9}Co_{0.1})_{73.5}Cu_1Nb_3Si_{13.5}B_9$ annealed at 450°C holding time one hour			$Fe_{73.5}Cu_1Nb_3Si_{13.5}B_9$ (FINEMET) as as-cast condition		
	$T_{p_1}{}^0C$	$T_{p_2}{}^0C$	T_{p_2}- T_{p_1} in^0 C	$T_{p_1}{}^0$ C	$T_{p_2}{}^0C$	T_{p_2}- T_{p_1} in^0 C	$T_{p_1}{}^0C$	$T_{p_2}{}^0C$	T_{p_2}- T_{p_1} in^0 C
10	531	668	137	… ….	.....	…….	550	686	136
20	540	675	135	548	688	140	554	700	146
30	550	685	135	554	693	139	561	708	147
40	551	686	135	559	698	139	567	715	148
50	552	687	135	….	….	…..	…..	……	……
60	552	687	135	….	….	…..	…..	……	…….

The comparative value of DTA results for $(Fe_{0.9}Co_{0.1})_{73.5}Cu_1Nb_3Si_{13.5}B_9$ alloy, this alloy annealed at 450°C holding time one hour and for original FINEMET sample is given by in table 4.9(a) and 4.9(b). The results show in table 4.9(a) that the peak temperature corresponding to crystallization decreases with addition of Co and the same condition annealed sample but slightly increase as-cast present alloy. So, due to

replacement of Co, the evolution of expected nanocrystalline α-FeCo(Si) phase can be found at a lower temperature. From table 4.9(a) it also found that the temperature gap between successive crystallization is less for the present sample than the FINEMET's. Also, it is clear from table 4.9(b) that the activation energy for formation α-FeCo(Si) phase and Fe_2B phase is higher than that the original FINEMET composition due to replacement of Co. These results indicate that the role of Co is to facilitate to formation of nanocrystalline phase and consistent with the findings of researches on Co-replaced by Fe in FINEMET sample.

Table 4.9(b): Comparison of activation energies of original FINEMET [4.12] and $(Fe_{0.9}Co_{0.1})_{73.5}Cu_1Nb_3Si_{13.5}B_9$ alloy.

$(Fe_{0.9}Co_{0.1})_{73.5}Cu_1Nb_3Si_{13.5}B_9$ as-cast ribbon		$(Fe_{0.9}Co_{0.1})_{73.5}Cu_1Nb_3Si_{13.5}B_9$ annealed at 450°C holding time one hour		$Fe_{73.5}Cu_1Nb_3Si_{13.5}B_9$ (FINEMET) as as-cast condition	
E_1(α-FeCoSi) in eV	E_2 (Fe_2B) in eV	E_1(α-FeCoSi) in eV	E_2 (Fe_2B) in eV	E_1(α-FeCoSi) in eV	E_2 (Fe_2B) in eV
4.1	6.31	3.58	5.73	3.21	3.81

4.2 Microstructural Analysis of Amorphous and Nanocrystalline $(Fe_{0.9}Co_{0.1})_{73.5}Cu_1Nb_3Si_{13.5}B_9$ alloy by XRD Analysis

A key tool in both the routine characterization and the in depth study of nanocrystalline materials has been X-ray diffraction techniques. In the present work, in order to study the crystallization onset temperature, XRD spectra have been recorded for the nominal composition $(Fe_{0.9}Co_{0.1})_{73.5}Cu_1Nb_3Si_{13.5}B_9$ annealed at 400^o to 650^o for one hour using MTI Corporation built 1700X-S High Temperature Muffle furnace. The appropriately annealed sample was subjected to XRD by using a Philps X'Pert PRO X-ray diffractometer to examine the micro structural evaluation as a function of annealing temperature. From the experiment, results of three kinds of structural parameter including lattice parameter, grain size and silicon content of nanocrystalline grain. XRD results indicate that no α-FeCo(Si) phases are present in

the alloys annealed at 400^{o}C for one hour annealed time with appearance of a broader diffused pattern, which are characteristics of amorphous materials.

X-ray pattern at annealed sample for 500^{o}C, clearly confers the presence of crystalline phase identification as a result a no α-FeCo(Si) phase solid solution developed in the amorphous matrix, lattice parameters for all the annealed samples have been determined from [110] diffraction peak using formula $a_0 = d\sqrt{2}$, while grain size have been calculated. Silicon content in the nanograins was calculated from established quantitative relationship between lattice parameter and Si-content in Fe-Si alloy by Bozorth [4.13]. All the results of θ, d-values, FWHM, a_0, D_g , Si-content from XRD analysis are listed in table 4.9

4.2.1 Identification of Phases by XRD Experiment

Above 400^{o}C it is clearly evident that crystallization starts with increasing annealing temperature peaks become narrow and sharper with higher intensity, which indicates that the crystallite size of α-FeCo(Si) grain are growing larger gradually. The XRD patterns for the $(Fe_{0.9}Co_{0.1})_{73.5}Cu_1Nb_3Si_{13.5}B_9$annealing at 500^{o}C, 550^{o}C, 575^{o}C, 600^{o}C, 625^{o}C and 650^{o}C each for one hour are presented figure 4.8. It is evident from figure 4.8 when the sample annealed below 500^{0}C, i.e. at 400^{0}C, it exhibited only one broad peak around 2θ = 45^{0}C at the position of d_{110} reflection which is generally known as diffuse hallow.

This diffuse hallow indicates the amorphous nature of the sample. It means at the annealing temperature below 500^{0}C, no crystallization peak has been detected. So the onset crystallization temperature determined from these results is 500^{0}C. The value of FWHM of the peak at the annealing temperature 550^{0}C is 0.7071, which is 600^{o}C is 0.5769. For the higher annealing temperatures, the FWHM value is getting smaller. It shows that the crystallization occurs to a good extent at the higher annealing temperature. The crystallization onset temperatures from DTA experiment for different heating rates were found in the range of 507^{0}C to 529^{0}C, which shows a good consistency with the XRD results.

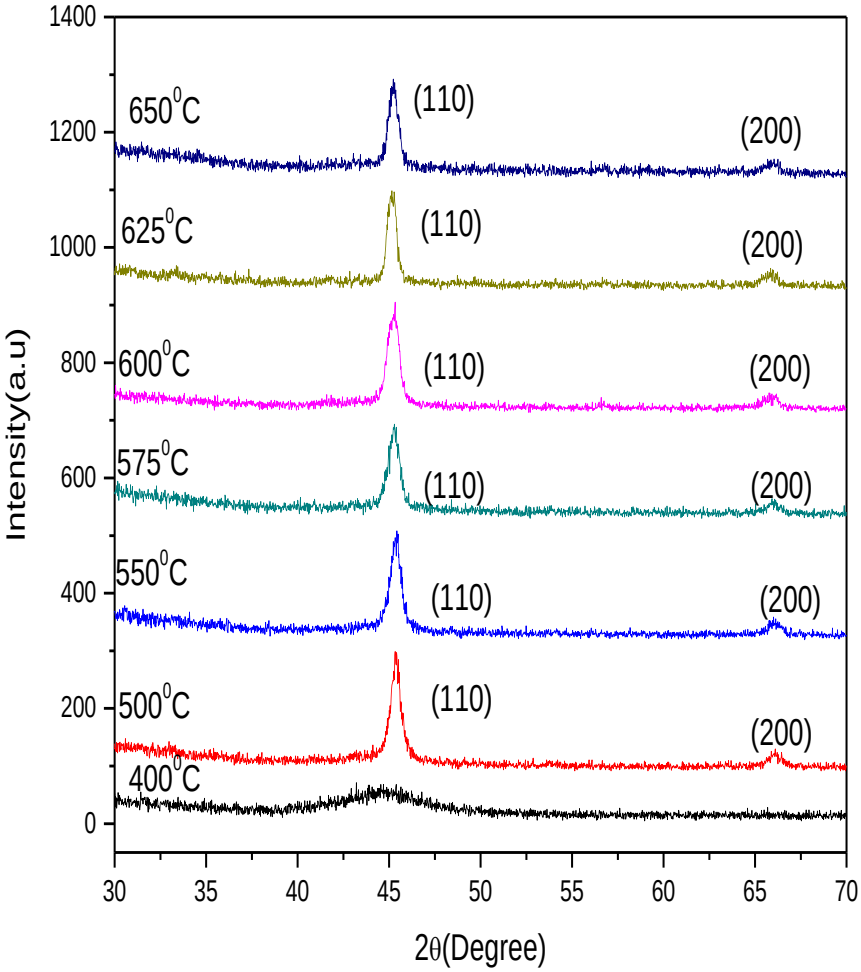

Figure 4.8: XRD spectra of $(Fe_{0.9}Co_{0.1})_{73.5}Cu_1Nb_3Si_{13.5}B_9$ alloys of annealed at different temperatures at constant annealing time one hour

For annealing at higher temperature i.e. 500^{0}C, 550^{0}C, 575^{0}C, 600^{0}C, 625^{0}C, and 650^{0}C the α-FeCo(Si) phases were found at the lower values of 2θ at 45.36^0, 44.35^0, 45.26^0, 45.22^0, 44.20^0 and 45.15^0 respectively with 100% peak intensity on (110) line. Other fundamental peaks corresponding to no α-FeCo(Si) on (200) diffraction lines for annealing temperature at and above 500^{0}C is obtained in this figure 4.8. But due to their low intensity they are not clearly visible.

From DTA result it is expected that no α-FeCo(Si) phase would form beyond 500^{0}C. The XRD pattern illustrated in figure 4.8 reveal that the difference in Bragg's peak as well as the intensity of the fundamental reflection becomes gradually stronger as the temperature of the heat treatment increases. This increase in the sharpness of

the intensity peaks with the annealing temperature indicates that crystalline volume fraction has been increased and also grains become coarser with increased crystallinity. The systematic but negligible shift of peak towards the larger angles with increasing temperature indicates that lattice parameter of the phase gradually decreases due to the increasing of Si-content of α-FeCo(Si) phase.

From DTA result it is expected that the formation of crystalline phase other than no α-FeCo(Si) in the XRD pattern has not been detected after annealed 650^{o}C for the expected from the DTA analysis of $(Fe_{0.9}Co_{0.1})_{73.5}Cu_1Nb_3Si_{13.5}B_9$ alloys. Absence of Fe_2B phase in XRD spectra is possibly due to very small volume fraction of broide phase [5.14 – 5.15]. The lattice parameter, the silicon content in bcc nanograins and grain size of α-FeCo grain can easily be calculated from the fundamental peak of (110) reflections. All results are shown in table 4.10.

Table 4.10: Experimental XRD data of $(Fe_{0.9}Co_{0.1})_{73.5}Cu_1Nb_3Si_{13.5}B_9$ alloys of annealed at different temperature at constant annealing time one hour.

Annealing temp in ^{0}C	θ(deg)	d($\overset{o}{A}$)	FWHM (deg)	a_o($\overset{o}{A}$)	D_g(nm)	Si at (%)
400	…….	…….	…….	…….	……	……
500	22.6811	1.9992	0.7071	2.8273	12.	22.46
550	22.6776	1.9995	0.7073	2.8277	12	22.27
575	22.6323	2.0033	0.7156	2.8331	12	19.76
600	22.6137	2.0048	0.7517	2.8353	12	18.73
625	22.6079	2.0053	0.6559	2.8359	13	18.41
650	22.5773	2.0079	0.5769	2.8396	15	16.71

4.2.2 Lattice Parameter Measurement

Determined the lattice parameter using only that particular reflection using equation:

$$2d\sin\theta=\lambda \text{ and } \alpha_0=d\sqrt{2} \qquad (4.3)$$

Where λ=1.54178 Å is the wavelength of Cu-K_α radiation and a_0 is determined lattice parameter of the grain, d is the inter-planar spacing and θ is the diffraction angle. Lattice parameter of crystalline α-FeCo(Si) was determined at different annealing temperatures of the experimental alloys. Figure 4.9 shows that, with the increase in

annealing temperature lattice parameter increasing. The lattice parameter of pure Fe is 2.8664Å. But the lattice parameter at various annealing temperature for the present alloy are significantly less than that of pure Fe. Si having a smaller atomic size compared to Fe, diffuses in the α-FeCo lattice during annealing at temperatures which results in a contraction of FeCo lattice. Increase of lattice parameter with annealing temperature suggests negligible peak shift to staking fault as in general peak is observed experimentally.

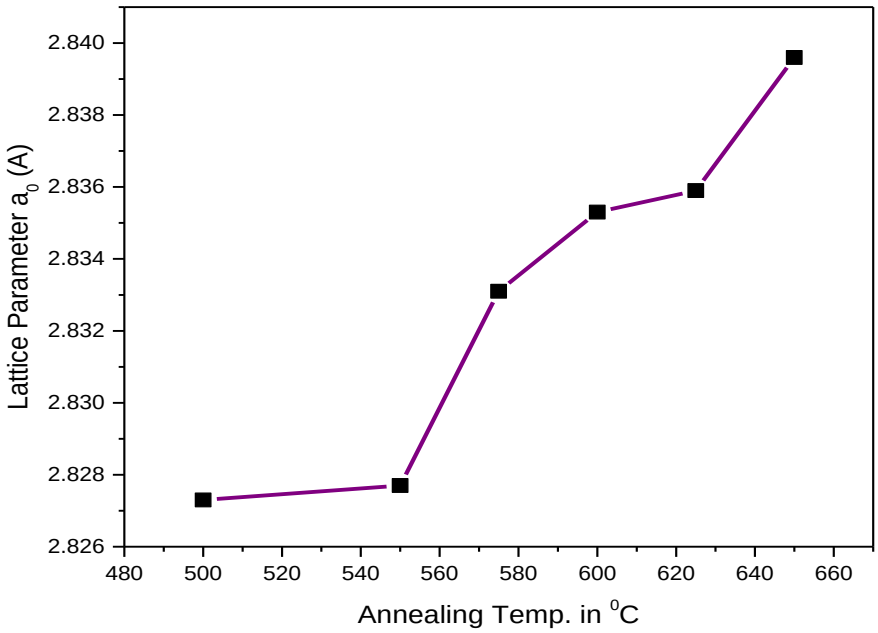

Figure 4.9: Variation of lattice parameter with annealing temperature.

As the presence of Co produce, a decrease in the lattice parameter, the actual Si content would be less in the crystalline phase. So contribution of Si content for the change of lattice parameter would be less might be the reason for which the variation in lattice parameter with annealing temperature is not obvious for present sample comparing to original FINEMET. The behavior of lattice parameter with annealing temperatures provides interesting information about composition of nanocrystalline phase formed by primary crystallization. All the obtained values of lattice parameter in this work are always significantly smaller than that of pure α-Fe.

4.2.3 Silicon Content in Nanograins

The silicon contents of the alloy $(Fe_{0.9}Co_{0.1})_{73.5}Cu_1Nb_3Si_{13.5}B_9$ at different annealing temperature 500^0C to 650^0C for one hour annealing time are found to be in the range of 16.71% to 22.46%. All these results are presented in table 4.10 and the pattern of change in silicon content with respect to annealing temperature is presented in figure 4.10.

The percentage of partitioned Si in the nanocrystalline α-FeCo(Si) phase is maximum at 500^0C. After 500^0C, decrease in Si-content is observed up to 650^0C, explained by the fact that at higher temperatures silicon diffuses out of nanograins due to crystallization corresponding to formation of boride phase which is consistent with the result of other FINEMET's. Si having a smaller atomic size compared to Fe, diffuses in the α-FeCo(Si) lattice during annealing at different temperatures which results in a contraction of α-FeCo lattice. So the more diffusion of Si, there should be more contraction of the α-FeCo lattice and thereby, the decrease of parameter.

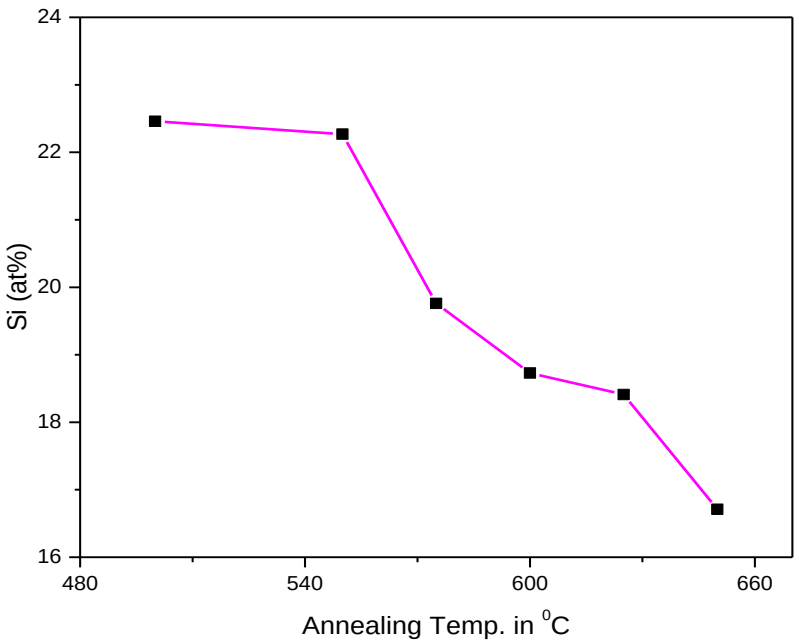

Figure 4.10: Variation of Si at % with annealing temperature.

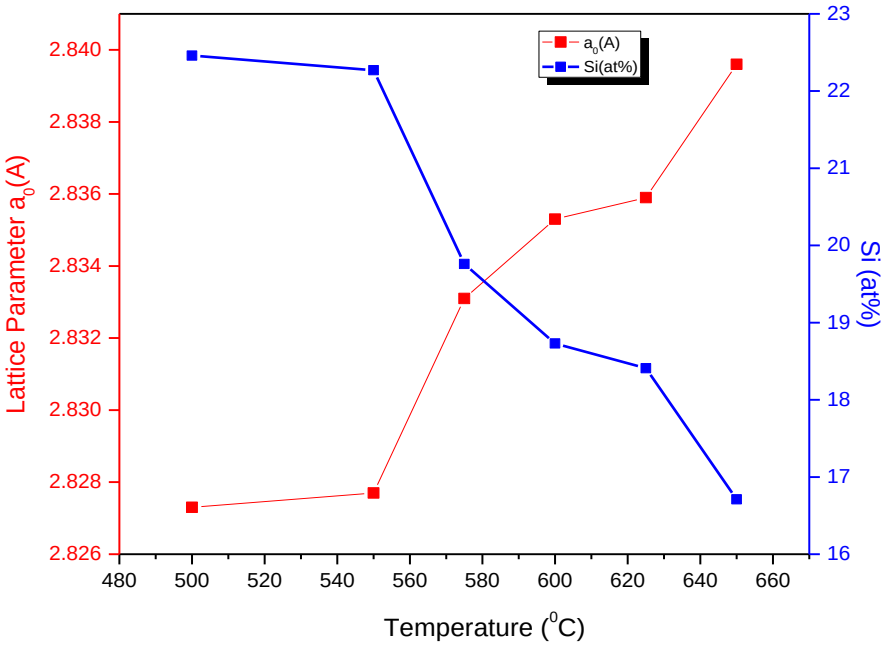

Figure 4.11(a): Variation of lattice parameter and Si at % with annealing temperature.

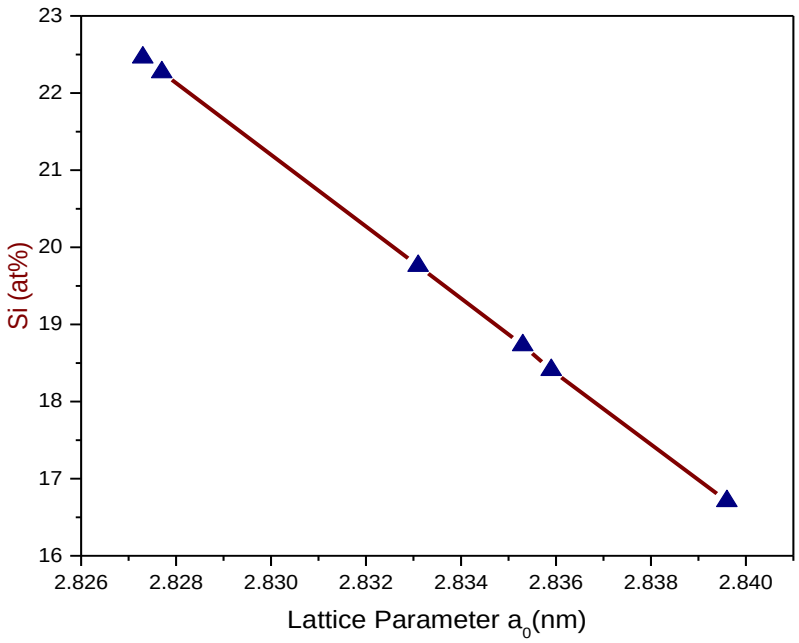

Figure 4.11(b): Variation of Si at % with lattice parameter.

Figure 4.11(b) shows the lattice parameter decreases with increases of silicon content, because diffuses in the bcc FeCo phase, to form the soft nanocrystalline α-FeCo(Si) phases. Figure 4.11(a) presents the inverse relationship between lattice parameter and silicon content. Figure 4.11(b) shows the silicon content linearly decreases with increasing lattice parameter. This kind of relation between lattice parameter and Si content was observed in the reports [4.16], which are verified in present work effectively. This is consequence of recrystallization when Si defuses out initiating formation of boride phase.

4.2.4 Grain Size Determination

Herzer [4.17] studied on theoretical explanation on the grain size dependence of superior soft magnetic properties based on his random anisotropy model (RAM) after the pioneer experimental invention of FINEMET alloy by Yoshizawa *et al.* [4.18]. The nanometric grains are consolidated to form a nanostructured materials, the magnetic properties are largely determined by the grain size and the exchange interaction between the adjacent grains. Grain size of all annealed samples of the alloy composition was determined using Sherrer method [4.19]. Grain size was determined using equation (4.4).

$$D_g = \frac{0.9\lambda}{\beta Cos\theta} \qquad (4.4)$$

The formation of the nanometeric microstructure corresponding to the grain growth with increase of annealing temperature is ascribed to be combined effects of Cu and Nb and their low solubility in Fe. Cu which is insoluble in α-FeCo, segregates prior to at the very beginning of nanocrystallization forming Cu-rich clusters and the nucleation of α-FeCo(Si) grains is thought to be multiplied by cluster Cu, which as the reason for the grain growth at the initial stage of crystallization. From table 4.9 it is clear that at lower annealing temperature 600^0C, the FWHM of the peak is large and with the increase of annealing temperature, the value of FWHM is getting smaller. The peaks are, therefore becoming sharper with the shifting of peak position towards higher 2θ value. The peak shifts indicate the change of the values of Si content of the nanograins and therefore, the change of values of lattice parameter of nanograins.

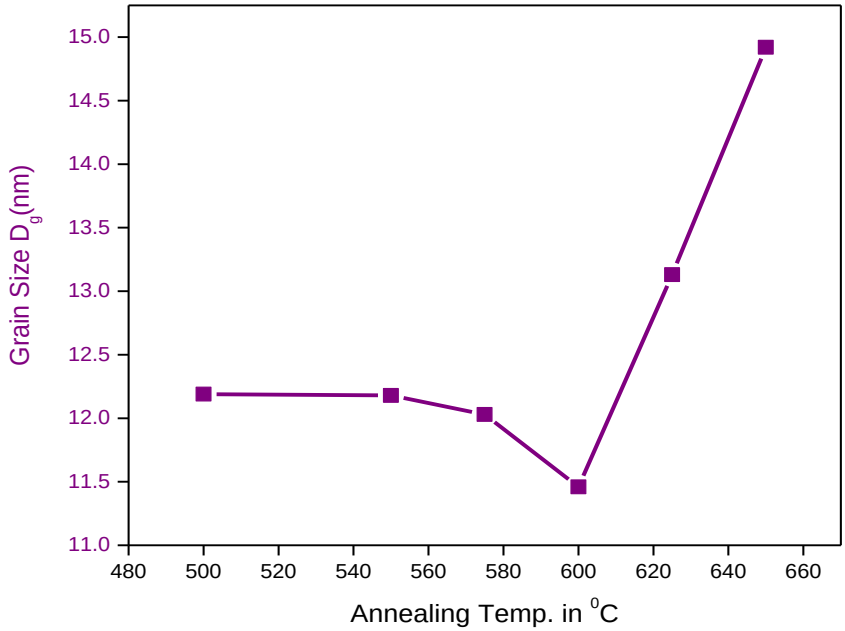

Figure 4.12: Grain size with annealing temperature.

Figure 4.12 and table 4.10 shown at 400^0C, no evidence of Si partitioning was found at the annealing temperature and hence grain growth is still not so evident. The increase of annealing temperature initiates partitioning α-FeCo(Si) phase and thus grain growth due to formation of nanocrystalline α-FeCo(Si) grains. In the range of annealing temperature 500^0C to 650^0C, the grain size remains in the range of 12 to 15nm corresponding to soft magnetic α-FeCo(Si) phases. Above 600^0C grain grow small change and attain maximum value 15nm at 650^0C indicating formation of Fe_2B phases. Formation of boride phase is detrimental to soft magnetic properties as showed in further experimental and also supported by different reports [4.20]. These facts reveal that heat treatment temperature should be limited within 500^0C to 650^0C to obtain optimum soft magnetic behavior, which constant grain size is12nm

4.3 Effect of Annealing Temperature on Specific Magnetization Measurement Nanocrystalline of $(Fe_{0.9}Co_{0.1})_{73.5}Cu_1Nb_3Si_{13.5}B_9$ Alloy at Room Temperature

The magnetization of as-cast $(Fe_{0.9}Co_{0.1})_{73.5}Cu_1Nb_3Si_{13.5}B_9$ amorphous and sample annealed for constant annealing time one hour at varying temperature from 500^0C to 650^0C has been measured as a function of magnetic field generated by an

electromagnet using a Vibrating Sample Magnetometer (VSM). In this type of magnetometer the sample is vibrated up and down in a region surrounded by several pick up coils. The magnetic sample is thus acting as a time changing magnetic flux; varying inside a particular region of fixed area. The magnetometer was calibrated using a high purity Ni disk considering the saturation magnetization of Ni is 54.75emu/gm at room temperature. The ribbon samples were cut into small shapes, weighed and glued to a standard sample holder.

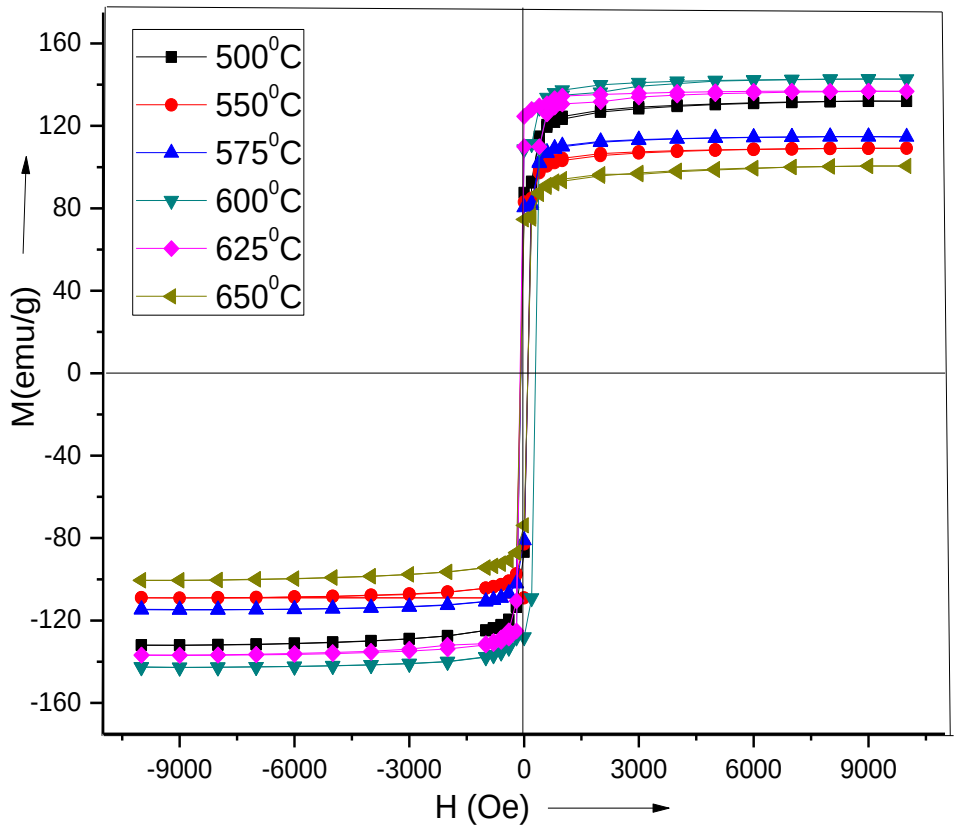

Figure 4.13: Specific magnetization versus magnetic field $(Fe_{0.9}Co_{0.1})_{73.5}Cu_1Nb_3Si_{13.5}B_9$ alloy at different annealing temperature for constant annealing time one hour of M – H loop.

Initially prepared Co-based FINEMET alloy well known that amorphous state is metastable. Metastability of glassy metal offers the possibility of phase separation diffusion of various species and structural relaxation even through the alloys remains amorphous when they grow nanocrystalline grains are annealed at temperature well below at 650^{o}C confirmed by DTA analysis. These are provides information about the

nature of residual strain in as prepared melt spun ribbons and their effect on domain wall pinning. This is important technical information about the possibility of using ribbons at elevated annealing temperature and optimum operating points of these ribbons, when they are used as soft magnetic materials under varying fields. These unique demands are fulfilled when the Co-based FINEMET types of nanocrystalline materials are thermally treated around their primary crystallization temperature which the evolution of nanometric size of the α-FeCo(Si) grains about 12 to 15nm that are exchanged couple the remaining thin residual amorphous interface.

Specific magnetization (M_S) at room temperature has been measured annealed sample, the annealing has been carried out for one hour constant annealing time at 500^{o}C to 650^{o}C shows the figure 4.13 and figure 4.14 are magnetization process of the nanocrystalline amorphous ribbons with different magnetic field. From these curves it is clearly evidenced that the magnetization is saturate for all the samples in the annealed states within an applied field 20kOe. Maximum saturation magnetization is reached at annealed sample at 600^{0}C. It can be seen that increasing annealing temperature M_S decrease up to 650^{o}C. Aranda *et.al* [4.21] has studied the approach to saturation in nanocrystalline FINEMET materials.

The magnetization prior to saturation is associated with reversible rotation and has been fitted to the law

$$M(H) = M_s \left[1 - \frac{a_1}{H} - \frac{a_2}{H^2}\right] + bH^{1/2} \qquad (4.5)$$

Where the term $\frac{a_2}{H^2}$ was described as being a direct consequence of the random anisotropy model, and attributable to α-FeCo(Si) grain. The coefficient a_2 reflects the Herzer's predicted effective magnetic anisotropy of the nanocrystalline material, where as in amorphous alloys it is postulated as being caused by local stress and magneto elastic coupling M_S is 132emu/g observed at 500^{0}C. After 550^{0}C M_s observed 109 emu/g to increase up to 142 emu/g for annealed samples at 500^{o}C to 600^{0}C compared with amorphous state is due to the irreversible structural relaxation, changing the degree of chemical disorder of the amorphous state [4.22] and enhance volume fraction of to α-FeCo(Si) nanocrystals that exchange coupled. The saturation magnetization is shown in figure in table 4.11.

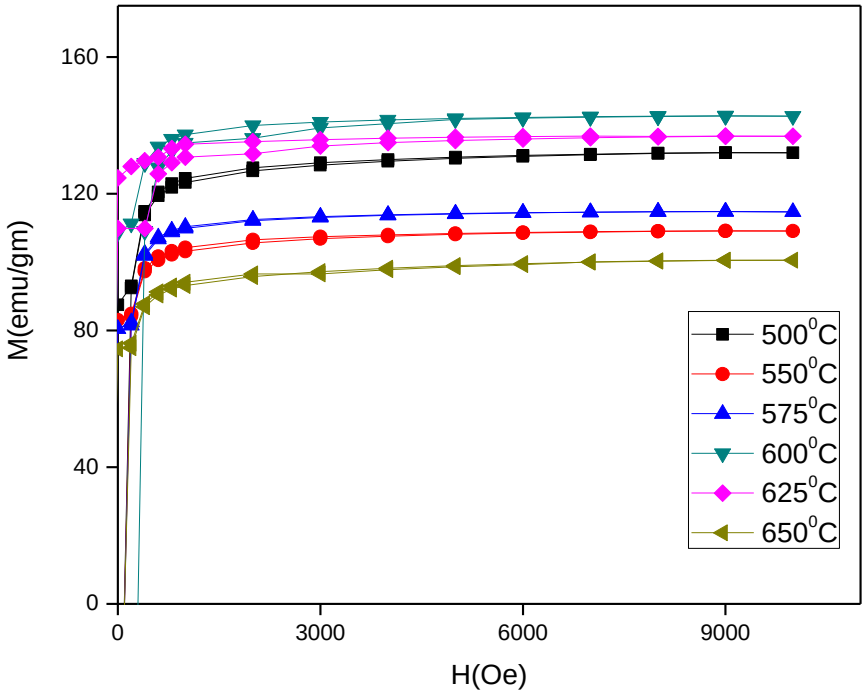

Figure 4.14: Specific magnetization versus magnetic field $(Fe_{0.9}Co_{0.1})_{73.5}Cu_1Nb_3Si_{13.5}B_9$ alloy at different annealing temperature for constant annealing time one hour.

It is to noted that an increase in M_s due to structural relaxation has also been detected in Fe-based glasses [4.23]. M_s is decrease in observed with increasing annealing temperature at 600^0C. The decreasing of M_S may be connected with the enrichment of the residual amorphous phase with Nb that weakens the coupling between ferromagnetic nanograins. Also role of Si diffuse into α-FeCo(Si) nanograins and these local environments also may be effect in decreasing M_S for the sample higher annealing temperature on ordering of Fe_3Si naograins can be not be rule out. If a small applied field suffices to produce saturation the nanocrystalline material is said to be magnetically soft.

Table 4.11: The values of saturation magnetization of $(Fe_{0.9}Co_{0.1})_{73.5}Cu_1Nb_3Si_{13.5}B_9$ alloy at different annealing temperature with constant annealing time one hour

Annealing temperature, in ^0C	Saturation magnetization, M_s in emu/g	Remanence magnetization, M_r in emu/g	Coercive force, H_c Oe
500	132	39	31
550	109	12	11
575	115	31	24
600	142	22	60
625	137	31	49
650	100	38	44

From these M – H loops at figure 4.14, the remanance induction (M_r) and coercive force (H_C) were determined shown in table 4.10. The M_S and H_C both decreasing with increasing annealing temperature again M_S and H_C are increasing with increasing annealing temperature, which distinguish reversible and irreversible types relaxation due to annealing temperature. Irreversible type of relaxation are those which are compared with thermally initiated microscope jumps of defects or ordering atomic pairs which corresponds to irreversible domain wall movements under external field. The different values of M_S and H_C are interpreted in quantitative way by means of domain theory.

CONCLUSIONS

5.1 Conclusions

Co-based nanocrystalline amorphous ribbon of FINEMET family with composition $(Fe_{0.9}Co_{0.1})_{73.5}Cu_1Nb_3Si_{13.5}B_9$ has been studied to find out the correlation between nanostructure size and soft magnetic properties depend on various stages of nanocrystallization during isothermal annealing around the crystallization temperature of their amorphous state. The amorphous stage of the as-cast ribbons has been confirmed by XRD. Crystallization kinetics and magnetic properties has been studied by DTA, XRD and VSM. From the systematic investigation on the crystallization structural and magnetic properties the following conclusions can be obtained:

(i) DTA experiment has been performed for six different heating rates 10^o to 60^oC/min in step of 10^oC/min up to a temperature 800^oC. DTA reveals the primary (T_{x_1}) and secondary (T_{x_2}) crystallization onset temperatures with manifestation of two well obtained exothermic peaks corresponding to nanocrystalline α-FeCo(Si) and Fe_2B phase respectively. The knowledge of the crystallization temperature has been fruitfully utilized during the isothermal annealing of this amorphous ribbon for nanocrystallization, which are controls the magnetic properties of partially substitution Fe by Co in FINEMET.

(ii) For heating rates 10^oC, 20^oC, 30^oC, 40^oC, 50^oC and 60^oC/min, onset of T_{x_1} were found 507^oC, 516^oC, 522^oC, 523^oC, 529^oC & 520^oC and that of the T_{x_2} were 634^oC, 646^oC, 656^oC, 658^oC, 662^oC & 652^oC respectively. The temperature difference between two crystallization peaks (T_{p_2}- T_{p_1}) are found to exists around 135^oC to 137^oC. This peak separation temperature is important for the stability of α-FeCo(Si) phase against Fe_2B phase while it is necessary for fabrication of higher quality inductors.

(iii) The sample annealed at 450^oC at constant annealing time is almost unchanged is still lower than DTA scan that of 1^{st} crystallization phase T_{x_1} = 540^oC at heating rat 20^oC/min. but the same condition sample annealed at 600^oC completely diffused T_{x_1} , α-FeCo(Si) phase has already vanish.

(iv) The activation energy of as-cast ribbon values of the α-FeCo(Si) is 4.1eV and Fe_2B phase is 6.31eV calculating using Kissenger's plots. The samples

annealed at 450^{o}C at constant annealing time thermal activation energies of α-FeCo(Si) is 3.58eV and Fe_2B is 5.73eV decreases than as cast ribbon.

(v) The evolution of nanocrystalline of α-FeCo(Si) and their sizes has been determined from the line broadening of fundamental peaks [110] from XRD pattern as affected by annealing around the crystallization temperatures. The grain sizes determined for the sample from 12 to 15nm for annealing temperature 500^{0}C to 650^{o}C. The crystallization onset temperature at 500^{0}C coincides well with the value obtained from DTA.

(vi) The lattice parameter and Si at% shows an inverse relationship indicating that Si diffuses in the crystalline phase at the initial stage of crystallization at 500^{o}C for which Si at% increased with decrease in lattice parameter.

(vii) The saturation magnetization (M_S) of annealed sample at 500^{o}C is 132emu/g decrease with increase of annealing temperature and increases for this nanocrystalline samples has slightly increased as maximum value of M_S = 142emu/g at 600^{0}C annealed sample, magnetization decrease after annealed condition. Small applied field suffices to produce saturation magnetization the nanocrystalline material thermal stage also magnetically soft. Achievement of soft magnetic Co-based nanocrystalline in the amorphous alloy in lower heat treatment temperature than the original FINEMET.

5.2 Scope for Future Work

These are much scope for further research in controlling the magnetic and structural kinetics by changing composition and heat treatment. Certain parameters like complex permeability, quality factor, transport properties, temperature dependence of magnetization, anisotropy and magnetostriction can be studied in detail for a better understanding of microstructure property relationship of FINEMET type alloys

REFERENCES

Chapter I

[1.1] Yoshizawa Y; Oguma O; Yamauchi K; "New Fe-base soft magnetic alloys composed of ultra-fine grain structure", J. Appl. Phy. 64, 6044 - 6046, 1988.

[1.2] Herzer G; "Grain size dependence of coercivity and permeability in nanocrystalline ferromagnetic", IEEE trans. Mag. 26, 1397-1402, 1990.

[1.3] Herzer G; "Magnetization process in nanocrystalline ferromagnets", Mat. Sci. Eng. A133, 1, 1-5, 1991.

[1.4] Herzer G; "Nanocrystalline Soft Magnetic Alloys", Chapter 3 in Hand Book of Materials Vol.10 ed. K.H.J. Buchow, Elsevier Pub. Co. p.417, 1997.

[1.5] Saroaut Noor, Sikder S. S. , Saha D. K. and Hakim M. A. "Time and Temperature dependence of Nanocrystalline and initial permeability of FINEMET alloy", Nuclear Science and application, 15 , 1, 9 -13, 2006.

[1.6] Mondal S. P., Kazi Hanium Maria, Sikder S. S.; Shamima Choudhury, Saha D. K. and Hakim M. A.; "Influence of annealing condition on nanocrystalline and ultra-soft magnetic properties of $Fe_{73.5}Cu_1Nb_1Si_{13.5}B_9$ alloy"; J. Mater. Sci. Technol. 28(1), 21-26, 2012.

[1.7] Hakim M. A. and Hoque S. M.; "Effect of structural parameters on soft magnetic properties of two phase nanocrystalline alloy of $Fe_{73.5}Cu_1Ta_3Si_{13.5}B_9$", J. Magn. Magn. Mater. 284, 395 - 402, 2004.

[1.8] Vlasak G., Svcc P. , Duhaj P. ;"Evolution of magnetostriction in $Fe_{73.5}Ni_xCu_1Nb_3Si_{13,5}B_9$ [x = 0,10,20,30,40] alloy in the course of transformation", J. Magn. Magn. Mater. , 254 -255, 225 - 227, 2003.

[1.9] Ohnuma M., Ping H., Abe D., Onodera T., Hono K., Yoshizawa.,; "Optimization of the microstructure and properties of Co-substituted Fe-Si-B-Nb-Cu nanocrystalline soft magnetic alloys", J. Appl. Phys., 93, 11, 9186 - 9194, 2003.

[1.10] Müller M., Grahl H., Mattern N., Kuhn U., Schnell B.; "The influence of Co on the structure and magnetic properties of nanocrystalline Fe Si B Cu Nb and Fe Zr B Cu-based alloys", J. Magn. Magn. Mater. 160, 284, 1996.

[1.11] Fernandez A., Perez M. J., Tajedor M., Madurga V.; "Thermo magnetic analysis of amorphous $(Co_x\ Fe_{1-x})_{73.5}Nb_3Si_{13.5}Bq$ metallic glasses", J. Magn. Magn. Mater, 338 - 344, 2000.

[1.12] Kolano - Burian A., Kalano R., Kulik T., Frence J.; "Magnetic properties of Co-doped FINEMET at elevated Temperature", Rev. Adv. Mater. Sci. 18, 545 - 548, 2008.

[1.13] Yoshizawa Y. and Yamauchi K; "Magnetic Properties of Nanocrystalline Fe-based Soft Magnetic Alloys composed of ultrafine grain structure", Mater. Trans. JIM, 31, 307, 1990.

[1.14] Noh T. H., Lee M. B., Kim H. J., Kang I. K.; "Relationship between crystallization process and magnetic properties of Fe-(Cu-Nb)-Si-B amorphous alloys", J. Appl. Phys. 67, 5568, 1990.

[1.15] Kazi Hanium Maria, Siba P. Mondal, Shamima Choudhury, Sikder S. S., Hakim M. A. and Saha D. K.; "Effect of Annealing Temperature on the Soft Magnetic Properties of $Fe_{75.5}Cu_1Nb_1Si_{13.5}B_9$ Amorphous Alloys", Journal of Engineering Trends Sciences (JETEAS) 2(1):102-108, 2011.

[1.16] Bigot J., Lecaude N., Perron J. C., Millan C., Ramiarinjaona C. and Rialland J. F., "Influence of annealing condition on nanocrystallization and magnetic properties in $Fe_{73.5}Cu_1Nb_3Si_{22.5-X}B_9$ [X = Cu, Ag & Au] alloy", J. Magn. Magn. Matter., 133**,** 29, 1994.

[1.17] Kane S. N, Sarabhai S., Gupta A., Varga L. K, Kulit T.; "Effect of quenching rate on crystallization in $Fe_{73.5}Cu_1Nb_3Si_{22.5-X}B_9$ alloys"; J. Magn. Magn. Mater., 215-216**,** 372, 2000.

[1.18] Müller M. and Matern N.; "The influence of refractory element addition on the magnetic properties and on the crystallization behavior of nanocrystalline soft magnetic Fe-B-Si-Cu alloys", J. Magn. Magn. Mater. 136,79,1994.

[1.19] Ayers J. D., Hans V. G., Sprague J. A., Elan W. T.; "On the role of Cu and Nb in the formation of nanocrystals in amorphous $Fe_{73.5}Cu_1Cr_xNb_3Si_{13.5}B_9$**",** Appl. Phys. Let., 64, 974, 1994.

[1.20] Herzer G.; "Grain structure and Magnetism of Nano crystalline Ferromagnetic"; IEEE Terns. Magn., 26, pp 1397 – 1402, 1990.

[1.21] Kubaschewsky O.; "Iron-binary phase diagrams", Springer Verlag, Berlin, Heidelberg, N. Y., Verlag Stahleisen mbH, Dusseldorf, 1982.

[1.22] Vlasak G., Svcc P., Duhaj P.; "Evolution of magnetostriction in $Fe_{73.5}Ni_xCu_1Nb_3Si_{13,5}B_9$ [x = 0, 10, 20, 30, 40] alloy in the course of transformation", J. Magn. Magn. Mater. , 254 -255, 225 - 227, 2003.

[1.23] Ohnuma O., Pins D. H., Abe T., Onodera H., Hono K. and Yoshizawa Y.; "Optimazitation of the microstructure and properties of Co-substituted Fe-Si-B-Nb-Cu nanocrystalline soft magnetic alloys"; J. Appl. Phys.; Vol. 93, No.11, 1 pp. 1986 – 9194, June 2003.

[1.24] Um C. Y. and McHenry M. E.; "Magnetic properties of Fe-Nb-Ta-Mo-B alloys", IEEE Trans. Magn. 40(4), 2724 -2726, 2004.

[1.25] Hakim M. A. and Hoque S. M.; "Effect of structural parameters on soft magnetic properties of two phase nanocrystalline alloy of $Fe_{73.5}Cu_1Ta_3Si_{13.5}B_9$", J. Magn. Magn. Mater. 284, 395 - 402, 2004.

[1.26] Franco V, Conde C. F., Conde A. and Kiss L. F.; "Super paramagnetic behavior in $Fe_{76}Cu_1Nb_3$ $Si_{10.5}B_{9.5}$ alloy", J. Magn. Magn. Mater., 215-216, 400-403, 2000.

[1.27] Slawska-Wanicwska A.,Nowicki P., Lachowicz H. K., Gorria P., Barandiardiaran J.M. and Hernando A.; "Magnetic interactions in Fe-Zr-B-Cu nanocrystalline materials at elevated temperatures", Phys. Rev. B 50(9), 6465-6467, 1994.

[1.28] Bean C. P., Livingston J. D.; "Superparamagnetism", J. Appl. Phys. 30(4), S120, 1959.

Chapter II

[2.1] Duwez P., Willens R. H. and Klement W.; J. Apply.phys.31, 1136, 1960.

[2.2] Duwez P.; J. Am. Inst. Metal. Eng., 191, 765, 1951.

[2.3] Duwez P.; Trans. Am SOC Met. 60: 607, 1967.

[2.4] Duwez P.; Ann Rev. Mat. Sci. 6: 83, 1967.

[2.5] Mader S., Nowick As.; Appl. Phys. Lett. 7: 57, 1965.

[2.6] Tsuei C. C., Duwez P.; J. Appl. Phys., 37: 435, 1960.

[2.7] Mc Henry M. A., Willard M. A. and Laughlin D. E.; "Amorphous and nanocrystalline materials for applications as soft magnets", Prog. Mat. Sci., 44, 291- 433, 1999.

[2.8] Mizoguchi T.; IBM Research report, RC 6045, 1976

[2.9] Alben R., Budnic J. I. and Gargil G. S.; "a_{111}Metalicglasess: American SOC. for metals"; pp304, 1978

[2.10] Yoshizawa Y. and Yamauchi K; "Fe-based soft magnetic amorphous alloys composed of ultrafine grain structure", Mater. Trans., 31, 307, 1990a..

[2.11] Hono K. and Sakuria T.; "Atom probe studies of nanostructured alloys"; Appl. Surf. Sci., 87/88, 166, 1995.

[2.12] Hono K., Hiraga K., Wang Q., Inoue A. and Sakurai T.; "The Microstructure Evolution of $Fe_{73.5}Si_{13.5}B_9Nb_3Cu_1$ Nanocrystalline Soft Magnetic Material", Acta Metal. Mater., 40, 2137-2147, 1992.

[2.13] Ayers J. D., Harris V. G., Sprague J. A. and Elan W. T.; "On the role of Cu and Nb in the formation of nanocrystals in amorphous $Fe_{73.5}Nb_3Cu_1Si_{13.5}B_9$", Appl. Phys. Lett. 64, 974, 1994.

[2.14] Herzer G.; "Nanocrystalline Soft Magnetic Alloys"; Hand Book of Materials, K. H. J. Buchow (ed), 10, 415 – 462, 1997.

[2.15] Yoshizawa Y. and Yamauchi K.; "Magnetic Properties of Nanocrystalline Fe-Based Soft Magnetic Alloys", Mater. Res. SOC. Symp. Proc. 232, 183 1991a.

[2.16] Herzer G.; In: Proc of Int. Symp. On 3ab Transition-Semi Metal Thin Films. Magnetism and Processing (Japan SOC for the promotion of Science, Committee, Sendia, Japan) **131** 130, 1991.

[2.17] Koster U., Schoncmann M., Blank - Bewersdorff S. Brauer, Sutton M. and Stephemon G. B.; "Nanocrystalline materials by crystallization of metal-metalloid glasses", Mat. Sci. Eng. **A133,** 611-615, 1991.

[2.18] Warliment H.; Mater. Sci. Eng. 99, 1988.

[2.19] Makino A., Inoue A. and Masumoto T.; Mat. Trans. JIM **36,** 924, 1995.

[2.20] Jones H.; Rep. Prog. Phys., **36,** 1425, 1973.

[2.21] Turnbull D.; J. dc physique, **35,** C4-1,1974.

[2.22] Takayama S.; "Amorphous structure and their formation and stability"; J. Materials Sci. Vol. 11(1) 164-185, 1976.

[2.23] Irvine J. T. S., Amano E., Huanosta A., Valenzuela R. and West A. R.; "Solid State should peak at T_c"; Ionic 40/41, 220, 1990.

[2.24] Cohen M. H. and Turnbull D.; "Composition Requirements for Glass Formation in Metallic and Ionic Systems"; Nature 189131-132, 1961.

[2.25] Gargil G.; III: J. Appl. Phys, 41, 2248, 1970.

[2.26] Chen H. S.; Acta. Mat., 22, 1505, 1974.

[2.27] Nagel S. R. and Taue J.; "Nearly- free- electron Approach to the theory of Metallic Glass Alloys"; Phys. Rev. Lett., 35, 380, 1975.

[2.28] Berkowitz A. E., Walter J. L. and Wall K. F.; "Magnetic Properties of amorphous particles produced by Spark Erosion"; Phys. Rev. Lett., 46, 1484.

[2.29] Murray P. and White J.; "Kinetics of the thermal dehydration of clays"; Trans. Brit. Ceram. SOC. 48, 187 - 206, 1949.

[2.30] Murray P. and White J.; "Kinetics of the thermal decomposition of clay 2, Isothermal decomposition of clay materials"; Trans. Brit. Ceram. SOC. 54, 151 - 187, 1955.

[2.31] Murray P. and White J.; "Kinetics of the thermal decomposition of clay 4, Interpretation of the differential thermal analysis of clays", Trans. Brit. Ceram. Soc. 54, 204 - 237, 1955.

[2.32] Sewel E. C.; "The consequences for differential thermal analysis of assuming a reaction to be first order"; Clay Minerals Bul. 2, 233 - 241, 1955.

[2.33] Kissinger H. E.; "Reaction Kinetics in Differential Thermal Analysis"; Anal. Chem. 29(11), 1702 - 1706, 1957.

[2.34] Boswell F. G.; "On the calculation of activation energies using a modified Kissinger method"; J. Therm. Anal., 18(2) 353 - 358, 1980.

[2.35] Cullity B. D.; "Elements of X-Ray diffraction"; Reading, M. A. Addison Wesley, 1978.

[2.36] Bozorth R.; "Ferromagnetism", D. Van Nostrand, Princeton N. J.76, 1951.

[2.37] Handrich K.; "Conditions for the Existence of Amorphous Ferromagnets" Phys. Stat. Sol.(b), 53, K17, 1972.

Chapter - III

[3.1] Turnbull D.; "Under what conditions can a glass be formed?", Contemp. Phys. 10, 473 - 488, 1969.

[3.2] Duwez P., Willens R. H. and Kelment Jr. W.; J. Appl. Phys. Lett., 31, 1136, 1960.

[3.3] Coey JMD and Sun H.; J. Magn. Magn. Mater., 87, 1251, 1991.

[3.4] Schnitzke K., Schultz L., Wecker J. and Katter M.; J. Appl. Phys. Lett., 57, 2853, 1990.

[3.5] Le Chatelier H.; Bull SOC. France Mineral, 10, 204, 1987.

[3.6] Pearson W. B.; "A Hand book of Lattice spacing and Structures of Metals and Alloys" (Oxford Pergamon), 1958.

[3.7] M. A. Mazid and M. A. Chowdhury; "Design and Construction of Forner type VibratingSample Magnetometer"; AECD/MMD/1 (Bangladesh).June, 1986.

[3.8] Simon Foner; "Versatile and Sensitive Vibrating Sample Magnetometer"; Rev. Sci. Instr. 30, 160, 1959.

Chapter -IV

[4.1] Clements W. G. and Cantor B.; "in rapidly quenched metal", Section-1, (Eds. Graut N. J. and Giessen B. C.) (MIT Press Cambridge, Mass) P. 267, 1976.

[4.2] Luborsky, F.E., Materials Sci. Engg-28, P.139, 1977.

[4.3] Mc Henry M. E., Willard M. A. and Laughlin D. E.; "Amorphous and nanocrystalline materials for applications as soft magnets." Prog. Mat. Sci., 44, 29-433, 1999.

[4.4] Manjura Hoque S., Hakim M. A., Chau N.; "Ultra soft magnetic properties devitrified Fe75.5Nb2.4Cu0.6Si13B8.5 alloy" Mat. Chem. Phys. 101, 112-117, 2007.

[4.5] Saha D. K. and Hakim M. A.; Journal of Bangladesh Academy of Sciences; 30, 2, 177-187, 2006.

[4.6] ChenC. L. and Hasegawa R. S.; "Mössbauer study of glassy alloy $(Fe-Mo)_{80}B_{20}$; J. Appl. Phys. 49(3) 1721, 1978.

[4.7] Moorjan K., Chatak S. K., Rao K. V., Kramer B. and Chen H. S.; Int. Conf. on liquid and amorphous metals, Grenmole, France 1980.

[4.8] Herzer G.; "Elsevier Hand Book of Magnetic Materials", 10, 427, 1997.

[4.9] Yoshizawa Y., Oguma S. and Yamachi K.; "New Fe-based soft magnetic amorphous alloys composed of ultrafine grain structure"; J. Appl. Phys. 64(10), 6044 - 6046, 1988.

[4.10] Hono K., A-Inoue, Sakuri T.; Appl. Phys. Lett., 58, 2180, 1991.

[4.11] Kissinger H. E.; "Reaction Kinetics in Differential Thermal Analysis" Anal. Chem., 29(11), 1702-1706, 1957.

[4.12] Noor S.; "Effect of two-step annealing on complex permeability of Fe-Cu-Nb-Si-B nanocrystalline soft magnetic materials", M. Phil. Thesis, March 2005, KUET, p70-72.

[4.13] Bozorth; "Ferromagnetism", D. Van Norstrand Company, Inc. Pinceton, NJ, P.64, 1964.

[4.14] Chen W. Z., Ryder P. I.; "X-ray and differential scanning calorimetry study of amorphous $Fe_{63.5}Co_{10}Cu_1Nb_3Si_{13.5}B_9$ alloy", Mater. Sci. Eng. B(34), 204 – 209, 1995.

[4.15] Borrego J. M., Conde C. F., Conde A. and Greneche J. M.; "Crystallization of Co-containing FINEMET alloys", J. Non. Crys. Solids, 287, 120 -124, 2001.

[4.16] Franco V., Conde C. F., Conde A., "Changes in magnetic anisotropy distribution during structural evolution of $Fe_{76}Si_{10.5}B_{9.5}Cu_1Nb_3$" J. Mang. Mang. Mat. 185, 353 – 359, 1998.

[4.17] Herzer G.; "Grain Structure and Magnetism of Nanocrystalline ferromagnets", IEEE Trans. Magn., 25(5), 3327-3329, 1989.

[4.18] Yoshizawa Y., and Yamachi K.; "Fe-based soft magnetic alloys composed of ultrafine grain structure", Mater. Trans. JIM 31, 307, 1990a.

[4.19] Cullity B. D.; "Elements of X-ray Diffraction", Adison-Wisley Publishing Company Inc., London, England, p.262, 1959.

[4.20] Pearson W. B.; "A Hand book of Lattice spacing and Structures of Metals and Alloys" (Oxford Pergamon), 1958.

[4.21] Aranda, G. R. Gonzalez, J. Kulakowski, K.; J. Appl. Phys. (1998) 83:6341.

[4.22] Lovas A., Kiss L. F., Balong L.; "Saturation magnetization and amorphous Curie point changes during the early stage of amorphous nanocrystalline transformation of a FINEMET type alloy"; J. Magn. Magn. Mater. (2000) 215-216, 463.

[4.23] Berkowitz A. E., Walter J. L. and Wall K. F.; "Magnetic properties of amorphous particles produced by Spark Erosion", Phys. Rev. Lett. 46, 1484, 1981.

Conference Paper

M. A. Hossain, **K. Sarkar**, M. N. I. Khan and S. S. Sikder,; "Study of Structural in the Effect of Partly Substitution of Fe by Co in FINEMET", International Conference on Physics – 2018, 08 -10 March, 2018, University of Dhaka, Dhaka-1000, Bangladesh